Max-Planck-Institut für Metallforschung
Stuttgart

Atomistic simulation of interface controlled solid-state phase transformations

Cornelis Bos

Dissertation
an der
Universität Stuttgart

Bericht Nr. 175
November 2005

Max-Planck-Institut für Metallforschung
Stuttgart

Atomistic simulation of interface controlled solid-state phase transformations

Cornelis Bos

Dissertation
an der
Universität Stuttgart

Atomistic simulation of interface controlled solid-state phase transformations

Development and application of a multi-lattice kinetic Monte Carlo method

Von der Fakultät Chemie der Universität Stuttgart

zur Erlangung der Würde eines Doktors der Naturwissenschaften
(Dr. rer. nat.) genehmigte Abhandlung

vorgelegt von

Cornelis Bos
geboren in Enschede

Hauptberichter:	Prof. Dr. Ir. E.J. Mittemeijer
Mitberichter:	Prof. Dr. B.J. Thijsse
Tag der Einreichung:	27. September 2005
Tag der mündlichen Prüfung:	25. November 2005

INSTITUT FÜR METALLKUNDE DER UNIVERSITÄT STUTTGART
MAX-PLANCK-INSTITUT FÜR METALLFORSCHUNG STUTTGART

2005

voor mijn ouders

CONTENTS

1. Introduction

1.1 Simulation of interface controlled *solid-solid* transformations

Most mechanical and engineering properties of metallic materials are determined by the microstructure of the material. Therefore, it is of great technological importance to obtain a fundamental understanding how the microstructure of a material is influenced by processing parameters such as deformation and heat treatment. In the processing of alloys many microstructural changes occur with the material in the solid state. Typical examples are phase transformations to different crystal structures, grain growth and recrystallisation. Here, the transformation takes place by the movement of *solid-solid* interfaces in the material. Basically, the transformations can be divided in two classes: martensitic (military) and diffusional (civilian). Martensitic transformations occur by a cooperative, usually a-thermal, movement of the atoms, whereas diffusional transformations are assumed to take place by independent thermally activated atomic jumps [1]. To understand the kinetics of diffusional transformations it is important to discern between transformations that are rate-controlled by processes at the interface (interface controlled transformations) and those that are rate-controlled by long-range diffusion of any of the alloying elements. Grain growth and recrystallisation are always interface controlled transformations. Typical interface controlled phase transformations are the massive transformations, which can be observed in many steel alloys.

The mobility of an interface in an interface controlled transformation is determined by the atomic rearrangement process occurring at the interface. However, the mechanism of the atomic rearrangement process is still not well understood [1]. The experimental study of the atomic mechanism of the interface movement is difficult because observations must be made of moving interfaces at an atomic resolution. Such observations have been made but data are still scarce [2, 3]. This is why atomistic simulations are used more often to study these phenomena. For example, molecular dynamics simulations have been used successfully in the study of martensitic transformations [4–6]. Unfortunately, the time scale associated with most interface controlled transformations is too long for molecular dynamics simulations. Because in diffusional transformations the interface should move by independent thermally activated jumps [1], a kinetic Monte Carlo approach similar to
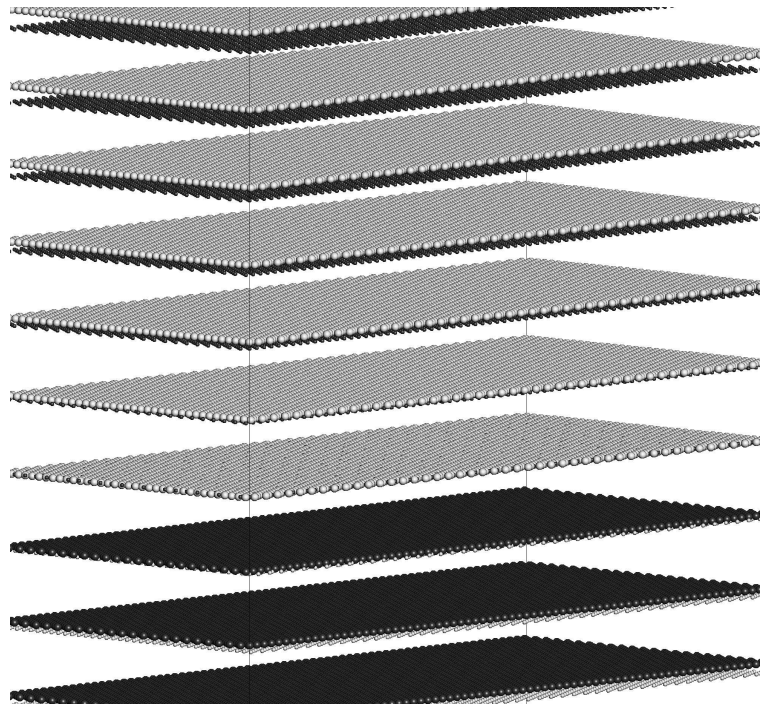
Fig. 1.1: Schematic drawing of the two interpenetrating partially occupied lattices. Bcc sites are represented by dark spheres and fcc sites by light spheres. Occupied sites are drawn larger than empty sites. The space between the planes has only been inserted here to obtain a clearer view.

those used for the simulation of *solid-liquid* interface movement [7–11] seems feasible. However, normal atomistic kinetic Monte Carlo methods use a rigid lattice of possible positions for the atoms [12, 13]. Clearly, for a phase transformation at least two different crystal lattices are required. Therefore, a new multi-lattice kinetic Monte Carlo method has been developed and is presented here in this work.

1.2 Multi-lattice kinetic Monte Carlo

In the multi-lattice kinetic Monte Carlo method a simulation starts with two interpenetrating partially occupied lattices, as shown in figure 1.1 for an face centered cubic (fcc) to a body centered cubic (bcc) phase transformation simulation. From figure 1.1 it becomes clear that in the multi-lattice kinetic Monte Carlo method the orientation relationship between the two crystals is a simulation parameter and must be chosen by the user. In this way the influence of different interface orientations (as determined by the orientation relation) can be systematically studied.

After creating the initial configuration (e.g. figure 1.1) the transformation is simulated by allowing the atoms at the interface to jump to a neighbouring empty site on either of the two lattices. Which jump actually is made at each time step is determined by chance, us-
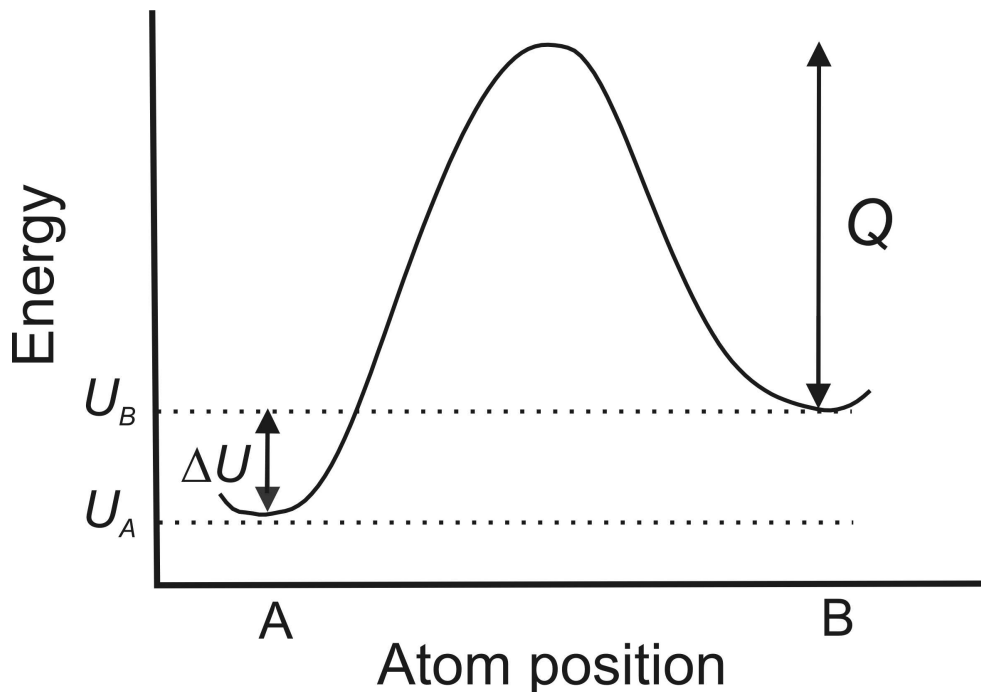
Fig. 1.2: For an atomic jump from position A to B the change in system energy, ΔU, is shown together with the change in system energy *during* the jump giving the energy barrier part, Q, of the activation energy. Q can either be a simulation parameter or calculated for every jump separately.

ing a weighted random selection procedure where the energetically most favourable jump is most likely to be chosen. For the calculation of the energy change associated with the jumps an atomic interaction model is required. In the multi-lattice kinetic Monte Carlo method virtually any interaction model can be used, the only limitation being the computational cost associated with the interaction model. A too complex model could extend the calculation time beyond practical limits. As the results presented in this thesis will show, it can be beneficial to work with a simple interaction model. With a more simple model there often is a better control over the atomic behaviour. With this control over the atomic behaviour, normally unchangeable materials properties (for example the energy difference between two phases) can be set as a simulation parameter, allowing the systematic investigation of the influence of these materials properties on the transformation behaviour.

If the goal of the simulations is to study the transformation behaviour for a specific material then the most accurate interaction model available should be used. Especially in the comparison with real laboratory experiments, it becomes important that not only the energy change in the system caused by a jump, ΔU, is modeled accurately but also that for the activation energy of an atomic jump a value is used that takes into account the (unique) arrangement of the neighbouring atoms. Therefore, depending on the re-

quired level of accuracy, two different types of simulations have been developed within the multi-lattice kinetic Monte Carlo framework. When a more quantative description of the kinetics is less important, simulations are run where the same constant energy barrier part of the jump activation energy, Q see figure 1.2, is used for every jump. In the other cases Q is calculated for every jump separately. However, here it is important to realize that the separate calculation of the activation energy for every jump is a computationally extremely costly procedure.

To limit this extra cost in computation time as much as possible, a two step procedure has been developed that allows the much faster calculation of the jump specific activation energies with the help of a trained neural network. As an interface moves there will be many different atomic jumps. However, the total number of really different jumps is limited due to the periodicity of the crystal lattices. By calculating the activation energy for a very large number of jumps a neural network can be trained that uses the information of the arrangement of the neighbouring atoms as input parameters to predict the activation energy for a jump. The collecting of the training data and the actual training of the neural network is the first step. Then as the second step the trained neural network is used to calculate the activation energies for the jumps during the simulations.

1.3   Thesis overview

The multi-lattice kinetic Monte Carlo method has been used to study the growth behaviour of the α (bcc) phase, in a γ (fcc) to α (bcc) phase transformation in a (model) single element system. In Chapter 2 the basics of the multi-lattice kinetic Monte Carlo method are presented, together with results of a study on the influence of the driving force and interface energy on the growth mode of the bcc phase. Then Chapter 3 presents lateral growth simulations performed to study the activation energy of the interface mobility. These simulations have led to a new interpretation of the interface mobility activation energy in terms of series of jumps of groups of atoms. The simulations as described in Chapter 3 were performed with a bond-counting atomic interaction model and with a constant energy barrier for all atomic jumps. Chapter 4 shows that the same results are obtained for simulations with an (iron) embedded atom method interaction potential and with variable per jump calculated activation energies. In Chapter 2 the growth mode was shown to depend on the driving force and the interface energy. In Chapter 5 it is shown that with the same driving force the growth mode can change from plane-by-plane to continuous by a change of the interface orientation. In Chapter 6 the interface mobility activation energy is compared to the boundary self-diffusion activation energy.

2. A kinetic Monte Carlo method for the simulation of massive phase transformations

C. Bos, F. Sommer and E.J. Mittemeijer

Abstract

A multi-lattice kinetic Monte Carlo method has been developed for the atomistic simulation of massive phase transformations. Beside sites on the crystal lattices of the parent and product phase, randomly placed sites are incorporated as possible positions. These random sites allow the atoms to take favourable intermediate positions, essential for a realistic description of transformation interfaces. The transformation from fcc to bcc starting from a flat interface with the fcc(111)//bcc(110) and fcc[11$\overline{2}$]//bcc[00$\overline{1}$] orientation in a single component system has been simulated. Growth occurs in two different modes depending on the chosen values of the bond energies. For larger fcc-bcc energy differences, continuous growth is observed with a rough transformation front. For smaller energy differences, plane-by-plane growth is observed. In this growth mode two-dimensional nucleation is required in the next fcc plane after completion of the transformation of the previous fcc plane.

2.1 Introduction

The massive transformation is a long-range diffusionless phase transformation during which the matrix phase is converted to a product phase with a different crystal structure but with the same composition [2]. This massive transformation is accomplished by diffusional jumps across the interface between the two phases. In many iron-based alloys the austenite, γ, to ferrite, α, transformation is of massive nature. Recently, the massive transformation has received much renewed attention [2, 14, 15]. The mechanism of the transformation is a topic of active discussion [16]. Most experimental data were collected after the transformation was completed. Data on the interface structure obtained during the transformation would greatly enhance the understanding of the transformation mechanism, but such data are scarce [3, 16].

Molecular dynamics (MD) simulations would allow the study of the structure of a moving interface in full atomic detail, as simulations of the martensitic transformation have shown [4–6]. Unfortunately the timescale required for massive transformations is too demanding computationally. In MD simulations the full continuous trajectories of the atoms are described. To enhance the timescale that can be simulated, kinetic Monte Carlo (kMC) simulations can be made. However, then the possible atom positions are restricted to a set of discrete sites. The movement of the atoms is then treated as a stochastic process.

Monte Carlo methods have been employed successfully in simulating *solid-vapour* and *solid-liquid* transformations [7–11]. The simulations have provided detailed information on the interface structure during crystal growth for different types of materials [10, 11]. Unfortunately these methods cannot be applied directly to *solid-solid* transformations. Because a kinetic Ising model provides the basis of kMC simulations it follows that the atoms are placed on a rigid lattice [12, 13]. Hence, a description of a *solid-solid* transformation requires at least two lattices. Until now such an approach was computationally too demanding [17]. However, increased computational power makes it possible to develop a full multi-lattice method now and such a method is presented for the first time in this paper.

For a massive γ to α transformation simulation, two different crystal lattices are required: fcc and bcc. A crucial extra imposition is the use of random sites in the method proposed here. These sites are distributed randomly throughout the system. This allows the occurrence of deviations of the crystal structure arrangement, in particular at the transformation front (see section 2.2).

This paper thus describes a multi-lattice kinetic Monte Carlo model for the simulation of a massive transformation (section 2.2). To describe the atomic interactions a nearest neighbour bond counting model is used (section 2.2.1). Although the model is not at all material specific, whenever materials properties had to be chosen, values that pertain to iron were selected. The first simulations performed with this model reported here were devised to test the applicability of this type of atomistic simulation.

The focus is on the transformation from the fcc to the bcc ($\gamma \rightarrow \alpha$) phase of a single element, starting with a flat, incoherent interface. Although a substantial amount of the bcc phase is present in the start configuration of the simulations, nucleation can still play an important role. A completely flat interface may require the formation of (2-dimensional) nuclei for further growth of the bcc phase. As described in section 2.3, simulations have been performed to study such 2-dimensional nucleation behaviour and to investigate the possibility of growth without such a separate nucleation phase. The results of the simulations are presented in section 2.4. The discussion in section 2.5 focuses on the nucleation and the growth behaviours.

2.2   Simulation method

As compared to earlier simulation models for crystal growth (e.g. see Ref [8]) the introduction of intertwining multiple crystal lattices is the cardinal step to be made in order to simulate *solid-solid* phase transformations. As described below, not only multiple lattices but also randomly distributed sites have to be introduced as possible positions for the atoms.

A system is created with a partially filled fcc (γ) lattice and a partially filled bcc (α) lattice. This means that the initial nucleation of the bcc phase is not simulated (see sections 2.1 and 2.3). A γ/α interface with a specific orientation is created. The events considered in the kMC model are atom jumps from a filled site to an empty site. The energy change ΔU associated with a jump is calculated on the basis of a nearest neighbour bond counting model as described in section 2.2.1. The jump probability p is taken as [12]

$$p = \frac{\exp\left(-\frac{\Delta U}{k_B T}\right)}{1 + \exp\left(-\frac{\Delta U}{k_B T}\right)}, \qquad (2.1)$$

where k_B is the Boltzmann constant and T is temperature. The simulation algorithm presented below has been developed from the following considerations.

Two sites (and atoms) are considered to be neighbours if the distance between them is less than $1.05r_f$ (the fcc nearest neighbour distance). In the simulations $r_f > r_b$ (r_b is the bcc nearest neighbour distance), the factor 1.05 has been chosen to prevent round-off errors. An atom is considered an interface atom if it has a neighbour of a type different from its own type or if it is next to a vacancy. Thereby the atoms next to vacancies are included in the collection of "interface" atoms in order to make movement of vacancies possible also when these vacancies are not positioned directly at the interface.

To prevent atoms from jumping through or into other atoms, not all empty neighbour sites can be valid target sites. There are two types of valid target sites. For the first type the site has to be within a radius r_{sj} of the source site. A jump to this type of target site is called a short jump. For the second type the target site has to be within the maximum jump distance $r_{maxjump}$ from the source site and there should be no other atom within a radius r_{vh} of the target site. If r_{vh} is chosen large enough then these target sites can be considered to be vacancies. These long jumps can then be considered to be vacancy jumps. The different ranges discussed are illustrated in fig. 2.1. A jump from site A to site B is valid (short jump) as site B is within r_{sj} of site A. A jump to site C is not valid because site D is within r_{vh} of site C.

The distinction between these two types of valid jumps has been made for computational efficiency reasons. It is unlikely that the target site of a short jump will have an occupied neigbour within r_{vh} (as the jumping atom is so near). Therefore the compu-
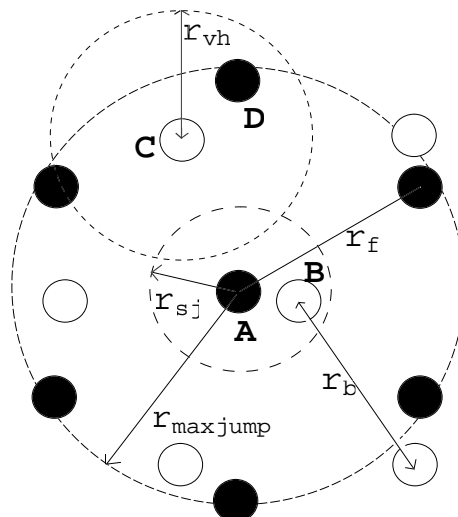
Fig. 2.1: The different ranges. Occupied fcc sites (black) and empty bcc sites (white) are shown. The maximum jump distance is r_{maxjump} for a long and r_{sj} for short jump (shown for atom A), r_{vh} is the minimum radius required for a vacancy hole. The bcc and fcc nearest neighbours distances are r_{b} and r_{f}, respectively.

tationally costly procedure of checking for an occupied neigbour within r_{vh} is not performed for these target sites. To deal with the unlikely case that the target site of a short jump *does* have an occupied neigbour within r_{vh} the atoms have been given a hard-sphere core. When two atoms are within a distance smaller than the hard-sphere diameter d_{hs}, the atoms experience a (infinitely) large repulsion. This ensures that two atoms will never overlap (see also section 2.2.1) because of a short jump.

All simulations have been done with $r_{\mathrm{sj}} = 0.35r_b$, $r_{\mathrm{vh}} = 0.85r_{\mathrm{b}}$ and $r_{\mathrm{maxjump}} = 1.025r_{\mathrm{f}}$.

If only fcc and bcc lattice sites are included in the simulation then the transformation must be accomplished by direct jumps from fcc to bcc sites. However, recognizing the complexity of actual interface structures, it is considered possible that the atoms first visit an 'intermediate' position. The location of these intermediate positions is not known and therefore difficult to include in the simulation. By including uniformly distributed randomly placed sites within the system it is assured that at least some of these extra positions are available for the atoms at the interface. The amount of available computer memory limits the number of random sites that can be included. Because these sites are distributed randomly they have a chance of being located at positions that will never be occupied. The efficiency of the random sites can be enhanced by continuously assigning new random positions until they have been occupied. In other words, the random sites 'search' for the (relevant) intermediate positions. Simulations have shown that without random sites no significant progress of the transformation is possible.

Finally, a time step is defined such that after one time step every interface atom has made one jump attempt.

The simulation algorithm then can be given as follows:

1. At random, select an interface atom

2. At random, select a valid empty neighbour site of that interface atom

3. Calculate the energy change ΔU for the jump to this empty site

4. Calculate the corresponding jump probability p according to eq. (2.1)

5. Generate a random number $r \in [0, 1)$ from a uniform distribution

6. Accept the jump if $r < p$

7. Continue step 1 until all interface atoms have been selected once and only once

8. Update the time step counter by one

9. Give the random sites that have remained unoccupied a new position.

10. Expand or contract the system in the direction perpendicular to the original interface (see section 2.3)

11. Continue with step 1

2.2.1 The atomic interaction model

The model for the atom interaction has been devised to comply with three requirements:

1. The bulk bcc atoms must have a lower energy than bulk fcc atoms

2. It must cost energy to enlarge the interfacial area

3. Atoms very close to each other must repel one another

The atom-atom interactions are expressed in terms of bond energies u. As there are three different kind of sites, there are six different kinds of bonds. Three of these bonds have been given a fixed energy. These are the fcc-fcc bond-energy u_{ff}, the bcc-bcc bond-energy u_{bb} and the bcc-fcc bond-energy u_{bf}. Choosing specific values for u_{ff} and u_{bb} will fulfill requirement 1. For bcc-bcc and fcc-fcc the distance between two atoms is fixed (only nearest neighbours are considered), but for the fcc-bcc distance this is not the case. Yet, the fcc-bcc bond energy, u_{bf}, is taken as a constant. Requirement 2 can then be satisfied by choosing a specific value for u_{bf} (see also section 2.3.1).

The three other kinds of bonds involve atoms on random sites (random-bcc, random-fcc and random-random). The interaction between a random site and a fcc/bcc/random site is taken independent of the distance between these two sites, but the value of the interaction is made variable as it depends on the surroundings of the random site(s) as follows. If a random site is very close to a specific lattice site, it should behave like that lattice site. Therefore, the energy of a bond with an atom on a random site depends on the distance of that random atom to the nearest lattice site, r_{ran}. The maximum distance between a random site and an xcc (where x is b or f) site is $\frac{1}{2}r_{\text{x}}$, the minimum distance is zero. At the maximum distance the bond-energy with an xcc atom is given by u_{rx}. For distances between the minimum and maximum values the bond energy for a random - xcc atom pair is interpolated linearly.

There are eight different interpolation equations. Four of these concern a bond between a lattice site of type x (b or f) and a random site that behaves like a site of type y (b or f):

$$u = u_{\text{rx}} + (\lambda u_{\text{xy}} - u_{\text{rx}})\frac{\frac{1}{2}r_{\text{y}} - r_{\text{ran}}}{\frac{1}{2}r_{\text{y}}}, \tag{2.2}$$

where λ is a parameter that will be explained below. The other four concern bonds between a random site A that behaves like a site of type x, with a distance r_{ran_A} to that site, and a random site B that behaves like a site of type y, with a distance r_{ran_B} to that site:

$$u = \frac{1}{2}\left[u_{\text{rx}} + (\lambda u_{\text{xy}} - u_{\text{rx}})\frac{\frac{1}{2}r_{\text{y}} - r_{\text{ran}_B}}{\frac{1}{2}r_{\text{y}}} + u_{\text{ry}} + (\lambda u_{\text{xy}} - u_{\text{ry}})\frac{\frac{1}{2}r_{\text{x}} - r_{\text{ran}_A}}{\frac{1}{2}r_{\text{x}}}\right]. \tag{2.3}$$

If the distance between a random site and the considered nearest lattice neighbour site, r_{ran}, is very small, the random site is almost indistinguishable from that lattice site; i.e. from an energy point of view it becomes indifferent if an atom occupies the lattice site or the random site. This means that the chance that such a random site becomes occupied is large. Often, it is necessary to count the number of atoms of a specific type: for example, the number of bcc atoms to determine the fraction transformed material. In this case the atoms on random sites very close to bcc sites should be counted as bcc atoms too. One option to ascertain that these occupied random sites close to the bcc lattice sites are recognized as bcc atoms, is to separately assign a crystal structure type to every single random atom based on the local surroundings of each atom. However, this not trivial task is computationally extensive. A second option is to ensure that the atoms have a significantly higher chance to occupy the lattice site as compared to the chance that the random site will be occupied. This can be accomplished with the parameter λ in eqs. (2.2) and (2.3). By choosing a value smaller than one for λ, the maximum energy of a bond

with an atom on a random site is reduced (less negative). In all simulations a value of 0.8 has been used for λ (i.e. for r_{ran} the bond-energy is 80% of u_{xy}.

Requirement 3 is fulfilled by giving the atoms a hard-sphere core. The hard-sphere diameter d_{hs} has been chosen as

$$d_{\mathrm{hs}} = 0.68 r_{\mathrm{b}}. \tag{2.4}$$

With this value the hard-sphere core is just a little larger then the tetragonal interstitial holes in the bcc crystal structure. If two atoms are within the range d_{hs} of each other, they are given such a large (positive) bond-energy that a jump for which such a bond would be created is never accepted.

2.3 Simulation Details

All interfaces have been created with the orientation fcc(111)//bcc(110) and fcc[11$\overline{2}$]// bcc[00$\overline{1}$]. The interface is completely flat and lies parallel to the xy-plane. A start configuration has three bcc planes and between 35 and 45 fcc planes. All simulations have been performed with imposed periodic boundary conditions in the x- and y-directions. The system volume is rectangular. The cross sectional area of the xy-planes is kept constant during the simulations; volume change is accommodated by expansion/contraction in the z-direction.

The bcc(110) and the fcc(111) lattice spacings ($d_{\mathrm{b(110)}}$ and $d_{\mathrm{f(111)}}$) are generally not equal. This means that as fcc planes are transformed to bcc the system wants to expand or contract (depending on the densities of the crystals) in the z-direction. The system is allowed to do this by shifting those fcc sites that have not yet made a jump trial in the simulation. This means that by this shift deviations from the ideal fcc lattice can occur because some atoms in one fcc plane are shifted while others are not. However, these deviations are so small that the crystal structure is not disturbed. The shift of the fcc atoms is done once every five time steps, according to

$$\Delta z = \frac{N_{\mathrm{newbcc}}}{N_{\mathrm{bcc,plane}}} \left(d_{\mathrm{b(110)}} - d_{\mathrm{f(111)}} \right), \tag{2.5}$$

where N_{newbcc} is the number of newly formed bcc atoms and $N_{\mathrm{bcc,plane}}$ is the number of atoms in a bcc plane. This procedure is consistent with having zero pressure acting on the system in the z-direction, implying that the system can freely expand or contract in this direction.

The fcc and bcc lattices have been created such that the numbers of atoms in an fcc(111) and a bcc(110) plane are equal. With the chosen number density of $0.103 \cdot 10^{30}$ atoms/m^3 (this is approximately 1.3 times the density of iron) for bcc and an initial interfacial area of 19.4x8.7 nm, the number of atoms per plane is 3312.

To avoid large heterogeneity of the distribution of the random sites over the entire system, the random sites are not distributed completely uniformly across the system. Instead a so called restrictedly random distribution is adopted as follows. First, the system is divided in small cubic cells with a side length of $1.4r_b$. Then, 10 random sites are inserted into each cell according to a uniform distribution.

The simulation program was run on a single processor PC (Pentium 4 Xeon at 2.8 GHz).

2.3.1 Possible bond energy values

When the bond energies are chosen a number of conditions must be fulfilled. To ensure that bcc is energetically more favourable than fcc and recognizing the coordination numbers of the bcc and fcc lattices, the most important requirement is

$$8u_{\text{bb}} < 12u_{\text{ff}}. \tag{2.6}$$

Not *every* jump from an fcc to a bcc site leads to an energy decrease: this depends on the surroundings of the sites considered. An atom at the interface can have different numbers of bcc and fcc neighbours. When an atom only has a few bcc neighbours and a large number of fcc neighbours, the atom should favour an fcc site over a bcc site (and vice versa with many bcc neighbours).

In the simulation of crystal growth it is common to demand that an incoming atom (from the vapour or liquid) can only successfully attach on kink sites where it has a certain minimum number of solid neighbour atoms [8, 11]. Here an analogous requirement is imposed: every atomic jump from fcc to bcc where an atom forms less than five bcc-bcc bonds should lead to an energy increase ($\Delta U_{\text{jump}} > 0$). With less than five bcc neighbour atoms the atom does not have enough 'bcc character' yet and the jump is unfavourable. If five or more bcc-bcc bonds are formed the jump is favourable and it is required that $\Delta U_{\text{jump}} < 0$. These conditions can be met by selecting proper values for u_{bb}, u_{ff} and u_{bf}. By looking at the number and type of the bonds that are broken and formed in a jump and in view of the requirement of inequality (2.6), ranges with valid values for u_{bb}, u_{ff} and u_{bf} can be indicated.

With the chosen interface orientation, there are for every short jump from an fcc to a bcc site where four bcc-bcc bonds are formed, seven fcc-fcc bonds broken (in case of a long jump a vacancy is involved and these numbers change). In case of five bcc-bcc bonds formed there are six broken fcc-fcc bonds (see appendix 2.A for an explanation of these numbers). The change in the number of mixed (fcc-bcc) bonds depends on the

arrangement around the jumping atom. The energy change ΔU_{4bb} for a jump where four bcc-bcc bonds are formed is given by

$$\Delta U_{4bb} = 4u_{bb} - 7u_{ff} + \Delta N_{mixed}u_{bf}, \tag{2.7}$$

where ΔN_{mixed} is the change in the number of mixed fcc-bcc bonds. As it is demanded that for *every* short jump from fcc to bcc where four bcc-bcc bonds are formed $\Delta U_{jump} > 0$, only the limiting case of the smallest possible value for ΔU_{4bb} because of ΔN_{mixed} must be considered. All bond energies are negative, which makes ΔU_{4bb} minimal when ΔN_{mixed} is maximal. For the given interface orientation the maximum value for ΔN_{mixed} is four, which leads to

$$\Delta U_{4bb,min} = 4u_{bb} - 7u_{ff} + 4u_{bf}, \tag{2.8}$$

for the minimum energy change for a jump where four bcc-bcc bonds are formed. By introducing $x = u_{bb}/u_{ff}$ and using equation (2.8), the requirement $\Delta U_{4bb,min} > 0$ can be written as

$$(4x - 7)u_{ff} > -4u_{bf}. \tag{2.9}$$

Because u_{bf} and u_{ff} are negative, it follows that $x < \frac{7}{4}$. Together with inequality (2.6) the range of valid values of x can be indicated by

$$\frac{3}{2} < x < \frac{7}{4}. \tag{2.10}$$

Hence, for a chosen value of u_{bb}, the range (2.10) prescribes the valid values for u_{ff}. Further rewriting inequality (2.9) as

$$0 > u_{bf} > \left(\frac{4x - 7}{-4}\right) u_{ff} \tag{2.11}$$

the valid values for u_{bf} can be expressed as a function of x and u_{ff}.

For most simulations a value of -1.04 eV was selected for u_{bb}. The energy of a (bulk) bcc atom is then approximately equal to that of an iron bcc atom. Recognizing requirement (2.10), for x a value of 1.7 was selected, which corresponds with $u_{ff} = -0.610$ eV. Next, in view of requirement (2.11), u_{bf} was set to -0.0262 eV. The maximal (i.e. least negative) bond energies with random atoms, u_{rb} and u_{rf}, were set to values two-thirds of u_{bf} (see table 2.1 for the complete set of values).

2.3.2 Nucleation

All simulations start with three planes of bcc atoms present, implying that 3-dimensional nucleation is not required. However, because the start configuration is a flat interface, new bcc phase must nucleate in the fcc plane at the interface. This implies 2-dimensional nucleation. The associated critical nucleus size has been determined by inserting more

Tab. 2.1: Bond-energy values in eV, u_{xy} is the energy of a bond between an atom on a site of type x and an atom on a site of type y (bcc, fcc or random). With the values given here, requirements (2.10) and (2.11) are fulfilled.

u_{bb}	u_{ff}	u_{bf}	u_{rb}	u_{rf}
-1.04	-0.610	-0.0262	-0.0174	-0.0174

Tab. 2.2: Bond-energy values in eV, u_{xy} is the energy of a bond between an atom on a site of type x and an atom on a site of type y (bcc, fcc or random). With these values inequality (2.10) is *not* fulfilled.

u_{bb}	u_{ff}	u_{bf}	u_{rb}	u_{rf}
-0.959	-0.295	-0.0131	-0.00872	-0.00872

or less circular bcc seeds of different sizes into this fcc plane and measuring the energy change as a function of nucleus size. Then simulations of lateral growth have been performed. The simulations have been executed applying the bond-energy values from table 2.1 and a temperature set to 1771 K.

2.3.3 Growth

The first atom in the fcc plane at the interface to jump to a bcc site only forms two bcc-bcc bonds (see appendix 2.A). Therefore, with the bond energies from table 2.1, $\Delta U_{jump} > 0$ is positive and relatively large. This means that the chance that such a jump is accepted is very low ($\approx 10^{-16}$). Even for the next adjacent fcc atom in the interface plane considered that jumps to bcc and that thereby forms three bcc-bcc bonds, the chance for acceptance is still low ($\approx 10^{-9}$). Altogether, this makes the chance of 2-dimensional nucleation very low and it would take years of calculation time to establish a substantial transformation. Therefore, simulations have been performed with the bond-energy values given in table 2.2. With these values, jumps from fcc to bcc where three bcc-bcc bonds are formed have a negative ΔU_{jump}, this violates inequality (2.10). To further examine the influence of the fcc-bcc energy difference, simulations have been performed for several (lower) values of u_{bb}, maintaining the other bond energy values as given in table 2.2.

For all growth simulations the temperature was set to 1012K and 10 vacancies where inserted randomly into the fcc plane at the interface. The vacancies were inserted because they have a positive influence on the growth rate as will become clear from the discussion of the results in section 2.5.
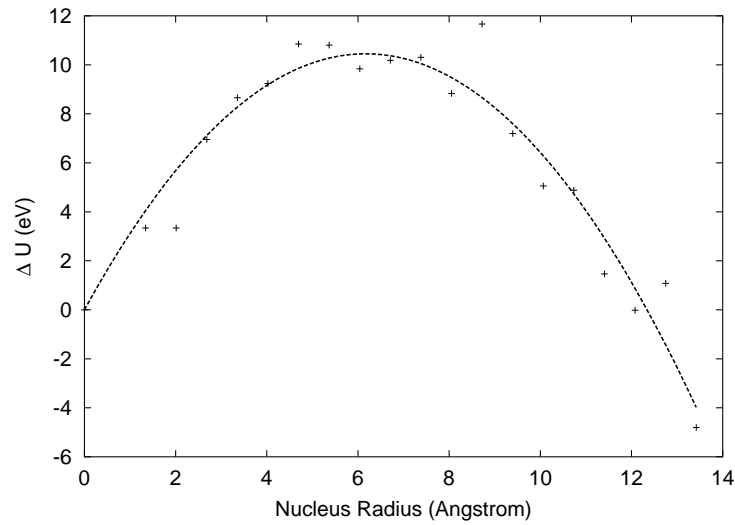
Fig. 2.2: Energy cost of building a bcc nucleus in an fcc plane at the bcc/fcc interface. Results of calculations with the bond energy values given in table 2.1. The dashed line represents the (least squares) fit of eq. (2.12) to the "measured" data points.

2.4 Results

2.4.1 Nucleation

The calculated energy cost of inserting a more or less circular bcc nucleus of height of one atomic plane in the fcc plane at the interface is shown in fig. 2.2 as a function of the nucleus radius. The size of the interface area parallel to the original interface does not change when a bcc nucleus is inserted in the fcc plane at the interface, also not upon its subsequent growth. Only the outer circumference of the nucleus contributes to a change in the total interface area. Therefore, the energy change for the creation of the circular nucleus, $\Delta U_{\mathrm{nucleus}}$, can be written as

$$\Delta U_{\mathrm{nucleus}} = \pi r^2 d \Delta U_V + 2\pi r d \gamma, \tag{2.12}$$

where r is the nucleus radius, ΔU_V is the fcc-bcc energy difference per unit volume, γ is the interface energy per unit area interface and d is the height of an atomic plane. A fit of eq. (2.12) to the calculated data is shown too in fig. 2.2 (dashed line). From the fit

$$\Delta U_V = (-7.4 \pm 0.4) \cdot 10^9 \ \mathrm{J/m^3}$$

and

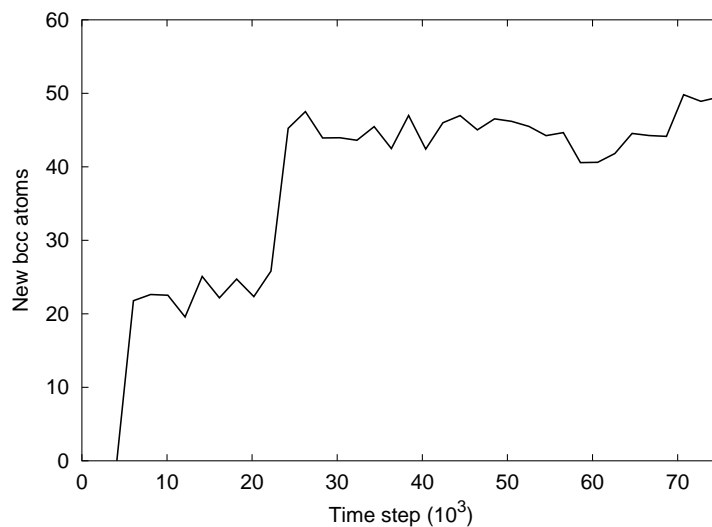$$\gamma = (4.5 \pm 0.2) \ \mathrm{J/m^2}$$

are obtained.

Fig. 2.3: Lateral growth of a bcc nucleus with a start radius of 10.7 Å($\hat{=}$73 bcc atoms). Result of simulation with the bond energies from table 2.1.

The simulations have demonstrated that nuclei with a radius smaller than the critical radius (≈ 6.1 Å) shrink and disappear and that nuclei larger than the critical size grow. It should be noted that this lateral growth is irregular (see fig. 2.3). When vacancies are added in the neighbourhood of the nucleus the same kind of irregular growth is observed but the growth rate then is much higher (cf. figs. 2.3 and 2.4). Growth is confined to the plane in which the nucleus was created and no other nuclei form spontaneously in the time of simulation.

2.4.2 Growth

Adopting the bond energies given in table 2.2, the entire system quickly transforms continuously from fcc to bcc, as shown in fig. 2.5. The insertion of a 2-dimensional nucleus is not required; the bcc phase grows spontaneously. The transformation does not result in a perfect bcc crystal. A single bcc plane after transformation is shown in fig. 2.6. The plane contains a few defects in the form of atoms placed on random sites, sometimes accompanied by one or two atoms on fcc sites.

When the fcc-bcc energy difference is lowered by giving u_{bb} less negative values, the transformation curve changes significantly. For three different values of u_{bb} a part of the transformation curve is shown in fig. 2.7. At $u_{\text{bb}} = -0.70$ eV the growth mode is no longer continuous, but is of plane-by-plane nature. In the continuous growth mode the transformation takes place in several planes simultenously (fig. 2.8). In the plane-by-plane growth mode, a single plane is completely transformed before bcc nucleates in the next fcc plane.
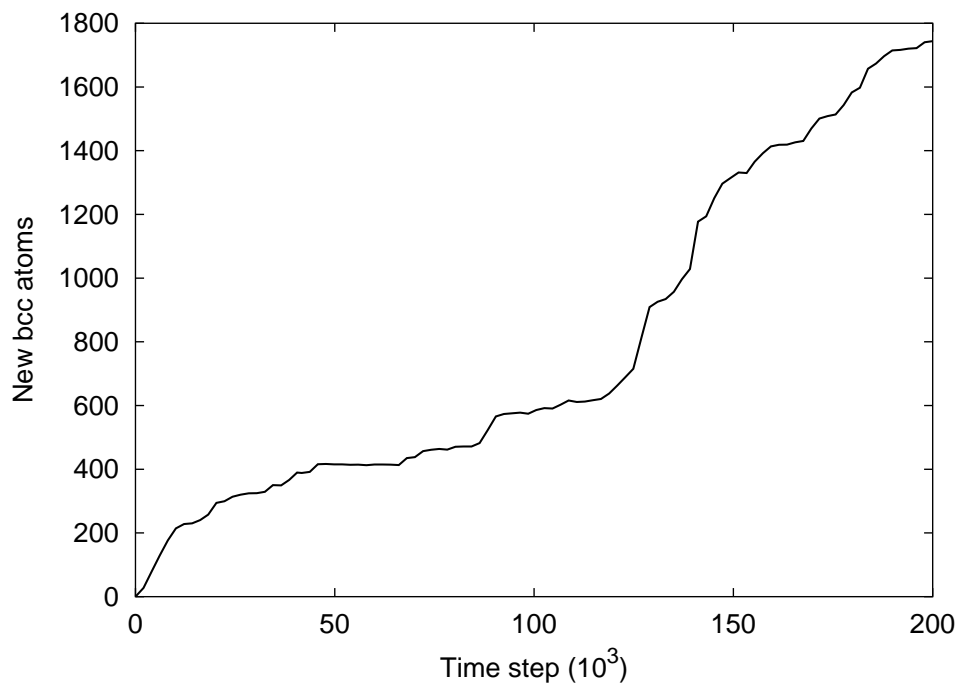
Fig. 2.4: Lateral growth of a bcc nucleus with a start radius of 10.7 Å($\hat{=}$73 bcc atoms), with seven vacancies in the vicinity of the nucleus. Result of simulation with the bond energies from table 2.1.
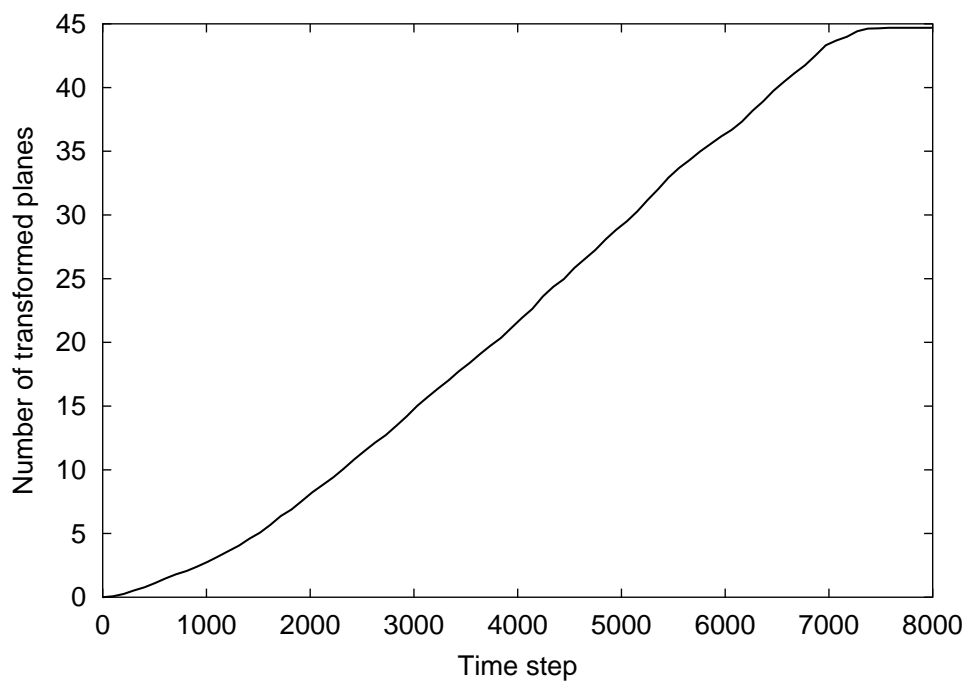
Fig. 2.5: Number of transformed planes as a function of time; result of simulation using the bond-energies from table 2.2.
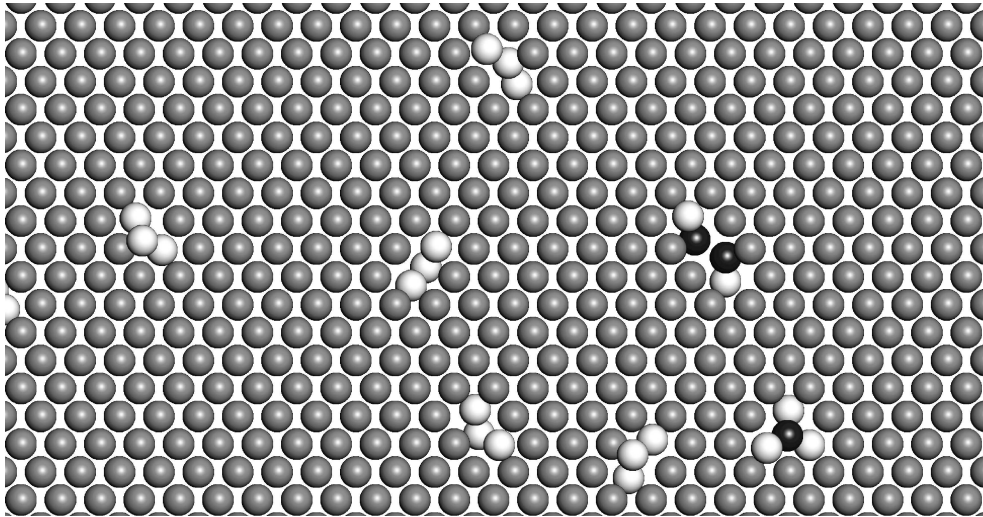
Fig. 2.6: A close-up of a single bcc plane, parallel to the x, y axes, after transformation (simulation with the bond-energies from table 2.2). The black atoms are residual fcc atoms, the grey atoms are bcc atoms and the atoms on random sites are white. Atoms that seem to overlap are placed above each other (i.e. have different z coordinates).
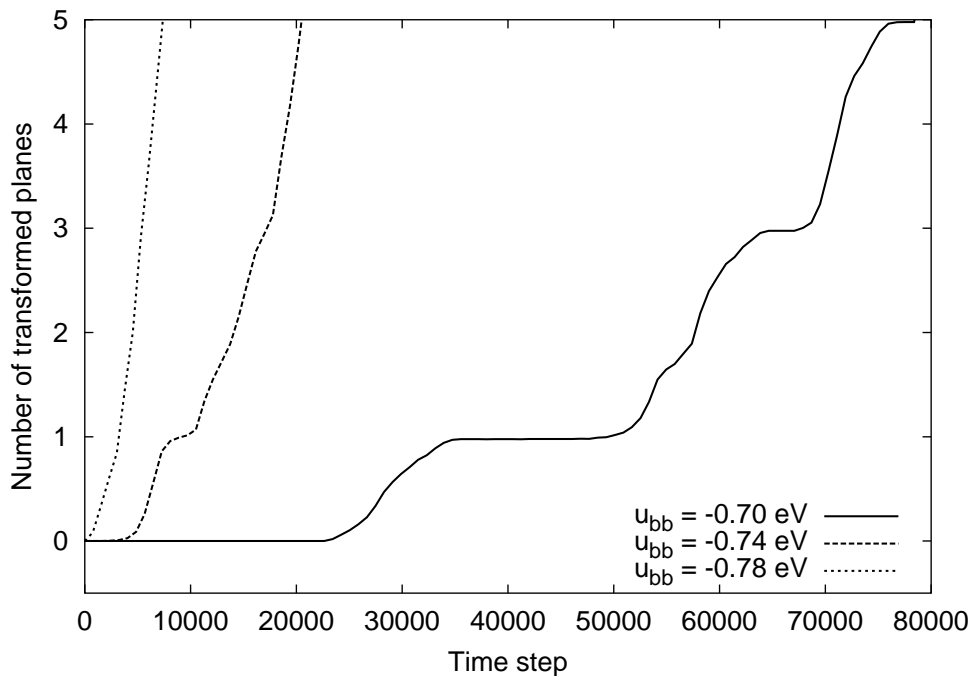
Fig. 2.7: Number of transformed planes as a function of time for three values of u_{bb} (the other bond energies are equal to the values given in table 2.2).

Fig. 2.8: A continuous fcc → bcc transformation in progress. The extra space between the planes is not real, it has been inserted to provide a clearer view. Fcc atoms are black, bcc grey and random atoms are white. The arrows indicate spots where the bcc phase is already growing in plane B before plane A has been transformed completely. Simulation with bond energies from table 2.2.

2.5 Discussion

2.5.1 Nucleation

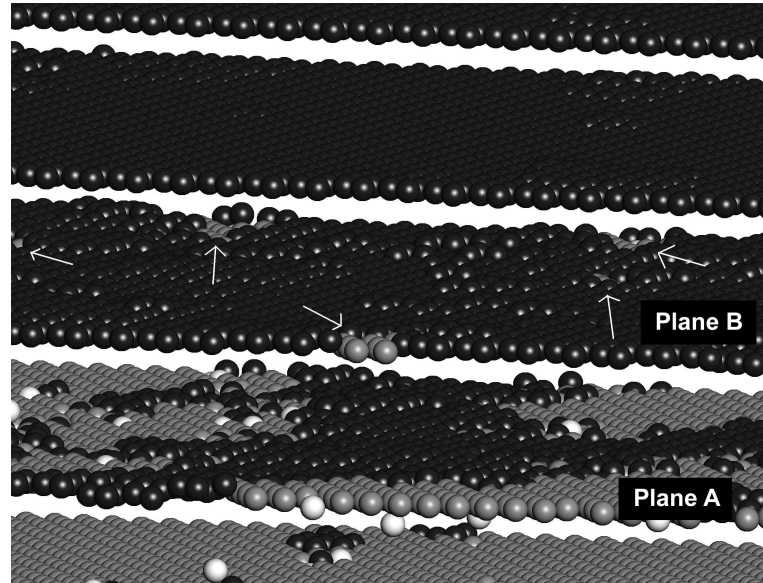The values that have been found for ΔU_V and γ can be directly related to the bond energy values (from table 2.1). Upon transformation the gain in bulk energy per unit volume of the nucleus considered is

$$\Delta U_V = N_{\text{transf}} \Delta U_{\text{bcc,fcc}}, \tag{2.13}$$

with N_{transf} as the number of transformed atoms per unit volume of the nucleus and $\Delta U_{\text{bcc,fcc}}$ the (bulk) fcc-bcc energy difference per atom ($= \frac{1}{2}(8u_{\text{bb}} - 12u_{\text{ff}})$). From the values chosen for the bcc density and the bond energies (cf. section 2.3 and table 2.1) it thus follows:

$$\Delta U_V = -8.1 \cdot 10^9 \text{ J/m}^3.$$

This calculated, theoretical value for ΔU_V agrees fairly well with the value obtained from the fit of eq. (2.12) to the simulated data: $(-7.4 \pm 0.4) \cdot 10^9$ J/m^3. In the theoretical calculation a perfect circular disc is taken as the form of the nucleus. However, the real form of a nucleus can be different because it is made of a discrete number of atoms, which causes the difference between the measured (simulated) and theoretical values of the critical size.

For a theoretical prediction for the interface energy, the number of interface atoms per unit interface area, N_{iatoms}, must be known. To this end the numbers of fcc and bcc atoms adjacent to the nucleus-matrix interface have been counted (again only the interface area perpendicular to the outer circumference of the disc has to be considered cf. section 2.4.1). For different nucleus sizes N_{iatoms} is not constant, but shows small deviations from the average value (in the range of nucleus sizes considered here) which is $3.45 \cdot 10^{19}$ atoms/m^2. N_{iatoms} consists out of two parts: fractions due to fcc atoms, f_{fcc}, and due to bcc atoms, f_{bcc}. These fractions are not constant but depend on the nucleus size. Therefore, average values will be used for f_{fcc} and f_{bcc}. Atoms at the disc circumference have, in comparison to the other atoms in the plane of the disc, depending on the local structure, one or two kin-like bonds replaced by mixed (fcc-bcc) bonds. Thus, as a first order approximation, it is assumed that for every atom at the disc circumference, upon becoming a disc circumference atom, one kin-like bond is replaced by a mixed bond, and γ can then be assessed as

$$\gamma = \left(\overline{f}_{\text{fcc}} \left(u_{\text{bf}} - u_{\text{ff}} \right) + \overline{f}_{\text{bcc}} \left(u_{\text{bf}} - u_{\text{bb}} \right) \right) \overline{N}_{\text{iatoms}}, \qquad (2.14)$$

With $\overline{f}_{\text{fcc}} = 0.58$, $\overline{f}_{\text{bcc}} = 0.42$, $\overline{N}_{\text{iatoms}} = 3.45 \cdot 10^{19}$ atoms/m^2 and the bond energies from table 2.1, it then follows

$$\gamma = 4.2 \text{ J/m}^2.$$

This value is close to the value obtained from the simulations ((4.5 ± 0.2) J/m^2).

The lateral growth of a 2-dimensional nucleus is not smooth and continuous (see figs. 2.3 and 2.4). This reflects that an increase in nucleus size beyond the critical size does not always lead to an energy gain, as demonstrated by the results shown in fig. 2.2. Because of local variations of the interface structure, the interface energy is not constant. Apparently, for certain nucleus sizes and shapes, the overall interface energy is that high that further growth again costs energy rather then delivers energy, although the nucleus size is already larger than the critical size. This effect can be ascribed to the limited number of different positions the atoms can take: the atoms can occupy random sites, but it is not guaranteed that these random sites are located at energetically favourable positions. Therefore, the interface is unlikely to be fully relaxed. This explanation is supported by the simulation with the vacancies added in the neighbourhood of the nucleus (cf. fig. 2.4). The vacancies are dissolved quickly in the interface, thereby providing extra space at the interface and consequently more relaxation possibilities for the interface atoms. This explains the observed higher growth rate as compared to the simulation without vacancies (cf. figs. 2.3 and 2.4).

2.5.2 Growth

Spontaneous growth of the bcc phase, within practical finite times of transformation, occurs on adopting the bond energy values from table 2.2, as shown in fig. 2.5. It is observed that during transformation of the first full five planes, the transformation rate increases gradually to a value that remains practically constant for the remaining part of the transformation. In the last part of the transformation the rate drops again because the total interface area starts to decrease as there is no more material to transform. Defects can occur in the transformed planes (fig. 2.6), in particular for the first few transformed planes. Therefore these planes contain a few more atoms than the normal total of 3312 (cf. section 2.3). This corresponds with an increase of the number of vacancies in the untransformed part of the system. The presence of vacancies increases the growth rate (cf. discussion in section 2.5.1), as is observed (fig. 2.5).

Depending on the value of u_{bb} the growth mode is either continuous (see fig. 2.7, $u_{bb} = -0.78$ eV) or plane-by-plane (see fig. 2.7, for $u_{bb} = -0.70$ eV). In case of plane-by-plane growth it takes a certain time before a new bcc nucleus is formed in the next fcc plane adjacent to the transformation front. After nucleation, the fcc plane transformes relatively fast. In case of continuous growth, no such nucleation phase can be distinguished: the transformation front is a rough interface (see fig. 2.8). Note that even in this case the product, fcc phase is contiguous. At an intermediate value for u_{bb} (see fig. 2.7, for $u_{bb} = -0.74$ eV) the growth mode is mixed: for transformation of the first and second fcc planes a clear nucleation phase can be discerned, but then growth becomes continuous (the steps in the transformation curve disappear). Although not clearly shown in fig. 2.7, the same effects happens for $u_{bb} = -0.70$ eV after longer simulation times. Equations similar to eq. (2.8) can be written for the energy changes ΔU_{2bb} and ΔU_{3bb} for jumps from an fcc site to bcc sites with two and three bcc neighbours, respectively

$$\Delta U_{2bb} = 2u_{bb} - 9u_{ff} + 8u_{bf} \tag{2.15}$$

and

$$\Delta U_{3bb} = 3u_{bb} - 8u_{ff} + 4u_{bf}. \tag{2.16}$$

Using eqs. (2.15) and (2.16), the jump probabilities p_2 and p_3 for jumps to sites with two and three bcc neighbours, respectively, can be calculated by applying eq. (2.1) as a function of u_{bb}; the results are shown in fig. 2.9. An fcc interface atom surrounded by fcc atoms only in its own (111) plane and that jumps to a bcc position makes a p_2-jump (see also Appendix 2.A). In the range -0.8 to -0.7 eV for u_{bb}, p_2 is very low (see fig. 2.9) and hence only few of these jumps will be accepted. An accepted p_2-jump is the first step of the formation of a new bcc nucleus. If p_3 is also very low then this one-atom-nucleus
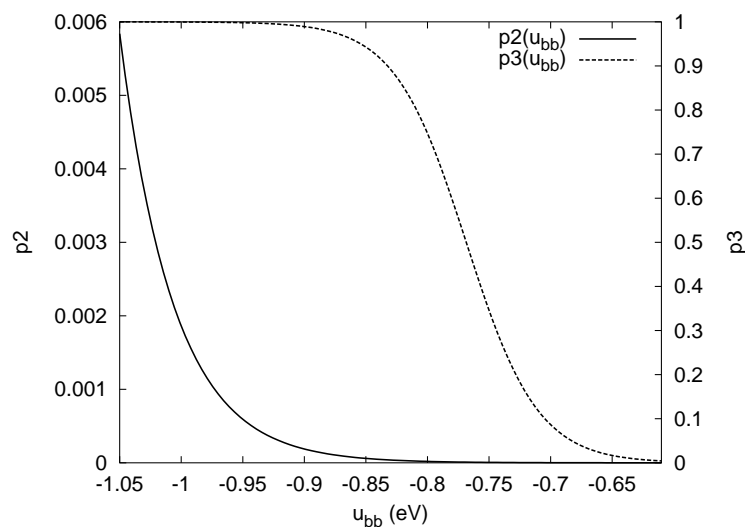
Fig. 2.9: The jump probabilities p_2 and p_3 as a function of u_{bb} (cf. eq. (2.1) and eqs. (2.15) and (2.16)), with other bond energies as indicated in table 2.2 and at $T = 1012$ K.

will quickly dissolve because no stabilizing extra bcc atoms will attach to it. The value for p_3 increases rapidly in the u_{bb} range from -0.8 to -0.7 eV and thus at $u_{bb} =$-0.70 eV the formation of a new bcc nucleus is much more difficult than at $u_{bb} =$-0.78 eV (cf. fig. 2.7).

The change of growth mode upon continued transformation and the associated roughening of the transformation interface are consequences of the increase in the number of vacancies in the untransformed planes (see above discussion): the presence of vacancies makes nucleation easier, because energetically more favourable atom positions can be occupied (see also section 2.5.1).

The surface roughening transition has been observed in crystal growth simulations with temperature as variable instead of a bond energy [7, 9, 11]. Obviously, according to eq. (2.1), a change in p_2 and p_3 can be induced by a temperature change as well as by a change in u_{bb}. Hence a similar growth mode variation can be caused by both temperature and bond energy changes.

2.5.3 Final remarks

The ledge mechanism has been suggested as a transformation mechanism for the massive transformation [2]. With ledges there is no need for 2-dimensional nucleation as long as some mechanism operates that makes the formation or the preservation of ledges possible. The simulations with the laterally growing nucleus (figs. 2.3 and 2.4) demonstrate that ledge-wise growth is a possible mechanism. Thus plane-by-plane growth can be con-

ceived as a form of ledge-wise growth, in association with "spontaneous" formation of new ledges.

With the atomic interaction model used here (see section 2.2.1) the energy of a bond between two atoms does not depend on the distance between those two atoms. As future work it is planned to use a more realistic atomic interaction model such as the Embedded Atom Method potential [18, 19]. This potential is known to work well for metals, even for the description of defect structures. With the use of such a potential a molecular dynamics approach can then be used to examine separately the activation energy for different (individual) jumps, an aspect that has thus far not been taken into account.

2.6 Conclusion

For the first time a massive transformation has been simulated departing from a multi-lattice basis in a kinetic Monte Carlo approach. An essential ingredient of the model is the incorporation of "random sites", not belonging to the product or parent lattices. In this way relevant intermediate atomic positions are identified and irregularities in the atomic structure of transformation interfaces can be accounted for.

Transformation mechanism and kinetics can be simulated for the massive fcc to bcc transformation adopting a bond counting model for the calculation of atomic jump probabilities. Starting with a completely flat initial interface, this model allows direct assessment of the critical nucleus size and interface energy values in terms of the bond energies.

Two different kinds of transformation mechanisms can be identified: plane-by-plane growth in association with 2-dimensional nucleation, resembling the ledge mechanism, and continuous growth in association with the occurrence of a rough transformation interface. Which mechanism is dominant, depends on the values of the bond energies and the temperature. Increasing the fcc-bcc energy difference (i.e. making the energy difference more negative), causes the growth mode to change from plane-by-plane to continuous.

The transformation does not lead to a perfect bcc crystal. Point defects are formed especially in the initial stage of the transformation. This corresponds with an increase of the vacancy concentration in the untransformed part of the system close to the interface. These vacancies influence the interface energy and lead to an increase of the transformation rate.

2.A Calculation of the number of broken and formed bonds

In a bcc (110) plane an atom has four (nearest) neighbours. In the bcc crystal in the planes above and below this plane the atom has another two neighbours, leading to a total of eight neighbours. In an fcc (111) plane an atom has six neighbours and three in the fcc

planes above and below, leading to a total of 12 neighbours. The planes near the interface have been labeled A, B, C and D. They are stacked in alphabetical order, A and B are bcc (110) planes and C and D are fcc (111) planes. The interface lies between plane B and C.

A bcc atom in plane B has four bcc neighbours in that plane and two bcc neighbours in plane A. The number of possible mixed fcc-bcc bonds with atoms in plane C turns out to be one, two or three depending on the local situation. For an fcc atom in plane C: six fcc-fcc bonds occur in plane C, three fcc-fcc bonds with atoms in plane D and one, two or three mixed fcc-bcc bonds with bcc plane B. The change in the number of bonds for a jump can be determined from these considerations. For example, when an fcc atom in plane C moves to a bcc site two new bcc-bcc bonds are formed (with atoms in plane B) and nine fcc-fcc bonds are broken (six with atoms in fcc plane C and three with atoms in fcc plane D). These broken fcc-fcc bonds are replaced with bcc-fcc bonds, the exact number depends on the local arrangement.

Different example (cf. section 2.3.1). Two bcc atoms in plane C, surrounded by fcc. If a common fcc neighbour (in plane C) also becomes bcc then there are four new bcc-bcc bonds formed (two with plane B and two with plane C) and seven fcc-fcc bonds broken (four with plane C and three with plane D). Mixed bonds still depend on the local arrangement.

3. An atomistic analysis of the interface mobility in a massive transformation

C. Bos, F. Sommer and E.J. Mittemeijer

Abstract

A new multi-lattice kinetic Monte Carlo method has been used for an atomistic study on the interpretation of the interface mobility parameter for a massive face-centred cubic (fcc) to body-centred cubic (bcc) transformation in a single element system. For lateral growth of bcc in a system with an fcc(111)//bcc(110) and fcc[11$\overline{2}$]//bcc[00$\overline{1}$] interface orientation the overall activation energy for the interface mobility parameter is governed by energetically unfavourable atomic jumps. The atoms on the fcc lattice often cannot jump directly to bcc lattice sites because neighbouring atoms block the empty bcc sites. By single unfavourable jumps and by groups of unfavourable jumps a path from fcc to bcc is created. The necessity of these unfavourable jumps leads to an overall activation energy considerably larger than the activation energy barrier for a single atomic jump.

3.1 Introduction

A typical example of interface controlled phase transformations is the massive transformation. Because the massive transformation is composition invariant, the transformation rate is determined by processes at the interface and not by long range diffusion of any of the alloying elements. In a previous paper [20] a multi-lattice kinetic Monte Carlo (kMC) method was presented for the first time for the atomistic simulation of massive transformations. In that work the focus was on the influence of the driving force on the growth mode. Now, this method has been extended to study the so-called interface mobility parameter for the face-centred cubic (fcc) to body-centred cubic (bcc) transformation in a single element system. With the (modified) method presented here, time book-keeping is introduced to enable the determination of the transformation rate. Analysis of the transformation rate as a function of temperature is required to determine the interface mobility parameter.

The interface mobility relates the interface velocity with the (occurring) driving force for the transformation. The interface mobility, M, is generally written as [1]

$$M = M_0 \exp\left(-\frac{\Delta G^a}{k_B T}\right), \tag{3.1}$$

with M_0 as the pre-exponential factor, ΔG^a as the activation energy, k_B as the Boltzmann constant and T as the temperature. Many factors influence the activation energy: e.g. interface structure, impurities. This leads to various expectation values for the activation energy. Generally, the experimental values found for ΔG^a differ significantly from the expected values [1]. To achieve a better understanding of the atomic processes that determine ΔG^a in massive transformations, the multi-lattice kMC method is used here for simulation of the interface movement in a γ(fcc)/α(bcc) transformation.

This paper describes the modifications applied to the original multi-lattice kMC method (section 3.2) needed to extract interface dynamics from the simulations. The fcc to bcc transformation in a single element system is simulated, with an initial interface orientation of fcc(111)//bcc(110) and fcc[11$\overline{2}$][1]// bcc[00$\overline{1}$]. The atomic interactions are described by a nearest neighbour bond counting model (section 3.2.1). With this model it is possible to choose the bond energies in such a way that either continuous or plane-by-plane growth is obtained, as described in Ref. [20].

Eq. (3.1) is usually applied to cases of continuous growth [1]. In the simulations performed in this study the bond energies were set to obtain the plane-by-plane growth mode (cf. section 3.3). When the transformation rate is determined for lateral growth in a single plane only (i.e. parallel to the original interface), this lateral growth can be considered to be continuous growth, although the overall growth mode is plane-by-plane. The choice to study growth in a single plane was made because the simulation of lateral (planar) growth requires much less computation time than the simulation of a continuous transformation of the entire fcc volume.

3.2 Simulation method

The multi-lattice kMC method as described in [20] allows the simulation of a phase transformation from one crystal structure to another, by incorporating both crystal structures as possible sites for atoms. To allow the atoms at and near the moving interface to take intermediate positions between the lattice sites, a collection of randomly placed sites is also included. These intermediate positions allow for irregularities in the atomic structure of transformation interfaces.

---

[1] wrongly indicated as fcc [11$\overline{1}$] in Ref. [20]

In the original method the chance for a jump of an atom from one site to another site was based only on the energy change ΔU of the system caused by the jump. This can never lead to fully correct dynamics [21], because only the initial state and end state of a jump are taken into account. A classically exact description of reaction kinetics is obtained if the (reaction) rate constants, k, of all possible processes in the system are taken into account (in the phase transformation simulations the possible processes are the atomic jumps) [22].

Each rate constant should be determined from the potential energy change along the entire reaction path from the begin to the end state. Preferably, the rate constants are calculated from transition state theory, but even with the simple transition state theory (STST) approximation already good results can be obtained [22].

If at a given time in the simulation the number of possible jumps in the whole system is N_{jump}, the next occurring jump is selected by first calculating the total sum of the rate constants k_i of all possible jumps for the actual configuration (i.e. the present set of occupied sites):

$$K_{\text{sum}} = \sum_{i=1}^{N_{\text{jump}}} k_i. \tag{3.2}$$

and thus $1/K_{\text{sum}}$ represents the average number of jumps per unit of time. Then a random number R_1 between zero and K_{sum} is drawn and the actually occurring jump is identified as the first jump a for which

$$\sum_{i=1}^{a} k_i \geq R_1. \tag{3.3}$$

As the probability density of times Δt between successive jumps has an exponential distribution, the time spent before making the next jump, can be calculated with [23]

$$\Delta t = -\left(\frac{1}{K_{\text{sum}}}\right) \ln(R_2), \tag{3.4}$$

where R_2 is a random number between zero and one.

On this basis the transformation rate r_{tf} has been derived from the simulations (in atoms/sec). The complete simulation algorithm is given in Appendix 3.A.

3.2.1   Atomic interaction model

For the calculation of the rate constants of the jumps an atomic interaction model is required. The same nearest neighbour bond counting model as in [20] is used. In this model a bond energy, u, is ascribed to all possible combinations of atom pairs (bcc–bcc, fcc–fcc, fcc–bcc), independent of the distance between a pair of two atoms. The atoms at random
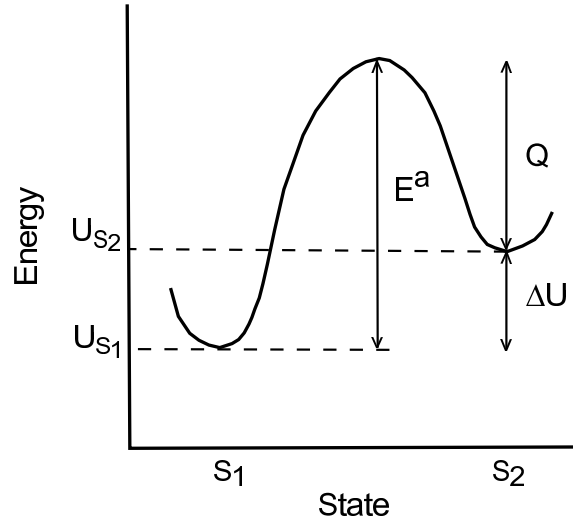
Fig. 3.1: A possible variation in energy along the jump path from state S_1 to S_2.

sites behave as the lattice site most nearest to them (see table 3.1 in section 3.3 for values of the bond energies).

Consider a jump taking the system from state S_1 to state S_2. The energy difference for this jump is

$$\Delta U = U_{S_2} - U_{S_1}. \tag{3.5}$$

Now assume that the energy of the system along the path of this jump varies as shown in fig. 3.1. According to STST (see for example Ref. [24]) the rate constant is given by

$$k = \nu_0 \exp\left(-\frac{E^a}{k_B T}\right), \tag{3.6}$$

with ν_0 a pre-exponential frequency factor and

$$E^a = Q + \Delta U = Q + U_{S_2} - U_{S_1}. \tag{3.7}$$

Obviously, for the jump back from S_2 to S_1 it holds

$$E^a = Q. \tag{3.8}$$

Hence, in general the rate constant can be written as

$$k = \begin{cases} \nu_0 \exp\left(-\frac{Q+\Delta U}{k_B T}\right) & \text{if } (\Delta U > 0) \\ \nu_0 \exp\left(-\frac{Q}{k_B T}\right) & \text{otherwise} \end{cases}. \tag{3.9}$$

The energy barrier that the atoms have to overcome to go from one site to another, actually depends through the atomic interaction energies on the (local) surroundings of the jumping atom. In this work Q is a freely adjustable simulation parameter. By taking Q

Tab. 3.1: Bond-energy values in eV, u_{xy} is the energy of a bond between an atom on a site of type x and an atom on a site of type y (bcc, fcc or random). With these value a bcc atom has the same binding energy as in iron bcc.

u_{bb}	u_{ff}	u_{bf}	u_{rb}	u_{rf}
-1.04	-0.663	-0.121	-0.0872	-0.0872

equal for every jump (and doing this also for ν_0) it is possible to study the effect of Q on the transformation rate, while keeping the driving force for the transformation constant. The driving force is determined by the values chosen for the bond energies u.

3.3   Simulation settings

The simulation program contains a number of parameters that prevent the atoms from coming unrealistically close to each other. Together these parameters determine whether an empty neighbour site qualifies as a valid target site for an atom to jump to. These parameters are: the maximum distance for a long jump $r_{maxjump}$ and for a short jump r_{sj}[2], the hard sphere core diameter d_{hs} and the minimum vacancy hole radius, r_{vh} (see fig. 1 in Ref [20]). The minimum vacancy hole radius determines the minimum distance to the nearest occupied neighbour site a (empty) site must have to be a valid target site for a long jump. The values used here for these parameters are: $r_{maxjump} = 1.025r_f$, $r_{sj} = 0.35r_b$, $d_{hs} = 0.68r_b$ and $r_{vh} = 0.85r_b$ unless noted otherwise (r_x is the xcc nearest neighbour distance).

The selected bond energies for the bond counting interaction model are given in table 3.1. These particular values result in a plane-by-plane growth mode (see section 3.1 and [20]) with an effectively impossible nucleation of bcc in an adjacent fcc plane. The λ-parameter that scales the energy of the atoms on random sites (see Ref [20]) was set to 0.8. Because (2-dimensional) nucleation is effectively impossible, the start configuration must contain a bcc seed as shown in plane B in fig. 3.2. The interface orientation is fcc(111)//bcc(110) and fcc[11$\bar{2}$]//bcc[00$\bar{1}$] and the interface lies parallel to the xy-plane. The fcc and bcc crystals were created with equal planar density for the planes parallel to the interface (with bcc volume density of $0.103 \cdot 10^{30}$ atoms/m^3). By choosing equal planar density no vacancies will be created or destroyed by the transformation. This facilitates the transformation. Furthermore, for the analysis of the data obtained from the simulations a constant number of vacancies is important as the vacancy content has a strong influence on the interface mobility (see section 3.4).

---

[2] The division of jumps in short and long jumps is purely artificial and has only been made for computational efficiency reasons [20].
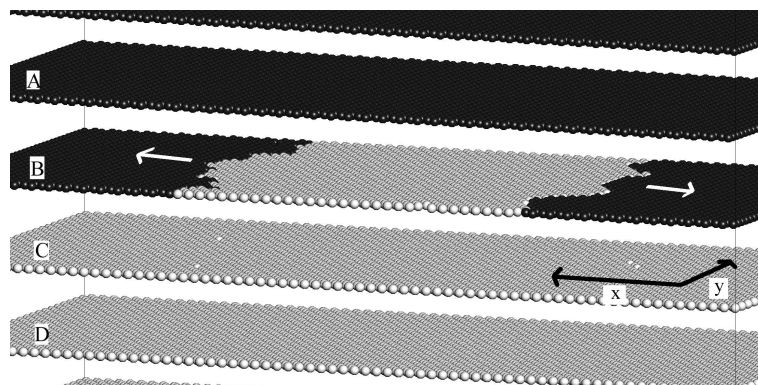
Fig. 3.2: The start configuration for the simulations, containing 15 vacancies. The extra space between the planes is not real, it has been inserted to provide a clearer view. Fcc atoms are black, bcc atoms are white. The white arrows indicate the bcc growth direction.

The initial interface area is 19.4x8.7 nm, the number of atoms per plane is 3312. If vacancies were inserted in the system then they were created in plane B shown in fig. 3.2 by removing fcc atoms. Periodic boundaries were used in both the x direction and the y direction. This leads to lateral growth of the bcc phase in the x direction, as indicated by the white arrows in fig. 3.2.

The random sites are distributed according to a restrictedly random distribution. First, the system is divided into small cubic cells with a side length of $1.4r_b$. Then, 10 random sites are inserted into each cell according to a uniform distribution.

In all simulations a value of 10^{13} (sec^{-1}) was used for ν_0.

The driving force for the transformation is taken to be temperature independent. Because the positions of the lattice sites are fixed, temperature also has no influence on the geometry of the interface through density changes. The only influence temperature has is on the transformation rate. With the chosen bond energies the temperature range that can be used for the simulation of lateral growth is very large, up to $10 \cdot 10^3$ K, because the chance for nucleation of bcc in the fcc plane adjacent to the interface (plane A in fig. 3.2) is so small. Because of computational efficiency reasons (see Appendix 3.B), most simulations have been performed at higher temperatures.

The simulation program was run on a single processor PC (Pentium 4 Xeon at 2.8 GHz).

3.4   Results

The transformation rate[3], r_{tf}, as a function of temperature with $Q = 1.744$ eV in a system

---

[3] An estimate for the transformation rate is determined by measuring the time between 20% and 80% completion of the transformation of the remaining fcc atoms of plane B in fig. 3.2 into bcc atoms.
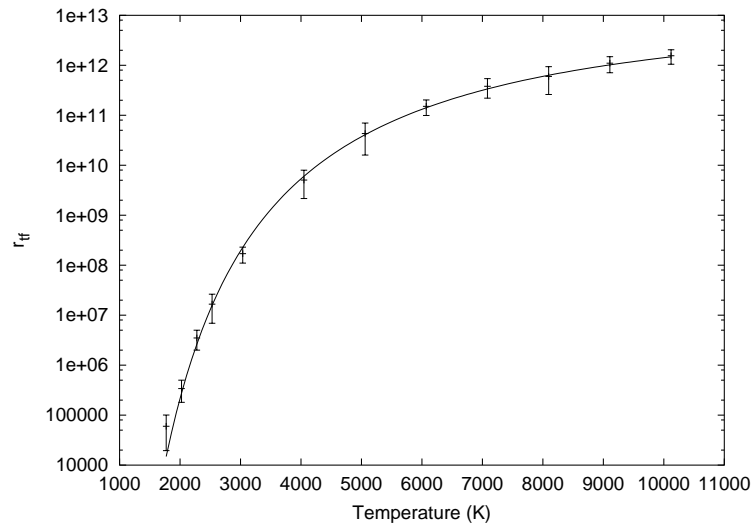
Fig. 3.3: The transformation rate as a function of temperature for a system containing 15 vacancies and with $Q = 1.744$ eV. All data points are an average from a minimum of 10 repetitions of the transformation simulation. The solid line is a fit of eq. (3.10).

containing 15 vacancies (created by removing fcc atoms from plane B in fig. 3.2) is shown in fig. 3.3. The transformation rate is given by [1]

$$r_{\text{tf}}(T) = C \exp\left(-\frac{\Delta G^a}{kT}\right)\left(1 - \exp\left(-\frac{\Delta U_{bcc,fcc}}{kT}\right)\right), \qquad (3.10)$$

with C a pre-exponential constant and $\Delta U_{bcc,fcc}$ the bcc–fcc energy difference (=0.174 eV). To obtain the overall activation energy for the mobility, ΔG^a, eq. (3.10) has been fitted to the simulation data[4]. Resulting values for ΔG^a and C are:

$$\Delta G^a = 3.65 \pm 0.05 \text{ eV}$$

and

$$C = (5.35 \pm 0.02) \cdot 10^{14} \text{ atoms/sec.}$$

Evidently, ΔG^a is about twice as large as the energy barrier for a single jump, Q (=1.744 eV; see above). The overall mobility activation energy, ΔG^a, has also been determined for three more Q-values. It followed that the difference between Q and ΔG^a is constant: ΔG^a can be written as

$$\Delta G^a = Q + E_{\text{off}}, \qquad (3.11)$$

where E_{off} is called here the activation energy offset.

---

[4] This implies, as usual, that only the internal energy part of the activation energy is determined; the entropy contribution is included in the pre-exponential factor

Tab. 3.2: The activation energy offset E_{off} for various values for the minimum vacancy hole radius r_{vh} and the number of vacancies in the system (σ is the standard error in E_{off} as obtained from the fit procedure [25] and r_{b} is the bcc nearest neighbour distance).

#vac	$r_{\mathrm{vh}}/r_{\mathrm{b}}$	E_{off}	σ
-	-	eV	eV
15	0.85	1.91	0.05
15	0.80	1.13	0.06
15	0.75	0.89	0.05
15	0.70	0.85	0.05
20	0.85	1.56	0.05
25	0.85	1.32	0.06

A single jump can have an activation energy (E^a) larger than the energy barrier (Q) if $\Delta U > 0$ (eq. (3.9)). Thus, because $E_{\mathrm{off}} > 0$, it would follow that r_{tf} is controlled by jumps with a positive ΔU. Detailed analysis of the jump possibilities of the fcc (parent) atoms at the interface has shown that at any given moment many fcc atoms cannot jump to a bcc (product) site, because all surrounding empty bcc sites are blocked by other atoms. Very often one or more unfavourable jumps (i.e. $\Delta U > 0$ (cf. fig. 3.1), for example to random sites) of the surrounding atoms (or the atom itself) are needed to create a 'path' to a bcc site. By decreasing r_{vh} an empty site is more likely to qualify as a valid target site. With more vacancies in the system, empty bcc sites are less likely to be blocked by other atoms. Therefore, by decreasing r_{vh} and/or increasing the number of vacancies, the transformation should proceed faster, which is confirmed by the correspondingly lower values found for E_{off} as shown in table 3.2. Because a smaller r_{vh} makes it easier to find a path from fcc to bcc for any position along the entire interface, whereas the transformation promoting influence of vacancies is locally confined, the effect of a change of r_{vh} is stronger than the effect of a change of the number of vacancies (cf. table 3.2).

In a simulation many atoms at the interface continuously jump back and forth. Such forward-and-back jumps do not contribute to the transformation. By removing these forward-and-back jump pairs from the jump history, only those jumps are selected that actually establish the transformation. In this way a histogram showing the number of effective jumps as a function of ΔU can be made: see fig. 3.4. E_{off} was 1.56 eV (table 3.2) for the settings chosen for the simulations giving the data shown in fig. 3.4. The histogram shows some intensity around 1.6 eV which is almost equal to E_{off}. This might suggest that the jumps with $\Delta U = 1.56$ eV are for some reason critical and therefore determine E_{off}. If rate determination by single unfavourable jumps would occur, ΔG^a (eq. (3.11)) can be identified with E^a (eq. (3.7)) and $\Delta U = E_{\mathrm{off}}$. In the simulations it is possible to selectively exclude all jumps within a certain ΔU-range. The results of such simulations, see table 3.3, show that if all jumps with ΔU-values near E_{off} (=1.56 eV)
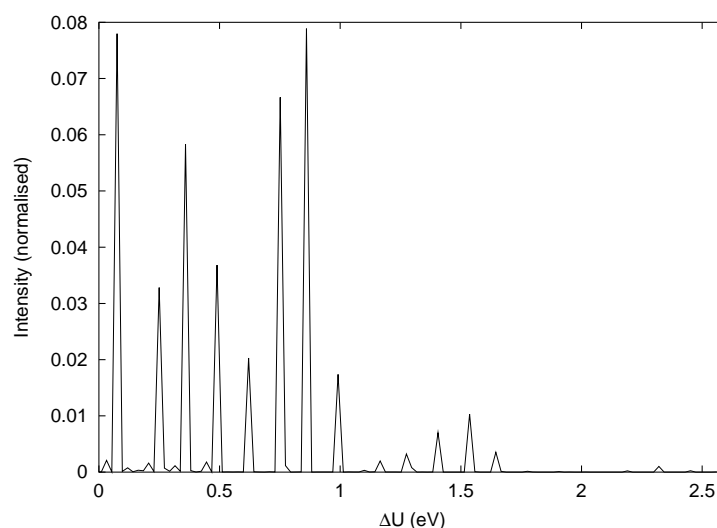
Fig. 3.4: A normalized histogram of ΔU-values of all effective jumps. The histogram is an average over 10 simulations with $Q = 1.744$ eV, $r_{\mathrm{vh}} = 0.85 r_{\mathrm{b}}$, $T = 6072$ K and 20 vacancies. Only the effective jumps with $\Delta U > 0$ are shown.

Tab. 3.3: The offset in the effective activation energy (E_{off}), for different ranges of excluded ΔU-values. Results from simulations with $Q = 1.744$ eV, 20 vacancies and $r_{\mathrm{vh}} = 0.85 r_{\mathrm{b}}$. σ is the standard error as obtained from the fit procedure [25].

Excl. ΔU (eV)	E_{off} (eV)	$\sigma (eV)$
-	1.56	0.05
1.13-1.31	1.95	0.12
1.44-1.70	1.65	0.11
1.74-1.92	1.56	0.11

are excluded the new activation energy falls within the excluded range. The activation energy offset changes strongly if jumps with ΔU-values considerably smaller than E_{off} are excluded. Because E_{off} can have a value in the middle of the excluded ΔU-range it becomes clear that E_{off} cannot be caused by single unfavourable jumps with $\Delta U = 1.56$ eV. This means that E_{off} must correspond to a composition of a group of jumps (a jump series) all with ΔU-values lower than E_{off} (for this reason E_{off} changes when jumps with ΔU-values $< E_{\mathrm{off}}$ are excluded, see table 3.3). These jump series have their own combined, effective activation energy, analogous to the overall activation energy of a series of consecutive chemical reactions. From reaction rate theory it is known that for such consecutive reactions the overall activation energy is the difference in energy between the energy of the top of the highest energy barrier and the energy of the initial state [26]. If a jump series is responsible for the observed overall interface mobility activation energy, then the energy variation of the system along the path from fcc to bcc must contain mul-
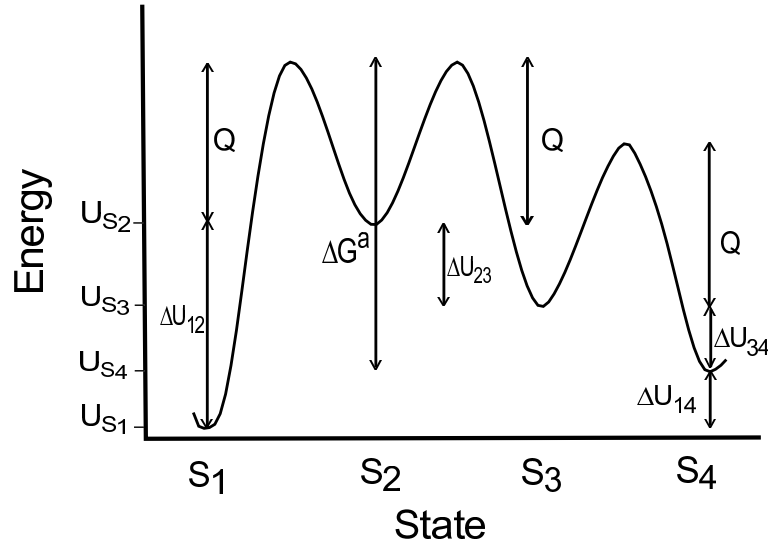
Fig. 3.5: A possible variation on a path from state S_4 to the most stable state S_1 with two intermediate states. The energy barrier between all states (i.e. for single jumps) is constant (Q). The overall activation energy for this process ΔG^a is the difference between the maximum energy level and the energy level of the start state and $E_{\text{off}} = \Delta U_{23} + \Delta U_{34}$ (all ΔU-values are positive in this figure).

tiple intermediate states; see, for example, fig. 3.5. The jump yield, Y_{jump}, is the number of transformed atoms per *single* jump. In all simulations Y_{jump} decreases with decreasing temperature as shown in fig. 3.6. As explained in Appendix 3.B, Y_{jump} can only decrease with temperature for a process with at least two intermediate states.

The simulations have shown that a jump series often contains jumps of different (neighbouring) atoms. This means that the energy of groups of atoms must be tracked during the simulations to determine the combined activation energy, but it cannot be known which groups. Effectively, this makes it impossible to determine exactly which ΔU-values combine into E_{off}. Here the important result is that jumps series incorporating groups of atoms are involved and that E_{off} is therefore not determined by single atom jumps.

3.5 General discussion

For incoherent boundaries the activation energy for diffusion of atoms in grain boundaries is often taken as an estimate for the activation energy of the interface mobility (ΔG^a in eq. (3.1)) [1]. However, experimental results on interface motion in massive transformations reveal values for this activation energy that are significantly larger than the activation energy for grain-boundary diffusion [27]. Similar results have been obtained for boundary motion in grain growth [1]. Two possible explanations have been offered: firstly, the atoms may be activated in groups rather than singly [28] or secondly, the presence of impurities or inclusions influences the temperature dependence of the growth rate, so the
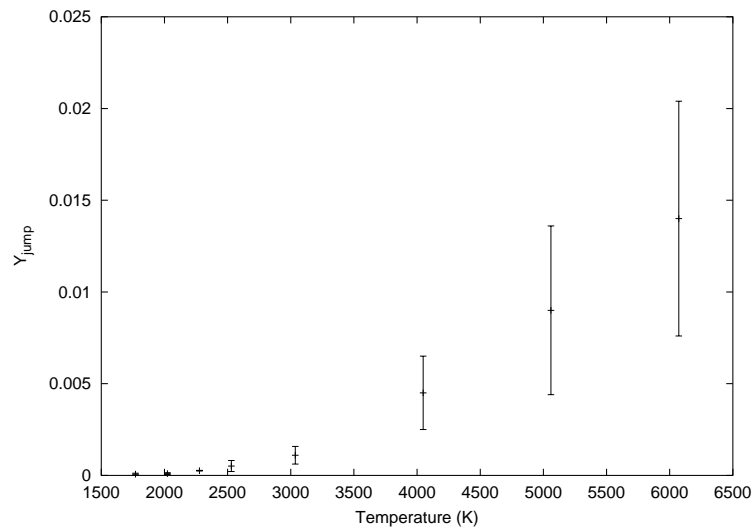
Fig. 3.6: The jump yield, Y_{jump}, as a function of temperature for a system containing 15 vacancies and with $Q = 1.744$ eV. All data points are an average from a minimum of 10 repetitions of the transformation simulation.

measured activation energy is no longer purely the activation energy for boundary movement [1]. The second explanation seems to be supported by, also very recent, molecular dynamics simulations on grain growth in single phase materials [29–31]: the activation energy for grain-boundary migration in pure metals as determined by the simulations was found to be actually much less than the activation energy observed experimentally. Strikingly, the activation energy determined in those simulations is even smaller than the activation energy for grain-boundary diffusion.

In the present simulations the energy barrier for every jump, Q, is constant. Therefore the activation energy for the process of bulk diffusion in the current model is also Q. Diffusion in the boundary will most likely also include unfavourable jumps and therefore in the present case the activation energy for boundary diffusion will be higher than for bulk diffusion. Work is in progress to incorporate realistic atomic interaction potentials (such as provided by the Embedded Atom Method [18, 19]). With such a potential it should be possible to include in the simulations not only ΔU-values but also Q-values that depend on the local surroundings of the jumping atoms. Only with these variable Q-values a meaningful comparison of the activation energies for the interface mobility, boundary diffusion and bulk diffusion can be made.

It has been suggested that during grain growth step-wise growth occurs for each grain [28], such that in each step a group of n atoms of the parent material become disordered or melt *simultaneously* and then take on the structure of the growing (product) crystal (with the total activation energy dependent on n). Although the groups are small and no melting or strong disordering is observed, the present simulations have shown that groups of atoms are involved in the phase transformation at the transformation interface.

The exact value for E_{off} is difficult to predict from the simulation settings. During the transformation, all along the interface, unfavourable jumps are required to provide a path from fcc to bcc. The energy change ΔU associated with each of these jumps depends on the local surroundings. Along the interface and with motion of the interface these local surroundings change continuously. This means that for the transformation jumps of many different ΔU-values (and combinations of ΔU-values for jump series) are required. Unlike in many other processes (such as diffusion) it is not one and the same, constant, activation energy barrier that is rate limiting as shown by the large uncertainty ranges in fig. 3.3 and table 3.3.

3.6   Conclusion

By calculating the atomic jump rates on the basis of simple transition state theory, the new multi-lattice kinetic Monte Carlo scheme can be used for the simulation of transformation kinetics in the fcc to bcc transformation in a single element system.

The observed effective overall activation energy for the interface mobility parameter is higher than the energy barrier for single atomic jumps (which was taken constant). It follows that the mobility activation energy is determined by energetically unfavourable jumps. During the transformation most fcc atoms at the interface cannot jump directly to empty bcc sites because the empty bcc sites are blocked by other neighbouring atoms. From the temperature dependence of the jump yield and from simulations in which a range of energetically unfavourable jumps was excluded it can be concluded that by series of unfavourable jumps performed by groups of atoms a path from fcc to bcc is created, albeit at the cost of an effective overall activation energy for the interface mobility larger than the activation energy barrier for a single atomic jump.

3.A   The simulation algorithm

1. *Create a list of all interface atoms*

2. *Calculate k for every valid jump of the interface atoms (using eq. (3.9))*

3. *Calculate K_{sum} (using eq. (3.2))*

4. *Generate a random number $R \in [0, K_{\text{sum}})$*

5. *Find the corresponding jump (eq. (3.3))*

6. *Let the atom jump*

7. *Generate a random number $R_2 \in [0, 1)$*

8. *Increase the simulation time by Δt as calculated with eq. (3.4)*

9. *Give the random sites that have remained unoccupied during the entire simulation a new (different) random position (this is only done after every 50000 jumps) [20]*

10. *Continue with step 1*

3.B The jump yield

First consider a transformation where the atoms can only jump between two states S_1 and S_2 with $U_{S_1} < U_{S_2}$ as shown for example in fig. 3.1. The rate for the transformation from state 2 to state 1 for this two state transformation, $r_{\text{tf},2}$, can be written as the difference between the number of atoms jumping from S_2 to S_1 and the number of atoms jumping in the opposite direction:

$$r_{\text{tf},2} = N_2 k_{21} - N_1 k_{12}, \tag{3.12}$$

where N_x is the number of active atoms[5] in state S_x. The rates constants k_{12} and k_{21} are given by (cf. eq. (3.6)):

$$k_{12} = \nu_0 \exp\left(-\frac{Q + \Delta U_{21}}{k_B T}\right) \tag{3.13}$$

and

$$k_{21} = \nu_0 \exp\left(-\frac{Q}{k_B T}\right). \tag{3.14}$$

Under the assumption $N_1 = N_2 = N$, $r_{\text{tf},2}$ can be rewritten into

$$r_{\text{tf},2} = \nu_0 N \exp\left(-\frac{Q}{k_B T}\right)\left(1 - \exp\left(-\frac{\Delta U_{21}}{k_B T}\right)\right). \tag{3.15}$$

By comparing eqs. (3.10)) and (3.15)) it is seen that the overall activation energy equals the height of the energy barrier ($\Delta G^a = Q$) in this two state situation.

The transformation rate gives the number of transformed atoms per unit of time. The jump rate r_j is the number of jumps per unit of time:

$$r_{j,2} = N(k_{12} + k_{21}). \tag{3.16}$$

The ratio of r_{tf} and r_j defines the jump yield Y_j, the number of transformed atoms per jump. For the two state system it follows from eqs. (3.12) and (3.16):

$$Y_{j,2}(T) = \frac{r_{\text{tf},2}(T)}{r_{j,2}(T)} = \frac{1 - \exp\left(-\frac{\Delta U_{21}}{k_B T}\right)}{1 + \exp\left(-\frac{\Delta U_{21}}{k_B T}\right)}. \tag{3.17}$$

---

[5] Only atoms that can actually make a jump attempt (active atoms), as atoms at the transformation front, must be taken into account.
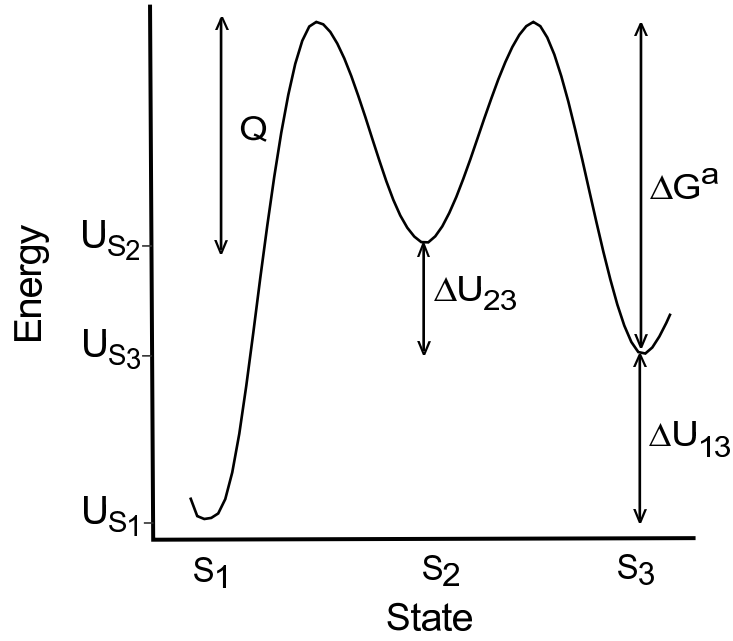
Fig. 3.7: A possible energy variation on a path from state S_3 (fcc in the simulations) to the most stable state S_1 (bcc) with one intermediate states. The energy barrier between all states is constant (Q). The overall activation energy for this process ΔG^a is the difference between the maximum energy level and the energy level of the start state.

Evidently, since $\Delta U_{21} > 0$, the jump yield decreases with increasing temperature.

In all simulations ΔG^a was found to be larger than the activation energy barrier for a single atomic jump, Q, and it was concluded that unfavourable jumps, i.e. with $\Delta U > 0$, govern the interface mobility. If ΔG^a is determined by single (independent) unfavourable jumps then an atom first makes one jump to an intermediate state and then a jump to the final (bcc) state occurs, as shown schematically in fig. 3.7 (hence $\Delta G^a = Q + \Delta U_{23}$). The transformation rate for this three state system is given by

$$r_{\text{tf},3} = \frac{1}{2} N_2 k_{21} - N_1 k_{12} \tag{3.18}$$

and the jump rate by

$$r_{j,3} = N_1 k_{12} + N_2 (k_{21} + k_{23}) + N_3 k_{32}. \tag{3.19}$$

Assuming steady state conditions(constant number of active atoms in all states) and $N_1 = N_3 = N$, the jump yield follows from eqs. (3.18) and (3.19):

$$Y_{j,3}(T) = \frac{r_{\text{tf},3}(T)}{r_{j,3}(T)} = \frac{\exp\left(\frac{\Delta U_{31}}{k_B T}\right) - 1}{4\left(1 + \exp\left(\frac{\Delta U_{31}}{k_B T}\right)\right)}. \tag{3.20}$$

As $Y_{j,2}$, $Y_{j,3}$ also decreases with increasing temperature, as shown in fig. 3.8.
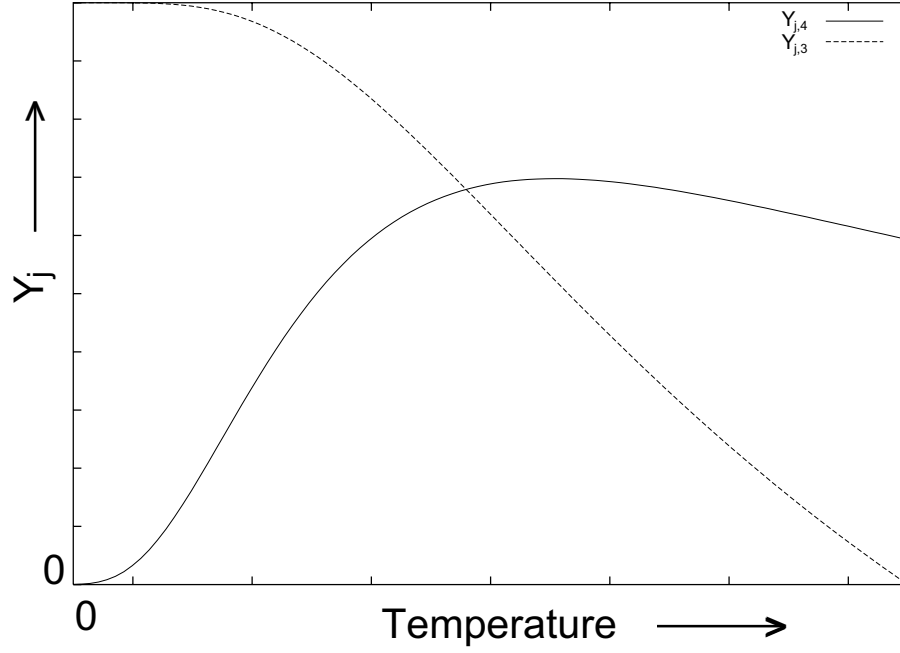
Fig. 3.8: The jump yield for a three state transformation process ($Y_{j,3}$, eq. (3.20)) and a four state transformation process ($Y_{j,4}$, eq. (3.23)).

Now consider a transformation process with two intermediate states as shown for example in fig. 3.5 (here $\Delta G^a = Q + \Delta U_{23} + \Delta U_{34}$). For this four state case the rate equations are

$$r_{\text{tf},4} = \frac{1}{2}N_2 k_{21} - N_1 k_{12} \tag{3.21}$$

and

$$r_{j,4} = N_1 k_{12} + N_2(k_{21} + k_{23}) + N_3(k_{32} + k_{34}) + N_4 k_{43}. \tag{3.22}$$

With $U_{S_1} < U_{S_4} < U_{S_3} < U_{S_2}$ and assuming steady state conditions and $N_1 = N_3 = N$, the jump yield follows from eqs. (3.21) and (3.22):

$$
\begin{aligned}
Y_{j,4}(T) &= \frac{r_{\text{tf},4}(T)}{r_{j,4}(T)} \\
&= \exp\left(\frac{U_{S_2} + U_{S_3}}{k_B T}\right)\left(\exp\left(\frac{U_{S_4}}{k_B T}\right) - \exp\left(\frac{U_{S_1}}{k_B T}\right)\right) \Big/ \\
&\quad \left[5\exp\left(\frac{U_{S_1} + U_{S_2} + U_{S_3}}{k_B T}\right) + 4\exp\left(\frac{U_{S_1} + 2U_{S_3}}{k_B T}\right) + \right. \\
&\quad \left. 4\exp\left(\frac{2U_{S_2} + 2U_{S_4}}{k_B T}\right) + 5\exp\left(\frac{U_{S_2} + U_{S_3} + U_{S_4}}{k_B T}\right)\right].
\end{aligned}
\tag{3.23}
$$

Although eq. (3.23) has been expressed in absolute energy levels U instead of energy differences ΔU, $Y_{j,4}(T)$ does not change when U_{S_1}, U_{S_2}, U_{S_3} and U_{S_4} are changed by the same amount. Now, and in contrast with $Y_{j,2}(T)$ and $Y_{j,3}(T)$, $Y_{j,4}(T)$ has a maximum at a certain temperature and below that temperature the jump yield decreases with decreasing

temperature, see fig. 3.8. This is the same behaviour as observed in the simulations (cf. fig. 3.6)). However this behaviour for $Y_{j,4}(T)$ is only obtained if $U_{S_4} < U_{S_3}$. If $U_{S_4} > U_{S_3}$ then $Y_{j,4}(T)$ will behave similar as $Y_{j,3}(T)$ in fig. 3.8. Apparently, the energy levels of the *intermediate* states must be arranged such that there is a decrease in energy (favourable single jump) against the direction of the transformation.

A higher jump yield means that less jumps are necessary to obtain the same amount of product phase. For this reason most simulations have been done at relatively high temperatures because less jumps must be simulated, which greatly shortens the calculation times.

4. Multi-lattice kinetic Monte Carlo simulation of interphase kinetics for an iron fcc to bcc transformation

C. Bos, F. Sommer and E.J. Mittemeijer

Abstract

Using an embedded atom method potential for iron, the kinetics of (lateral) growth in the massive austenite (γ) to ferrite (α) transformation was analysed applying a newly developed multi-lattice kinetic Monte Carlo simulation approach. On this basis, for the first time the variable, individual activation energy for each single atomic jump could be accounted for. It was shown that the transformation is rate controlled by series of energetically unfavourable jumps by groups of atoms, necessary to create a path from γ to α at the interphase.

4.1 Introduction

Massive transformations and grain growth are typical examples of thermally activated, interface controlled solid state transformations. Models that describe the resulting microstructure of these industrially important processes depend on an adequate description of the interface mobility. The textbook equation for the interface velocity, v, that usually presents a good description of the experimental observations, reads [1] (see also, figure 4.1):

$$v(T) = M \left(1 - \exp \left(-\frac{\Delta G}{kT} \right) \right) \tag{4.1}$$

with

$$M = M_0 \exp \left(-\frac{\Delta G^a}{kT} \right), \tag{4.2}$$

with M_0 a pre-exponential constant, ΔG^a the activation energy of the interface mobility M, k_B the Boltzmann constant, T the temperature and ΔG the (positive) Gibbs energy difference between the parent and product phase. One of the main difficulties in the use of equation (4.1) is to obtain reliable data for ΔG^a, especially as a function of interface
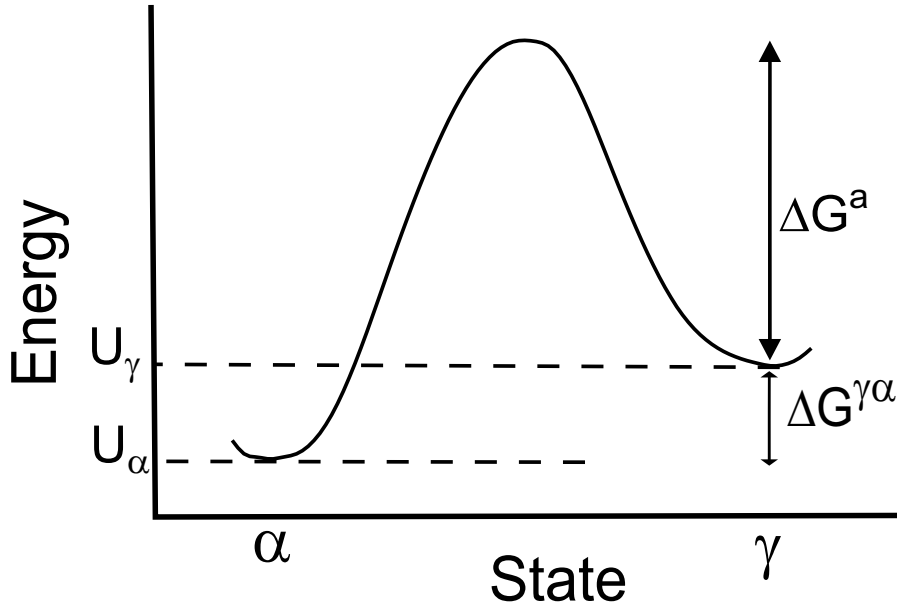
Fig. 4.1: A possible variation in system energy on a path from the γ phase to the α phase.

orientation/structure. The background of equation (4.1) is the assumption that the inter-face moves by independent jumps of atoms across the boundary, where each atom has to overcome an energy barrier in the jump. Thus, in a phase transformation from the fcc (γ) to the bcc (α) phase, atoms jumping from γ to α will experience a lower activation energy barrier than atoms jumping in the reverse direction, as shown in figure 4.1.

Recently, multi-lattice kinetic Monte Carlo [20] simulations of a massive fcc to bcc transformation in a single element system have shown that ΔG^a is determined by series of energetically unfavourable jumps[1] performed by groups of atoms [32]. This means that there are several intermediate states in the path from γ to α as shown schematically in figure 4.2. The overall activation energy (ΔG^a) is the difference between the maximum energy of the system and the energy of the initial state (on a path from γ to α). The groups of intermediate jumps are required because generally an fcc atom cannot jump directly to a bcc site because the bcc sites are blocked by neighbouring atoms.

In the multi-lattice kinetic Monte Carlo simulations the atomic jump rates, k, are calculated according to

$$k = \begin{cases} \nu_0 \exp\left(-\frac{Q+\Delta U}{k_B T}\right) & \text{if } (\Delta U > 0) \\ \nu_0 \exp\left(-\frac{Q}{k_B T}\right) & \text{otherwise} \end{cases}, \tag{4.3}$$

with Q the height of the energy barrier of a jump, ν_0 a (constant) frequency factor and ΔU the change in system energy caused by the jump considered. The observed difference between Q and ΔG^a was found to depend on the openness of the interface structure.

---

[1] An unfavourable jump implies that the energy of the system after the jump is larger than before the jump; i.e. in figure 4.1 a jump from α to γ.
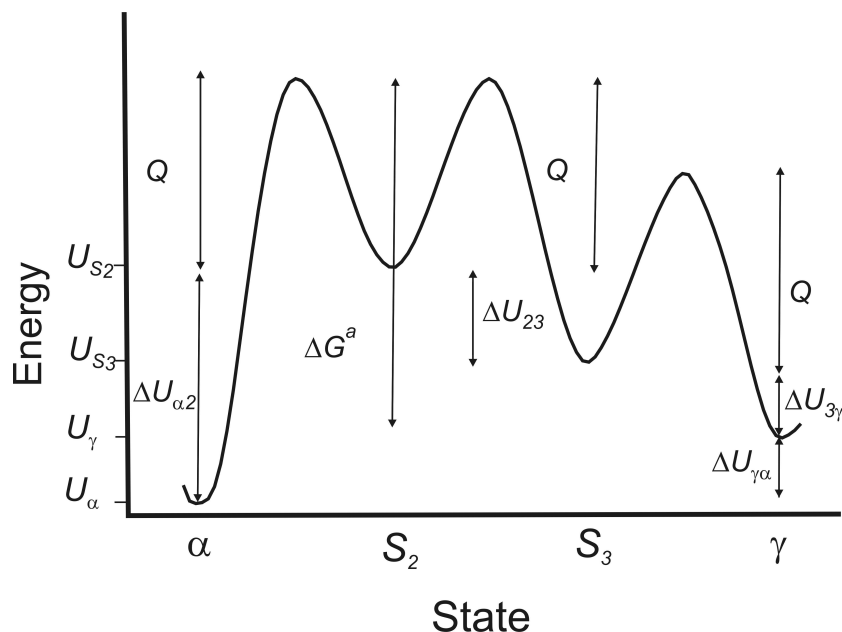
Fig. 4.2: A possible variation in system energy on a path from the γ phase to the α phase with two intermediate states. The energy barrier between all states (i.e. for single jumps) is constant (Q). The overall activation energy for this process ΔG^a is the difference between the maximum energy level and the energy level of the begin state.

In the previous work [20, 32] ΔU was calculated for each jump with a simple bond counting energy model and Q was taken constant for every jump, which are severe simplifications. To find out if the results obtained with these simplifications are generally valid, in the current work simulations have been performed incorporating the embedded atom method [18, 19] (EAM), a more accurate atomic interaction model than the bond counting model, that allows calculation of ΔU and the activation energy barrier Q both for each individual jump, thereby expressing the effect of the local surroundings of the jumping atoms.

4.2 Simulation method

The multi-lattice kMC method as described in [20] and [32] allows the simulation of a phase transformation from one crystal structure to another, by incorporating both crystal structures as possible sites for atoms. To allow the atoms at and near the moving interface to take intermediate positions between the lattice sites, a collection of randomly placed sites is also included. These intermediate positions allow for irregularities in the atomic structure of transformation interfaces.

In the present work two types of simulations have been performed. In the first type the atomic jump rate, k, is calculated with a constant energy barrier Q (cf. equation (4.3)).

Then Q is a simulation parameter. The energy difference ΔU for each jump is calculated with the Johnson-Oh EAM potential for iron [33].

The second type of simulation uses a variable activation energy barrier Q for the atomic jumps, by making the activation energy for each individual jump dependent on the local surroundings of the jumping atom. The jump rate equation can be written as

$$k = \nu_0 \exp\left(-\frac{E^a}{k_B T}\right), \qquad (4.4)$$

with $E^a = Q + \Delta U$ if $\Delta U > 0$ and $E^a = Q$ otherwise (cf. equation (4.3)). For every jump E^a is determined separately applying a constrained conjugate gradient energy minimization method as presented in reference [34]. In this method the jumping atom is pushed in a number of small steps from the start position towards the end position of the atom. After every step the energy of the system is minimized by a conjugate gradient method, i.e. by a (continuous) adjustment of the atomic positions, under the constraint that the jumping atom is allowed to move only perpendicularly to the line drawn from start to end position. This calculation can only be performed with an atomic interaction model which gives the interaction energy as a continuous function of the distance between two atoms (such as an EAM potential).

If every E^a would be calculated as described above with the constrained conjugate gradient energy minimization method, the calculation time for the simulations would become much too long. Therefore, a neural network [35] was trained on the basis of data of over five thousand jumps rigorously calculated with the constrained conjugate gradient energy minimization method. The thus trained neural network can be used in the simulations to calculate E^a for each individual jump. To obtain an accurate neural network description of E^a the right set of input parameters must be selected. Because E^a is primarily determined by the surrounding atoms of the jumping atom, the input parameters should in particular express the role of these surrounding atoms. A description that is accurate enough and yet allows fast simulation is the set of distances of the 14 neighbouring atoms closest in distance to the straight line drawn from begin to end position of the jumping atom. Together with the jump distance and the system energy before and after the jump these input parameters suffice to obtain a neural network that describes E^a for each individual jump within a mean square error of less than two percent.

4.3   Simulation setup

The start configuration contained a bcc seed for the simulation of lateral growth as shown in figure 4.3. The interface orientation is fcc(111)//bcc(110) and fcc[11$\bar{2}$]//bcc[00$\bar{1}$] and the interface lies parallel to the xy-plane. The fcc and bcc crystals were created with equal planar density for the planes parallel to the interface (with bcc number density of
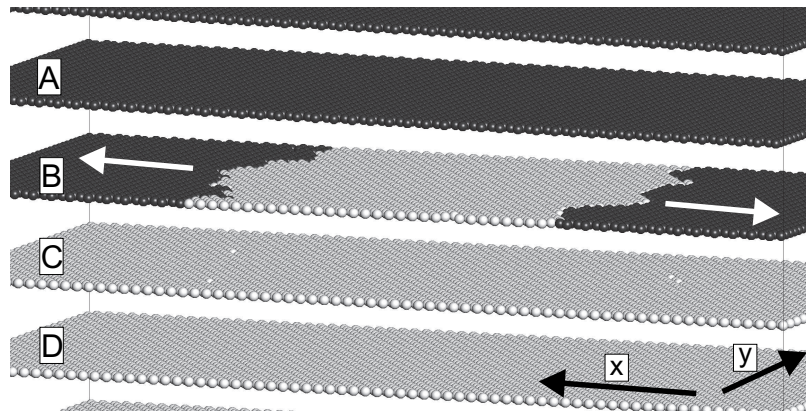
Fig. 4.3: The start configuration for the simulations, containing 17 vacancies. The extra space between the planes is not real, it has been inserted to provide a clearer view. Fcc atoms are dark grey, bcc atoms are light grey. The white arrows indicate the bcc growth direction.

$84.9 \cdot 10^{27}$ atoms/m^3). The number of atoms per plane is 3312. If vacancies were inserted in the system then they were created in plane B shown in figure 4.3 by removing fcc atoms. Periodic boundaries were used in both the x direction and the y direction. This leads to lateral growth of the bcc phase in the x direction, as indicated by the white arrows in figure 4.3.

The random sites were distributed according to a restrictedly random distribution. First, the system was divided in small cubic cells with a side length of $1.4r_b$ (with r_b the bcc nearest neighbour distance). Then, N_{ran} random sites were inserted into each cell according to a uniform distribution. Unless noted otherwise $N_{ran} = 10$.

In all simulations a value of 10^{13} (sec^{-1}) was used for ν_0.

The driving force for the transformation is determined by the (iron) EAM potential and, for the chosen densities of the fcc and bcc crystals, it is $\Delta U_{bcc,fcc} = 0.03$ eV. With this driving force and the chosen interface orientation the chance of bcc nucleating in plane A (cf. figure 4.3) is extremely small (cf. reference [20]). and therefore only lateral growth in plane B occurs. Because the positions of the lattice sites are fixed, temperature has no influence on the geometry of the interface through density changes. The only influence temperature has is on the transformation rate. For optimal calculation time efficiency [32] the simulations were performed in a temperature range from 1250 to 4000 K.

In the constant energy barrier simulations (see sections 4.2 and 4.4.1) a value of 0.872 eV was used for Q.
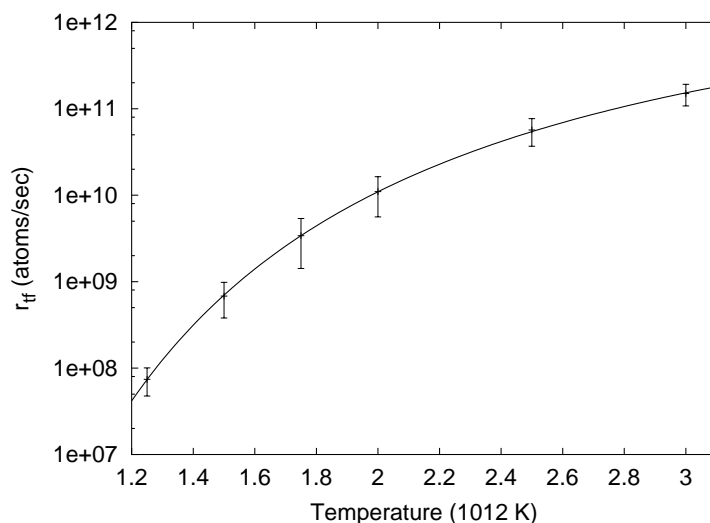
Fig. 4.4: The transformation rate as a function of temperature for a system containing 17 vacancies and with $Q = 0.872$ eV. All data points represent the average from a minimum of 10 repetitions of the transformation simulation. The error bars represent the corresponding standard deviation. The solid line is a fit of equation (4.5).

By calculating the transformation rate r_{tf}[2] of simulations at different temperatures, the overall activation energy for the interface mobility, ΔG^a, can be found by non-linear least-squares fitting to the obtained data of [3]

$$r_{\text{tf}}(T) = C \exp\left(-\frac{\Delta G^a}{kT}\right)\left(1 - \exp\left(-\frac{\Delta U_{bcc,fcc}}{kT}\right),\right).\tag{4.5}$$

with C a pre-exponential constant and $\Delta U_{bcc,fcc}$ the fcc-bcc energy difference (driving force, equal to 0.03 eV; see above and see equations (4.1) and (4.2)).

4.4   Results

4.4.1   EAM constant-Q simulations

The transformation rate is shown as a function of temperature for a system with 17 vacancies in figure 4.4. By fitting equation (4.5) to the data

$$\Delta G^a = 1.576 \pm 0.006 \text{ eV}$$

---

[2] An estimate for the transformation rate is determined by measuring the time between 20% and 80% completion of the transformation of the remaining fcc atoms of plane B in figure 4.3.

[3] This implies, as usual, that only the internal energy part of the activation energy is determined; the entropy contribution is included in the pre-exponential factor.

and

$$C = (5.721 \pm 0.006) \cdot 10^{14} \text{ atoms/sec.}$$

have been obtained. Evidently, ΔG^a is about twice as large as the energy barrier for a single jump, Q (=0.872 eV). This already shows that ΔG^a is controlled by unfavourable jumps ($\Delta U > 0$, cf. equation (4.3)). If it is one type of unfavourable jump that is rate limiting it should be possible to write ΔG^a as

$$\Delta G^a = Q + \Delta U_{\text{rl}}, \tag{4.6}$$

where ΔU_{rl} is the ΔU of the rate limiting jump. If equation (4.6) holds then $\Delta U_{\text{rl}} = \Delta G^a - Q = 0.704$ eV. Excluding all jumps with ΔU between 0.63 and 0.78 eV from the simulations a new overall activation energy

$$\Delta G^a_{\text{excl}} = 1.63 \pm 0.03 \text{ eV}$$

has been found. With equation (4.6) this gives $\Delta U_{\text{rl}} = 0.76$ eV which falls within the excluded ΔU-range. Therefore, it must be concluded that interpretation of the values found for ΔG^a on the basis of equation (4.6) is invalid and that ΔG^a is determined by multiple unfavourable jumps, i.e. by groups of unfavourable jumps as shown schematically in figure 4.2.

The jump yield Y is defined as the number of transformed (fcc to bcc) atoms per atomic jump. It can be shown that Y as a function of temperature can only have a maximum at $T \neq 0$ if the process has multiple intermediate states where at least two of the energy levels of the intermediate states must be arranged such that their energy level increases in the direction of the transformation (i.e. $U_{S_2} - U_{S_3} > 0$ in figure 4.2; see also figure B2 in [32]). The jump yield as a function of temperature for a system with 17 vacancies is shown in figure 4.5. The jump yield has an maximum at $T \neq 0$. Hence ΔG^a is determined by groups of unfavourable jumps.

In the simulation with the bond counting interaction model it was found that the difference between ΔG^a and Q is strongly influenced by the interface structure [32]. If more vacancies are added to the system the interface structure will become more open (because the vacancies dissolve at the interface), which should lead to a smaller ΔG^a. In figure 4.6 ΔG^a is shown as a function of the number of vacancies in the system. Indeed, ΔG^a decreases with an increasing number of vacancies.

As noted in sections 4.2 and 4.3 the system also contains a set of randomly placed sites. The role of these random sites is to allow the atoms to take intermediate positions at the transformation front. The series of unfavourable jumps by groups of atoms are required because the empty bcc sites are often blocked by neighbouring atoms which means that
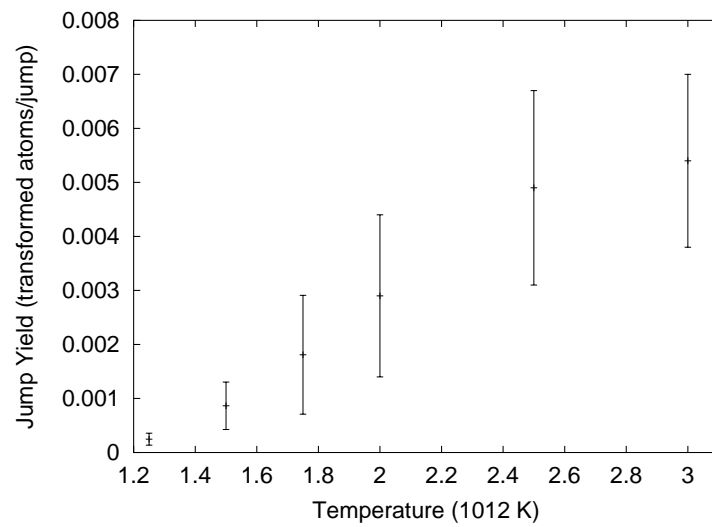
Fig. 4.5: The jump yield as a function of temperature for a system containing 17 vacancies and with $Q = 0.872$ eV. All data points represent the average from a minimum of 10 repetitions of the transformation simulation. The error bars represent the corresponding standard deviation.
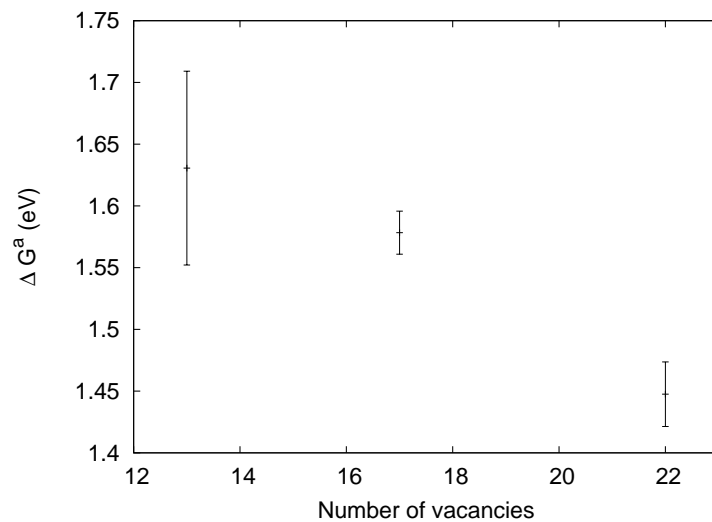

Fig. 4.6: The overall interface mobility activation energy as a function of the number of vacancies in the system (simulations with $Q = 0.872$ eV). The error bars show the standard error as obtained from the fit procedure.
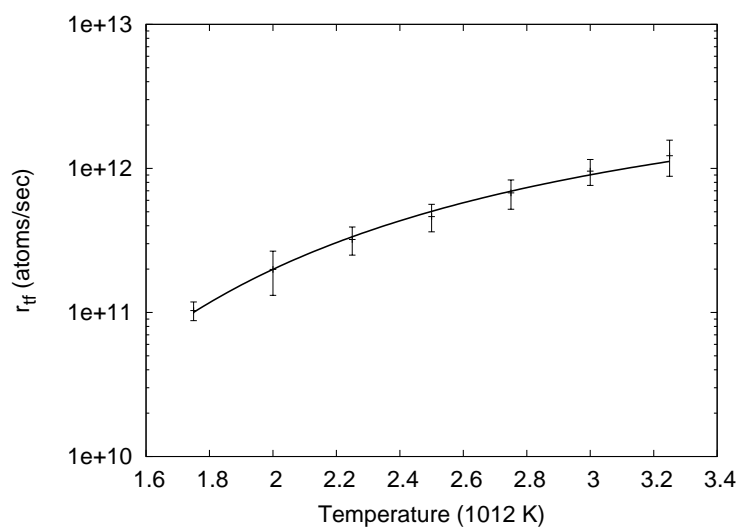
Fig. 4.7: The transformation rate as a function of temperature for a system containing 17 vacancies and with neural network calculated E^a-values. All data points represent the average from a minimum of 10 repetitions of the transformation simulation. The error bars represent the corresponding standard deviation. The solid line is a fit of equation (4.5).

most fcc atoms cannot jump directly to a bcc site. Or in different words: the groups of jumps provide a path from fcc to bcc. If more random sites are available it is easier for the atoms to find a path to bcc and ΔG^a decreases (confirmed by simulations with different values for N_{ran}). However, when too much random sites are added to the system the relative chance for a jump to a random site as compared to a jump to a lattice site becomes so large that all calculation time is spend on jumps to and from random sites instead of on jumps that could effectuate the transformation.

4.4.2　EAM variable-Q simulations

The transformation rate as a function of temperature for a system with 17 vacancies and with E^a (cf. equation (4.4)) calculated with the trained neural network is shown in figure 4.7. From a fit of equation (4.5)

$$\Delta G^a_{\mathrm{nn}} = 0.99 \pm 0.02 \text{ eV}$$

has been obtained for the overall interface mobility activation energy, ΔG^a_{nn}, of these neural network simulations. By filtering out all back-and-forth jumps from the jump history only those jumps that actually effectuate the transformation can be selected. A histogram that shows how often jumps with a specific E^a occur in this group of effective jumps is shown in figure 4.8. It follows that there is only a very minimal fraction of jumps
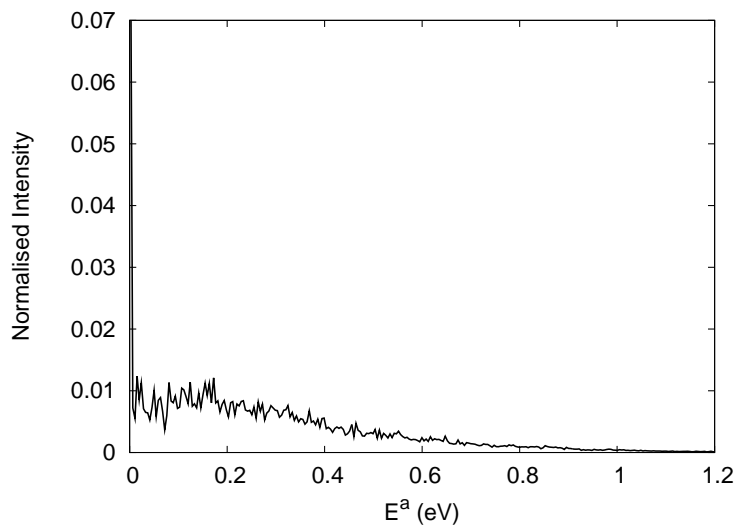
Fig. 4.8: The distribution of E^a-values of the effective, single jumps recorded for a system containing 17 vacancies at a temperature of 2530K.

with $E^a = \Delta G^a_{\mathrm{nn}}$. Excluding all jumps with E^a in the range of 0.91-1.12 eV leads to a new overall activation energy, $\Delta G^a_{\mathrm{nn,excl}}$:

$$\Delta G^a_{\mathrm{nn,excl}} = 1.00 \pm 0.02 \text{ eV}.$$

This value for the effective mobility activation energy is in the middle of the excluded range of activation energy values for single jumps, leading to the conclusion that the variable E^a simulations also demonstrate that ΔG^a is determined by groups of jumps (by the same line of reasoning as in section 4.4.1). Also, the jump yield as a function of temperature, shown in figure 4.9, again has a maximum at $T \neq 0$, supporting the conclusion that ΔG^a is determined by groups of jumps.

Finally, for simulations with different numbers of vacancies in the system the same trend as in figure 4.6 is observed; i.e. ΔG^a decreases with increasing vacancy content.

4.5 Discussion

All observations made with the original bond-counting with constant Q simulations have been confirmed for both the EAM with constant Q and the EAM with variable Q simulations. Apparently equation (4.1) remains a very good approximation for the transformation rate regardless of the exact shape of the energy variation along the path from γ to α as long ΔG^a is taken as the difference between the highest energy level and the start level energy along that path. For example, no significant change of the interface velocity
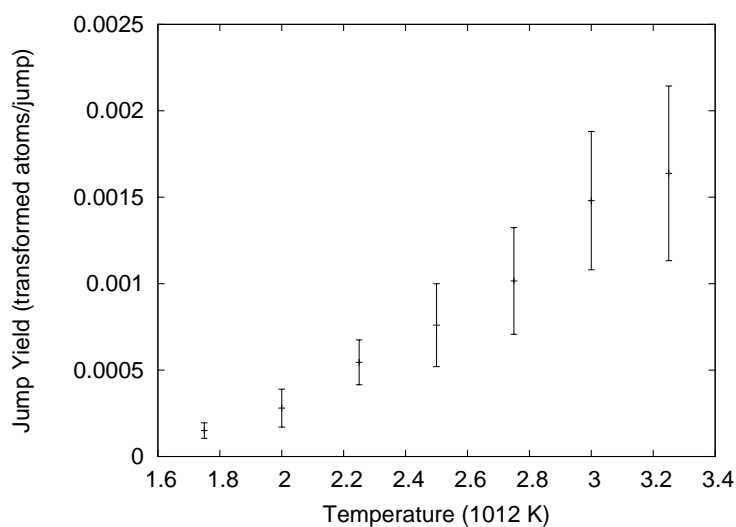
Fig. 4.9: The jump yield as a function of temperature for a system containing 17 vacancies and with neural network calculated E^a-values. All data points represent the average from a minimum of 10 repetitions of the transformation simulation. The error bars represent the corresponding standard deviation.

occurs if the energy barrier between state S_3 and state γ in figure 4.2 is much smaller than Q.

The introduction of the EAM based, variable, neural network calculated single jump activation energies is an important step forward in applying the multi-lattice kinetic Monte Carlo method as a quantative method. With the neural network approach it is possible to use even more accurate interatomic potentials, because the energy barriers for only a limited number of jumps (here about 5000 jumps) have to be calculated to obtain the data to train the neural network.

4.6 Conclusion

The results of the simulations performed here for the massive γ (fcc) to α (bcc) phase transformation fully support conclusions drawn on the basis of the previous simulations with a constant single jump activation energy barrier and a bond-counting atomic inter-action model; i.e. for both the embedded atom method (EAM) with constant activation energy barrier and the EAM with neural network calculated, variable single jump activation energy simulations, the overall interface mobility activation energy is determined by series of unfavourable jumps by groups of atoms. These groups of jumps are required to create a path from fcc to bcc as most fcc atoms cannot jump directly to bcc sites because they are blocked by neighbouring atoms. A more open interface structure leads to a smaller overall interface mobility activation energy.

5. Atomistic Simulations of Interface Controlled Phase Transformations

C. Bos, F. Sommer and E.J. Mittemeijer

Abstract

A multi-lattice kinetic Monte Carlo method has been used for an atomistic study on moving interfaces in interface-controlled phase transformations. Depending on the driving force of the transformation a continuous or a plane-by-plane lateral growth mode occurs. In case of plane-by-plane growth 2-dimensional nucleation is required to accomplish the transformation. To study the activation energy of the interface mobility for an fcc to bcc massive transformation in a single element system, lateral growth mode simulations have been performed. Series of unfavourable atomic jumps control the transformation rate because atoms on the fcc lattice in general cannot jump directly to bcc lattice sites since neighbouring atoms block the empty bcc sites. The magnitude of the difference between the mobility activation energy and the activation energy for diffusion is determined by the interface structure.

5.1   Introduction

A typical example of an interface controlled phase transformation is the massive transformation. The rate of transformation in a massive transformation is determined by processes at the interface. In many iron-based alloys the austenite, γ, to ferrite, α, transformation is of massive nature. Recently, the massive transformation has received much renewed attention [2, 14, 36, 37]. The mechanism of the transformation is a topic of active discussion [16]. Most experimental data were collected after the transformation was completed. Data on the interface structure obtained during the transformation would greatly enhance the understanding of the transformation mechanism, but such data are scarce [3, 16].

Molecular dynamics (MD) simulations would allow the study of the structure of a moving interface in full atomic detail, as simulations of the martensitic transformation have shown [4–6]. Recently, MD simulations have also been used in the simulation of elastically driven migration of flat grain boundaries [31, 38].

Unfortunately, the timescale required for the simulation of massive transformations is generally too demanding computationally. In MD simulations the full continuous trajectories of the atoms are described. To enhance the timescale that can be simulated, kinetic Monte Carlo (kMC) simulations can be made. However, then the possible atom positions are restricted to a set of discrete sites. The movement of the atoms is in this case treated as a stochastic process.

Monte Carlo methods have been employed successfully in simulating *solid-vapour* and *solid-liquid* transformations [7–11]. Unfortunately these methods cannot be applied directly to *solid-state* transformations, because a description of a *solid-state* transformation requires at least two lattices.

The recently introduced multi-lattice kinetic Monte Carlo (kMC) method [20] for the simulation of a solid-state phase transformation from one crystal structure to another incorporates both crystal structures as possible sites for atoms. To allow the atoms at and near the moving interface to take intermediate positions between the lattice sites, a collection of randomly placed sites can also be included. These 'random sites' allow for irregularities in the atomic structure of transformation interfaces. Depending on the driving force for the transformation and on the mobility of the atoms at the interface, these intermediate sites can be esssential to the transformation.

In this work results of the simulation of an fcc to bcc transformation in a single element system are presented. Both the activation energy of the interface mobility and the influence of the driving force on the growth mode have been investigated.

5.2   Simulation Method

The textbook equation for the interface velocity, v, reads [1]

$$v = M \left(1 - \exp \left(-\frac{\Delta G}{k_B T} \right) \right) \tag{5.1}$$

with

$$M = M_0 \exp \left(-\frac{\Delta G^a}{k_B T} \right), \tag{5.2}$$

where M_0 is a pre-exponential factor, ΔG^a is the activation energy of the interface mobility, k_B is the Boltzmann constant, T is the temperature and ΔG is the Gibbs energy difference between the parent and product phases. Eq. (5.1) is based on the assumption that the interface moves by (with respect to time and space) independent thermally activated jumps across the interface, where the atoms jumping from the parent phase to the product phase experience an effective energy barrier of ΔG^a and atoms jumping in the reverse direction experience an effective energy barrier of $\Delta G^a + \Delta G$.

Multi-lattice kMC allows the atomistic simulation of interface controlled transformations based on the same assumptions, i.e. the interface moves by independent thermally activated atomic jumps.

In the multi-lattice kMC method as employed here the jump rate, k, is calculated from simple transition state theory (see for example Ref. [24]) with

$$k = \nu_0 \exp\left(-\frac{E^a}{k_B T}\right),$$ (5.3)

with ν_0 a pre-exponential factor and E^a the activation energy for the jump. In the kMC method a jump is selected at random based on the relative chance of each jump[1]. Let K_{sum} be the sum of the jump rates of all possible jumps in the system,

$$K_{\text{sum}} = \sum_{i=1}^{N_{\text{jump}}} k_i,$$ (5.4)

where N_{jump} is the total number of possible jumps. The average number of jumps per unit of time is given by $1/K_{\text{sum}}$. Now, a random number R_1 between zero and K_{sum} is drawn and the actually occurring jump is identified as the first jump a for which

$$\sum_{i=1}^{a} k_i \geq R_1.$$ (5.5)

The time Δt between successive jumps can be calculated with [23]

$$\Delta t = -\left(\frac{1}{K_{\text{sum}}}\right) \ln(R_2),$$ (5.6)

where R_2 is a random number between zero and one.

For the calculation of E^a in Eq. (5.3) it is here assumed that every jump has the same energy barrier Q, as shown for a jump from position A to position B in Figure 5.1. This means that Eq. (5.3) can be rewritten as

$$k = \begin{cases} \nu_0 \exp\left(-\frac{Q+\Delta U}{k_B T}\right) & \text{if } (\Delta U > 0) \\ \nu_0 \exp\left(-\frac{Q}{k_B T}\right) & \text{otherwise} \end{cases},$$ (5.7)

where ΔU is the potential energy change of the system caused by the jump.

For the calculation of ΔU an atomic interaction model is required. In this work two different models have been used: an embedded atom method (EAM) potential [18, 19] and a bond-counting model (as described in Ref. [20]). In the bond counting model all possible bonds have been given a fixed energy regardless of the distance between two

---

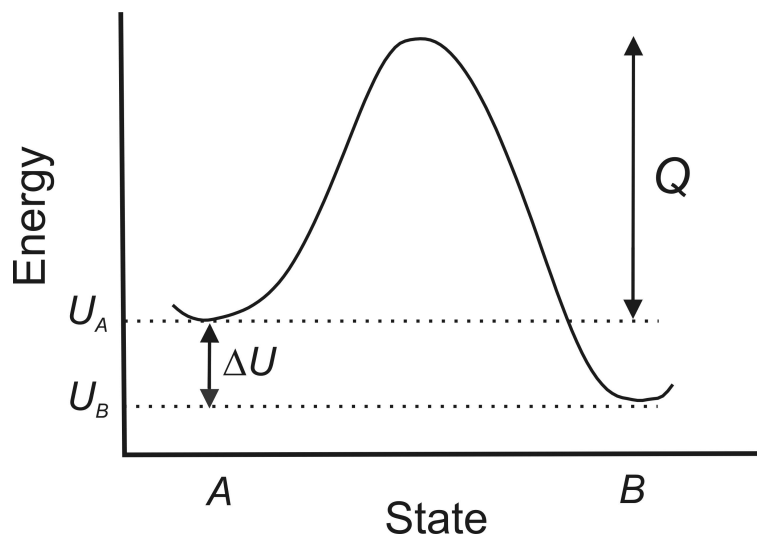[1] See Ref. [32] for a full description of the simulation algorithm

Fig. 5.1: The variation in energy along the atomic jump path from position A to position B and vice versa.

atoms. In total there are five different bond energies: u_{bb} for a bcc-bcc bond, u_{ff} for a fcc-fcc bond, u_{bf} for a mixed bcc-fcc bond, u_{rf} for a bond between an fcc atom and an atom on a random site and u_{rb} for a bond between an bcc atom and an atom on a random site. The EAM potential gives much more realistic interaction energies, but the bond counting model has the advantage that the driving force ($\Delta U_{bcc,fcc} = \frac{1}{2}(8u_{bb} - 12u_{ff})$) and bcc-fcc interface energy can be chosen almost arbitrarily.

5.3   Simulation settings

Besides the temperature, the constant energy barrier (Q), the densities of the crystal lattices, the number of random sites in the system, the interface orientation and the number of vacancies in the system, the simulations with the bond counting model, as compared with the EAM model, have one important extra parameter: the hard core diameter, d_{hs}, which prevents atoms from overlapping. Further, for simulations using the bond counting model two more parameters must be specified: the maximum distance for a long jump $r_{maxjump}$ and for a short jump r_{sj}. These two parameters mainly influence the computation efficiency of the simulation, as described in Ref. [20]. Here $r_{sj} = 0.15r_b$, $d_{hs} = 0.65r_b$ and $r_{vh} = 0.75r_b$ have been used (r_b is the bcc nearest neighbour distance).

For the EAM potential the Johnson-Oh [33] potential for iron was used. The three different sets of bond energies (sets A, B and C) that were used are given in Table 5.1. These different sets were used to vary the driving force for the transformation and to vary the bcc-fcc interface energy.

To study the interface mobility activation energy an fcc(111)//bcc(110) with fcc[11$\overline{2}$]// bcc[00$\overline{1}$] interface was created, with for bcc the equilibrium (iron) density and for fcc

Tab. 5.1: Bond-energy values in eV, u_{xy} is the energy of a bond between an atom on a site of type x and an atom on a site of type y (bcc, fcc or random).

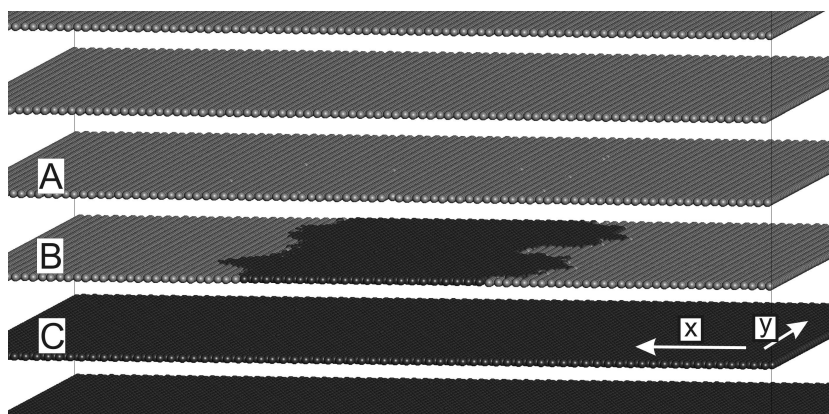| Set name	u_{bb}	u_{ff}	u_{bf}	u_{rb}	u_{rf}
A	-1.15	-0.663	-0.121	-0.0872	-0.0872
B	-1.18	-0.663	-0.567	-0.0872	-0.0872
C	-1.22	-0.663	-0.567	-0.0872	-0.0872

Fig. 5.2: A typical fcc(111)//bcc(110) with fcc[11$\overline{2}$]// bcc[00$\overline{1}$] configuration. The extra space between the planes is not real; it has been inserted to provide a clearer view. Bcc atoms are dark, fcc atoms are light gray. Periodic boundaries were used in the x and y directions.

a density was chosen such that the fcc(111) and bcc(110) planes have the same plane density. A typical configuration is shown in Figure 5.2. For the simulation of lateral growth of a bcc seed, as in plane B of Figure 5.2, the EAM potential was used.

To study the 2-dimensional nucleation behaviour the same system was used but now with the bond counting interaction model. Besides the fcc(111)//bcc(110) interface orientation, an fcc(252)//bcc(110) with fcc[$\overline{5}$20]//bcc[$\overline{1}$00] interface was also used. Because with this orientation equal plane density cannot be created (as fcc (252) is not a closed packed plane), this system was created with almost equal densities for fcc and bcc (fcc density was slightly smaller than the bcc density). By keeping the number of fcc and bcc sites in the simulation volume equal every fcc atom can in principle find a bcc site.

The random sites were distributed according to a restrictedly random distribution. First, the system was divided in small cubic cells with a side length of $1.4r_b$. Then, N_{ran} random sites were inserted into each cell according to a uniform distribution. Unless noted otherwise $N_{ran} = 10$.

In all simulations a value of 10^{13} (sec^{-1}) was used for ν_0. The default value for Q is 0.872 eV. Most simulations were done at temperatures around 2500 K. This is for computational efficiency reasons as explained in Ref. [32].
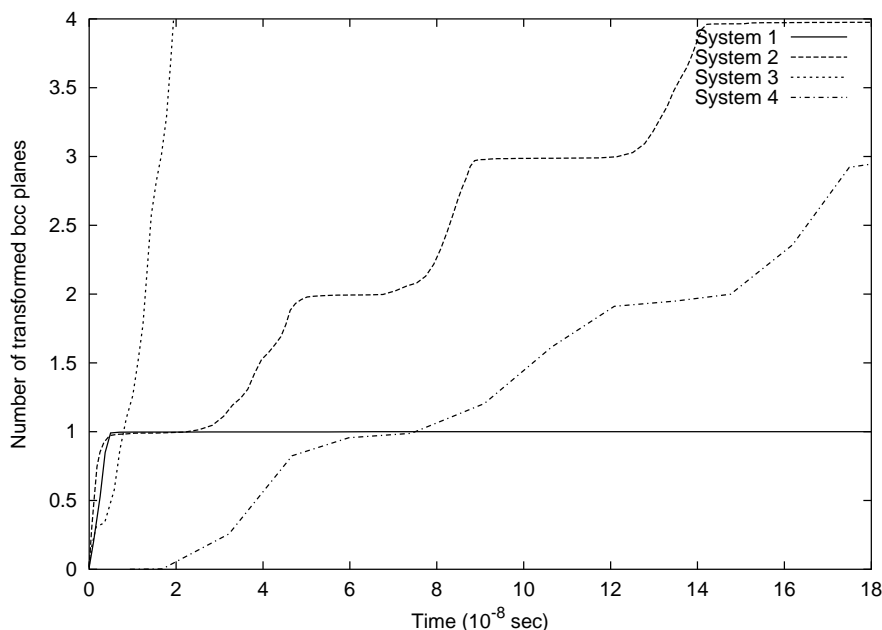
Fig. 5.3: Growth curves for four different simulation systems. Systems 1, 2 and 3 have an fcc(111)//bcc(110) and system 4 has an fcc(252)//bcc(110) interface orientation. For systems 1 and 4 the bond energies from set A, for system 2 the bond energies from set B and for system 3 the bond energies from set C (see Table 5.1) were used. All simulations pertain to $T = 2275$ K and were carried out with $N_{ran} = 0$.

5.4   Results

5.4.1   Nucleation behaviour

The growth curves of four different systems are shown in Figure 5.3. Systems 1, 2 and 3 have the same fcc(111)//bcc(110) interface orientation but pertain to different sets of bond energies.

With bond energy set A, i.e. system 1, (see Table 5.1) bcc is not able to nucleate in new planes (for example in plane A from Figure 5.2), only the artificially inserted bcc seed grows and then the transformation stops. With bond energy set B, i.e. system 2, which means a higher driving force and a lower interface energy (see Table 5.1), bcc is able to nucleate in new planes and a plane-by-plane growth mode is observed. For an even stronger driving force, bond energy set C (system 3), the continuous growth mode is observed, which means that the transformation takes place in several planes simultaneously. As opposed to system 1, for system 4 with an fcc(252)//bcc(110) interface orientation nucleation and growth with bond energy set A is possible.
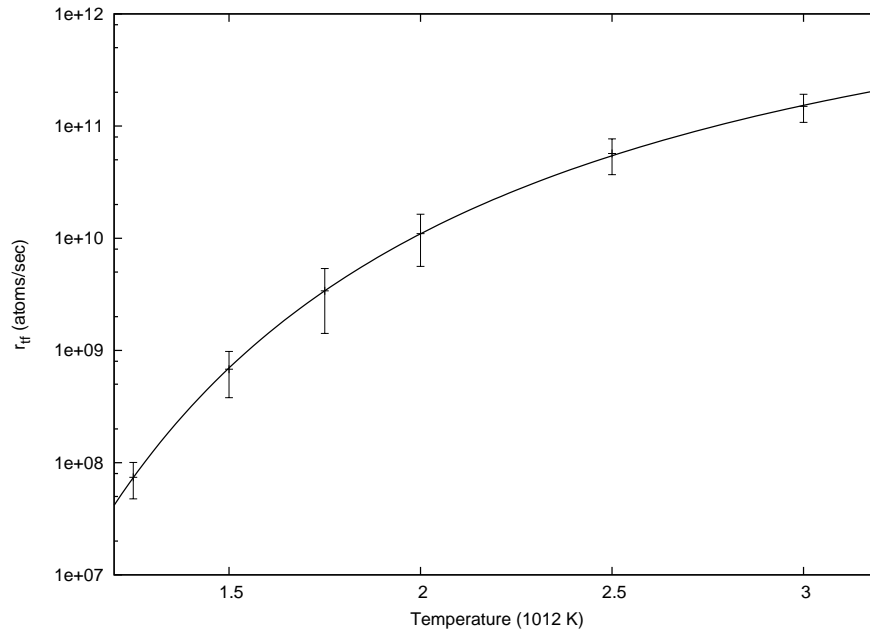
Fig. 5.4: The transformation rate as a function of temperature for a system containing 15 vacancies and with $Q = 0.872$ eV. All data points are an average from a minimum of 10 repetitions of the transformation simulation. The solid line is a fit of Eq. (5.8).

5.4.2 Interface mobility activation energy

Normally, the interface velocity, v is measured at a number of different temperatures and then the interface mobility activation energy, ΔG^a is found by fitting Eqns. (5.1) and (5.2). In the simulations the interface area is constant, which means that instead of v, the transformation rate, r_{tf} (in atoms/sec), can also be used to determine ΔG^a. The transformation rate is given by

$$r_{tf}(T) = C \exp\left(-\frac{\Delta G^a}{kT}\right)\left(1 - \exp\left(-\frac{\Delta U_{bcc,fcc}}{kT}\right)\right), \qquad (5.8)$$

where the entropy part of the driving force has been taken into the pre-exponential constant C and ΔG (cf. Eq. (5.1)) has been replaced with the fcc-bcc energy difference, $\Delta U_{bcc,fcc}$.

The transformation rate[2] as a function of temperature is shown in Figure 5.4 (for lateral growth in a fcc(111)//bcc(110) system using the EAM potential). By non-linear least squares fitting of Eq. (5.8) to the simulation data (with $\Delta U_{bcc,fcc} = 0.03$ eV)

$$\Delta G^a = 1.576 \pm 0.006 \text{ eV}$$

[2] An estimate for the transformation rate is determined by measuring the time between 20% and 80% completion of the transformation of the remaining fcc atoms of plane B in fig. 5.2 into bcc atoms.

is found. The value obtained for ΔG^a is almost twice as large as the value used for the single atomic jump energy barrier, Q (see Eq. (5.7) and Figure 5.1).

Simulations with different values for Q have shown that the difference between ΔG^a and Q is constant. This difference is called here the energy offset E_{off}, which can be written as

$$E_{\text{off}} = \Delta G^a - Q. \tag{5.9}$$

Because $E_{\text{off}} > 0$, it already follows that the transformation is controlled by energetically unfavourable jumps ($\Delta U > 0$, see Eq. (5.7)). It could be that one single type of jumps is rate determining, which would mean that $E_{\text{off}} = \Delta U_{\text{crit}}$. Here $E_{\text{off}} = 0.704$ eV. For simulations where all jumps with $\Delta U \in (0.628; 0.776)$ (in eV) were excluded, a new $E_{\text{off}}^{\text{excl}}$ of 0.76 ± 0.03 eV was found. Because $E_{\text{off}}^{\text{excl}} \in (0.628; 0.776)$ it follows that

$$E_{\text{off}} \neq \Delta U_{\text{crit}},$$

Hence, there is no single critical jump. It must be concluded that the interface mobility activation energy is determined by a series of jumps, i.e.

$$E_{\text{off}} = \sum_{i=1}^{N} \Delta U_i, \tag{5.10}$$

where N is the number of intermediate jumps. The exact size of N is unknown, but from the value of E_{off} and typical ΔU values N is expected to have a value of 4 or 5.

The series of unfavourable jumps performed by groups of atoms are required because most fcc atoms at the interface cannot directly jump to a bcc lattice site because all surrounding empty bcc sites are blocked by neighbouring (fcc) atoms (by overlap). Only by a complex multiple jump mechanism can every fcc atom find a place on the bcc lattice. On a local scale this means that the interface will often stop for a while (or even move backwards) and then suddenly move forward one or more atom rows.

If there is more room at the interface, the rearrangement process should be easier to accomplish. This has indeed been observed in our work for systems with different numbers of vacancies (created by removing atoms from plane B in Figure 5.2). Indeed, ΔG^a decreases with increasing vacancy content.

5.5 Discussion

Although both interface orientations considered in this work (fcc(111)//bcc(110) and fcc (252)//bcc(110)) are incoherent, the disorder at the interface is larger for the fcc(252)// bcc(110) orientation. This explains why the (2-dimensional) nucleation of new bcc planes is much easier in the fcc(252)//bcc(110) system (cf. system 1 vs. system 4 in Figure 5.3).
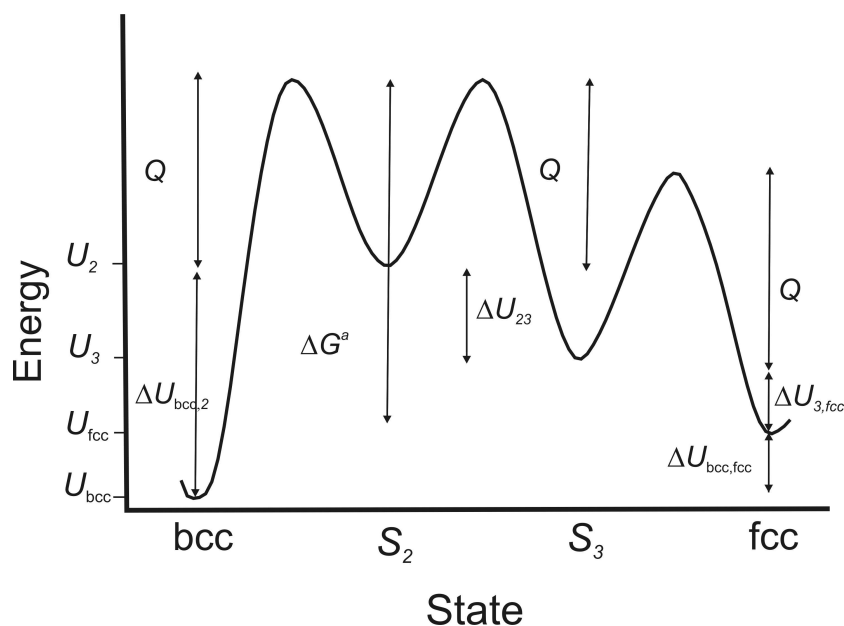
Fig. 5.5: A possible variation on a path from fcc to bcc (right to left) with two intermediate states. The energy barrier between all states (i.e. for single jumps) is constant (Q). The overall activation energy for this process ΔG^a is the difference between the maximum energy level and the energy level of the start state and thus $E_{\text{off}} = \Delta U_{23} + \Delta U_{3,fcc}$ (all ΔU-values are positive in this Figure).

In the fcc(111)//bcc(110) system the growth mode depends on the driving force and the bcc-fcc interface energy. With a high driving force and a low interface energy, the energy gain upon transformation is so large that the cost in energy on formation of a 2-dimensional bcc nucleus is no real barrier for nucleation. A more moderate driving force leads to a plane-by-plane growth mode. Which means that growth is much faster than nucleation, but nucleation can still occur. With an even smaller driving force, the growth mode parallels the well known ledge-wise growth mechanism and an external mechanism is required for the formation of new ledges.

Because ΔG^a is determined by series of unfavourable jumps by groups of atoms it follows that there are multiple intermediate states on the path from fcc to bcc, as schematically shown in Figure 5.5. On the basis of Figure 5.5 an exact expression for the interface velocity can be found (adopting the steady state constraint). If $U_{\text{bcc}} < U_{\text{fcc}} < U_2 < U_3$, ΔG^a is given by (cf. Eq. (5.1)):

$$\Delta G^a = Q + \sum_i^N \Delta U_i = Q + \Delta U_{23} + \Delta U_{3,\text{fcc}}. \tag{5.11}$$

If $U_3 < U_2$ (as in Figure 5.5) Eq. (5.1) is only a very good approximation (but holds over a large temperature range) [32].

As a first estimation for ΔG^a grain boundary diffusion activation energies, ΔG^a_{gb}, are often used [1]. However, experiments have shown that ΔG^a is often larger than ΔG^a_{gb} [27]. This difference is attributed to solute drag effects [1]. In the simulation system used here, the activation energy for volume diffusion ΔG^D_V is always equal to Q because $\Delta U = 0$ for bulk diffusion jumps. In reality ΔG^a_{gb} is smaller than ΔG^D_V because the activation energies for the atomic jumps in the grain boundary are lower. However, in the simulations the activation energy for any jump is always at least Q. Because many jumps in the boundary will have $\Delta U > 0$, ΔG^a_{gb} will be larger than Q. To be able to really compare ΔG^a, ΔG^a_{gb} and ΔG^D_V from simulations, all these activation energies should be determined with a variable (for every jump separately calculated) Q. This work is in progress.

5.6 Conclusion

The growth mode depends on the atomic interaction energies, i.e. the driving force and interface energy, and on the interface orientation. With the same atomic interaction settings, bcc will not grow unless an external nucleation mechanism is operative (comparable to ledge-wise growth) with an fcc(111)//bcc(110) and fcc[11$\overline{2}$]//bcc[00$\overline{1}$] interface orientation, whereas a system with an fcc(252)// bcc(110) with fcc[$\overline{5}$20]//bcc[$\overline{1}$00] interface orientation will grow by (2-dimensional) nucleation of new bcc(110) planes. This can be attributed to the more disordered structure of the fcc(252)//bcc(110) interface. By increasing the driving force for the transformation a plane-by-plane growth mode is obtained: growth is much faster then nucleation, but nucleation can occur. The continuous growth mode can be obtained by further increasing the driving force. Then nucleation is no longer an obstacle and growth takes place in several planes simultaneously.

Because the mobility activation energy is determined by energetically unfavourable jumps, the observed effective interface mobility activation energy is higher than the energy barrier for single atomic jumps. During the transformation most fcc atoms at the interface cannot jump directly to empty bcc sites because the empty bcc sites are blocked by other neighbouring atoms. Simulations where jumps within a certain energy range were excluded have shown that series of unfavourable jumps by groups of atoms are required for fcc atoms to find a path to the bcc lattice.

6. An atomistic study on the activation enthalpies for interface mobility and boundary diffusion in a massive transformation

C. Bos, F. Sommer and E.J. Mittemeijer

Abstract

In the multi-lattice kinetic Monte Carlo simulation of the fcc to bcc transformation in iron, the atoms can take position on the sites of the crystal lattices and on a number of sites randomly dispersed over the system to allow for irregularities in the atomic structure of transformation interfaces. Lateral growth simulations with an initial interface orientation of fcc(111)//bcc(110) and fcc[11$\overline{2}$]//bcc[00$\overline{1}$], provided data on the activation enthalpy for the interface mobility and the migration activation enthalpy for boundary diffusion. The results obtained allow a critical appraisal of rules of thumb proposed earlier for the relation between the activation enthalpies for interface mobility, grain-boundary diffusion and volume diffusion. In particular it is shown that, depending on the interface structure the interface migration activation enthalpy can be larger or smaller than the migration activation enthalpy for boundary diffusion.

6.1 Introduction

The massive transformation is a typical example of an interface controlled phase transformation. In the description of the kinetics of these transformations the interface mobility, M, is one of the key quantities. M, is generally written as [1]

$$M = M_0 \exp\left(-\frac{\Delta H^a}{k_B T}\right), \qquad (6.1)$$

with M_0 as the pre-exponential factor, ΔH^a as the activation enthalpy (the entropy part is contained in M_0), k_B as the Boltzmann constant and T as the temperature. The interface mobility is assumed to be determined by the mobility of the atoms at the interphase boundary and therefore it is usually claimed that the activation enthalpy for grain-boundary diffusion, ΔH^D_{GB}, would be a good estimate for ΔH^a for incoherent interfaces [1]. However,

experimental results [27, 39] show that on average values for ΔH^a are in between the activation enthalpy for boundary diffusion and the activation enthalpy for bulk diffusion, ΔH_{V}^D:

$$\frac{\Delta H_{\mathrm{GB}}^D}{\Delta H_{\mathrm{V}}^D} \in \left[\frac{1}{2}, \frac{2}{3}\right] \tag{6.2}$$

and

$$\frac{\Delta H^a}{\Delta H_{\mathrm{V}}^D} \geq \frac{2}{3}. \tag{6.3}$$

Recently, multi-lattice kinetic Monte Carlo (kMC) atomistic simulations have shown that the activation enthalpy for the interface mobility can be considerably larger than the activation enthalpy for a single jump at the boundary: ΔH^a is determined by series of energetically unfavourable jumps performed by groups of atoms rather than by single atomic jumps [32, 40]. A method, based on a neural network description, that allows the time efficient calculation of jump specific activation energies, E^a, was introduced in Ref. [40]. According to this method the activation energy for a jump can be calculated dependent on the local surroundings of the jumping atom.

The purpose of this work is to determine both ΔH_{GB}^D and ΔH^a from simulations with these variable, jump specific E^a-values. Then a valid comparison of these two activation enthalpies can be made.

Lateral growth of the α (bcc) product phase in a γ (fcc) to α (bcc) transformation in a single element system (iron) is simulated, with an initial interface orientation given by fcc(111)//bcc(110) and fcc[11$\overline{2}$]//bcc[00$\overline{1}$]. With this setup the temperature dependence of both the interface mobility and the boundary self diffusion have been examined.

6.2   Simulation method and settings

The multi-lattice kMC method as described in Refs. [20] and [40] allows the simulation of a phase transformation from one crystal structure to another, by incorporating both crystal structures as possible sites for the atoms. To allow the atoms at and near the moving interface to take intermediate positions between the lattice sites, a collection of randomly placed sites is also included. These intermediate positions allow for irregularities in the atomic structure of transformation interfaces [20].

The transformation is simulated by letting the atoms at the interface jump to a neighbouring empty site. The jump rate constant, k, is calculated by

$$k = \nu_0 \exp\left(-\frac{E^a}{k_B T}\right), \tag{6.4}$$

where E^a is calculated using a constrained conjugate gradient energy minimization method as presented in Ref. [34]. To reduce the calculation time of the simulations a neural net-
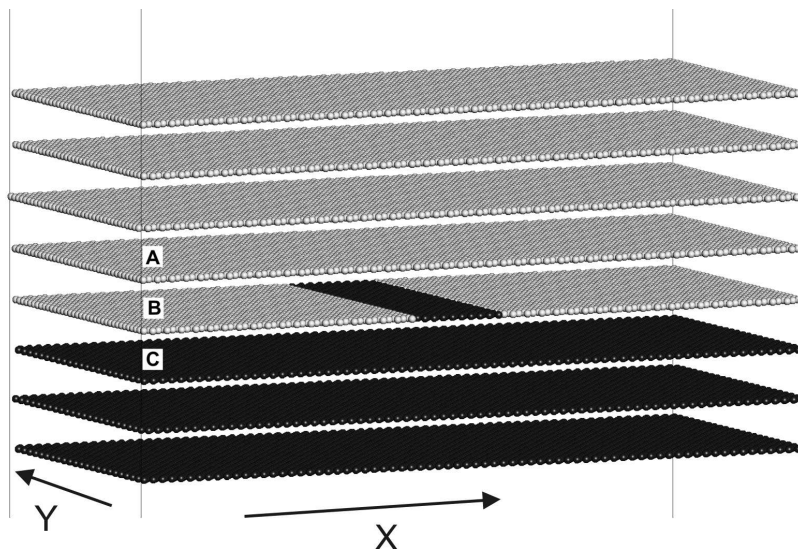
Fig. 6.1: A typical start configuration for the simulations. The extra space between the planes is not real; it has been inserted to provide a clearer view. Fcc atoms are light grey, bcc atoms are dark.

work is trained with data from over ten thousand jumps. The trained neural network is then used in the simulations to calculate E^a (with a mean square error of less than 2 percent).

The start configuration involves a bcc seed for the simulation of lateral growth in atomic plane B for the structure shown in Fig. 6.1.

The fcc and bcc crystals were created with equal planar density for the planes parallel to the interface (with bcc number density of $84.9 \cdot 10^{27}$ atoms/m^3). If vacancies were inserted in the system then they were created in plane B shown in Fig. 6.1 by removing fcc atoms. Periodic boundaries were used in both the x and y directions.

The random sites were distributed according to a restrictedly random distribution. First, the system was divided in small cubic cells with a side length of $1.4r_b$ (with r_b the bcc nearest neighbour distance). Then, N_{ran} random sites were inserted into each cell according to a uniform distribution.

In all simulations a value of 10^{13} (sec^{-1}) was used for ν_0 (cf. Eq. (6.4)). The atomic interaction energies were calculated using the Johnson-Oh embedded atom method potential for iron [33].

With these simulation settings the following analyses were made:

- The interface mobility activation enthalpy (here denoted as $\Delta H^{a,s}$, i.e. with an additional superscript 's'; cf. Eq. (6.1), to signify that it is the activation enthalpy as determined from the simulations, see also section 6.4) was determined by a non-

linear least squares fit to the obtained data for the transformation rate, r_{tf}[1], according to [32]:

$$r_{\text{tf}}(T) = C \exp\left(-\frac{\Delta H^{a,s}}{kT}\right)\left(1 - \exp\left(-\frac{\Delta U_{bcc,fcc}}{kT}\right)\right), \tag{6.5}$$

where C is a pre-exponential constant and $\Delta U_{bcc,fcc}$ (=0.03 eV) is the fcc-bcc energy difference.

- The activation enthalpy for vacancy migration in boundary self diffusion, ΔH_{GB}^m, was obtained from the determination of mean square atom displacements (MSD) [41] in a system with a completely flat interface (i.e. no bcc seed in plane B of Fig. 6.1) with a single vacancy at the interface (i.e. in plane B of Fig. 6.1). The summed square atom displacement (SSD) is given by

$$\text{SSD}(t, t_0) = \sum_{j=1}^{N_{\text{GB}}} \left(\mathbf{r}_j(t + t_0) - \mathbf{r}_j(t_0)\right)^2, \tag{6.6}$$

where t is time, N_{GB} is the number of atoms at the boundary (atoms with neighbours of both fcc and bcc type) and $\mathbf{r}_j$ is the position of atom j. If a represents the slope of a SSD vs. time plot then ΔH_{GB}^m can be found by a fit of

$$\ln(a) = C' - \frac{\Delta H_{\text{GB}}^m}{k_B T}, \tag{6.7}$$

with C' as a constant, to the data for a obtained at several temperatures, T.

For efficiency reasons all simulations were performed in the temperature range of 2000 to 3200 K (see also Appendix B of Ref. [32]).

6.3 Results

The results obtained for $\Delta H^{a,s}$ and ΔH_{GB}^m for different values of N_{ran} are shown in Table 6.1. The bcc bulk diffusion migration activation enthalpy, ΔH_{V}^m, (which is E^a from Eq. (6.4) for a vacancy jump in the bulk) was found to be

$$\Delta H_{\text{V}}^m = 1.34 \text{ eV}.$$

---

[1] An estimate for the transformation rate is determined by measuring the time between 20% and 80% completion of the transformation of the remaining fcc atoms in plane B as shown in Fig. 6.1.

Tab. 6.1: Interface mobility ($\Delta H^{a,s}$) and boundary self diffusion (ΔH_{GB}^m) migration activation enthalpies for different numbers of random sites in the system (σ is the standard error as obtained from the fit procedure [25]).

N_{ran}	$\Delta H^{a,s}$	$\sigma_{\Delta H^{a,s}}$	ΔH_{GB}^m	$\sigma_{\Delta H_{\mathrm{GB}}^m}$
-	(eV)	(eV)	(eV)	(eV)
0	1.14	0.06	1.46	0.02
4	1.06	0.06	1.37	0.03
8	1.04	0.05	1.45	0.11
15	0.98	0.03	0.80	0.12

6.4   Discussion

Usually, the activation enthalpy for the interface mobility (ΔH^a) is compared to the activation enthalpy for boundary self diffusion (ΔH_{GB}^D) and/or volume self diffusion (ΔH_{V}^D), where for incoherent boundaries ΔH^a is expected to be approximately equal to ΔH_{GB}^D, rather than equal to ΔH_{V}^D [1].

The activation enthalpy for self diffusion can be conceived as composed of a part due to migration (of a vacancy) and a part due to the formation of a vacancy [39]. Thus for boundary diffusion

$$\Delta H_{\mathrm{GB}}^D = \Delta H_{\mathrm{GB}}^m + \Delta H_{\mathrm{GB}}^f, \tag{6.8}$$

with ΔH_{GB}^f as the vacancy formation enthalpy at the boundary, and for volume diffusion

$$\Delta H_{\mathrm{V}}^D = \Delta H_{\mathrm{V}}^m + \Delta H_{\mathrm{V}}^f, \tag{6.9}$$

with ΔH_{V}^f as the bulk vacancy formation enthalpy. Normally, such a split is not made for ΔH^a. For reasons that will be explained below, here a comparison is now made of the migration activation enthalpies for volume diffusion (ΔH_{V}^m) and boundary diffusion (ΔH_{GB}^m) and the activation enthalpy for boundary mobility ($\Delta H^{a,s}$), as they were obtained from the simulations.

For all values of N_{ran}, $\Delta H^{a,s}$ is smaller than ΔH_{V}^m (Table 6.1). Only for the largest value of N_{ran}(=15) $\Delta H^{a,s}$ is larger than ΔH_{GB}^m; for the other values of N_{ran} (=0, 4 and 8) ΔH_{GB}^m is larger than $\Delta H^{a,s}$ (and, even, ΔH_{V}^m).

To interpret these results it is remarked that the activation energy for an atomic jump (E^a cf. Eq. (6.4)) can be written as

$$E^a = \Delta U + Q, \tag{6.10}$$

where ΔU is the change in system energy caused by the jump and Q is the energy barrier (see figure 6.2). For bulk vacancy diffusion $\Delta U = 0$ and Q always has the same
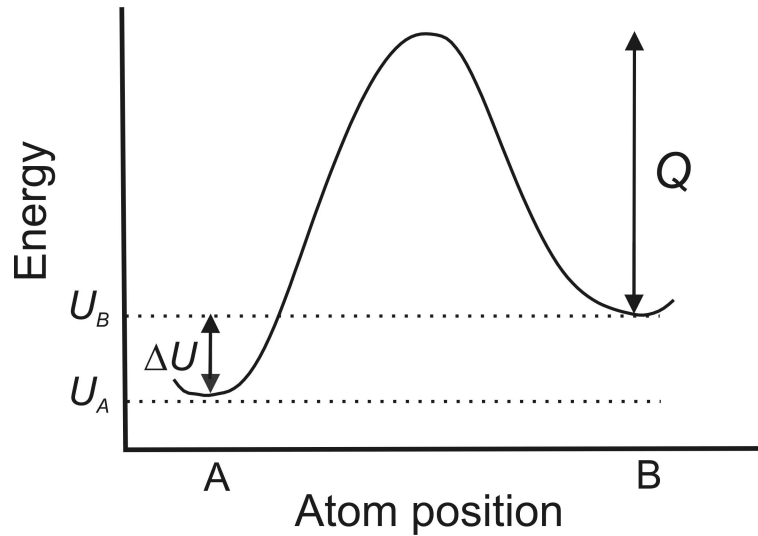
Fig. 6.2: For an atomic jump from position A to B the change in system energy caused by the jump, ΔU, is shown together with the change in system energy *during* the jump giving the energy barrier part, Q, of the activation energy.

value (here 1.34 eV; see section 6.3). For jumps at the boundary ΔU will generally be different from zero, because most atom positions at the boundary have different binding energies. Thus vacancies at the boundary can be trapped in energetically favourable positions (meaning that an unfavourable ($\Delta U > 0$) atom jump must be made for the vacancy to escape). At the boundary Q can be as large or smaller as in the bulk, but not larger. A 'vacancy trap' at the boundary where a positive ΔU-value is paired with a reasonably large Q-value can explain why $\Delta H_{\mathrm{GB}}^{m}$ can be larger than $\Delta H_{\mathrm{V}}^{m}$ (again note: activation enthalpies for *migration* of a vacancy are compared here). For relatively large numbers of random sites these traps are less likely to occur, because there will be more jump possibilities, which increases the chance that a jump with either a smaller ΔU or smaller Q-value can be found to escape the trap. Accordingly, $\Delta H_{\mathrm{GB}}^{m}$ becomes smaller than $\Delta H_{\mathrm{V}}^{m}$ for large values of N_{ran}, as observed.

For the movement of the interface (during the transformation from fcc to bcc) a number of difficult jumps could be required at a certain part of the interface and this would slow down the interface movement (locally). In the meantime relatively easy jumps in a neighbouring part of the interface could change the structure in such a way that the difficult jumps in the first mentioned part of the interface are no longer necessary. Visualization of the movement of the atoms during the transformation for the simulations performed in this work, has indeed shown that often a small part of the interface is not moving until a transformation in a neighbouring part of the interface takes place thereby allowing easier atom jumps at (the edges of) the (previously) immobile part. This means that the transformation can take place by relatively easy jumps only, explaining why, even with low values for N_{ran}, $\Delta H^{a,s}$ is always smaller than $\Delta H_{\mathrm{V}}^{m}$. In Refs. [32, 40] it was shown
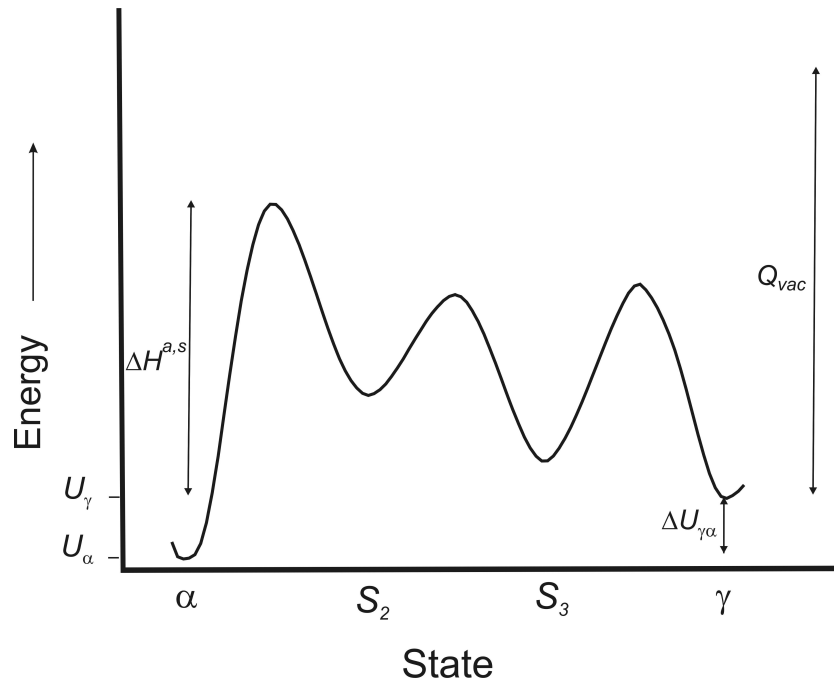
Fig. 6.3: A possible variation in system energy on a path from the γ phase to the α phase (right to left) with two intermediate states. For comparison the size of the energy barrier for migration in volume vacancy diffusion, Q_{vac}, has also been indicated. Q_{vac} is larger than the interface mobility activation enthalpy, $\Delta H^{a,s}$.

that $\Delta H^{a,s}$ is not determined by single jumps but by series of energetically unfavourable jumps performed by groups of atoms. Then, the result $\Delta H^{a,s} < \Delta H_V^m$, implies that all the jumps in the series of unfavourable jumps have significantly lower Q-values than the Q-value for volume diffusion, as shown schematically in figure 6.3.

Simulations with different vacancy content have shown that with more free space (more vacancies) at the interface, a path from fcc to bcc is easier found, leading to higher interface mobilities [32, 40]. Vacancies (artificially) inserted in the simulation system will often be 'smeared out' over the interface. The series of unfavourable atom jumps can be seen as rearrangements of the locally available free space to the necessary volumes and/or (continuous) shapes of free space to enable jumps from fcc to bcc. Therefore, $\Delta H^{a,s}$ can be said to contain a 'formation' enthalpy part of an appropriate volume of free space (probably up to the size of the atomic volume). This 'formation' part of the activation enthalpy must not be confused with a contribution of formation enthalpy to the activation enthalpy for the interface mobility due to the possible temperature dependence of the the amount of free space (vacancy content), which latter contribution does not occur in the current simulations because the amount of free space is kept constant and determined only by the (chosen) initial simulation configuration (the interface orientation and the number of (artificial) vacancies in the system). If, in nature, the intrinsic (configuration determined) amount of free space is sufficient the activation enthalpy for the interface mobility

ΔH^a will be given by $\Delta H^{a,s}$. If this intrinsic amount of free space is insufficient, then the effect of thermal activation of the amount of free space (vacancies) becomes significant and thus ΔH^f_{GB} must be included in $\Delta H^{a,s}$ to obtain ΔH^a. This is the reason that in the above discussion $\Delta H^{a,s}$ was directly compared to the *migration* activation enthalpies for boundary and bulk diffusion. It has been shown by simulations that, $\Delta H^{a,s}$ depends on the (constant, i.e. temperature independent) number of vacancies in the system [40]. This indicates that ΔH^a cannot be written as a simple sum of constant contributions $\Delta H^{a,s}$ and ΔH^f_{GB} (as in Eqns. (6.8) and (6.9)).

For different interface orientations the amount of intrinsic free space (see above) will be different. The simulations reported here, were all performed with a relatively high vacancy concentration[2]. Preliminary simulations with less vacancies suggest that, for the current interface orientation where the closest packed planes in γ (fcc) and α (bcc) are parallel at the interface, it is very probable that the amount of intrinsic free space is insufficient to induce the transformation.

The vacancy formation enthalpy will be higher in the bulk than at the interface [42]. Thereby, in particular for the highest (and therefore most realistic[3]) number of random sites in the system ($N_{\mathrm{ran}} = 15$, see Table 6.1) ΔH^D_{GB} can satisfy the range of values indicated by Eq. (6.2).

Now, in order to compare ΔH^a, ΔH^D_{GB} and ΔH^D_{V} there are two possibilities. Depending on the amount of intrinsic free space at the interface, either (i) a vacancy formation enthalpy must be added to $\Delta H^{a,s}$ to obtain ΔH^a, or (ii) a vacancy formation enthalpy must not be added to $\Delta H^{a,s}$ to obtain ΔH^a (see above). In the first case, the total combined interface mobility activation enthalpy (ΔH^a) will be larger than ΔH^D_{GB} (see Table 6.1 for the most realistic[3], high number of N_{ran} (=15) and where it is assumed that ΔH^f_{GB} and $\Delta H^{a,s}$ can be simply added to get ΔH^a; see the discussion above), which is in agreement with experimental observations indicated by Eq. (6.3). In the second case, $\Delta H^a < \Delta H^D_{\mathrm{GB}}$, which result agrees with molecular dynamics simulations on grain-boundary migration and self diffusion in copper [38].

6.5   Conclusion

Simulations with variable, surroundings specific, activation energies for atomic jumps have shown that the (migration parts of the) activation enthalpies for interface mobil-

---

[2] The bcc nucleus inserted in plane B of figure 6.1 does not fit perfectly in the surrounding fcc matrix, which means that less bcc atoms are inserted than fcc atoms are removed. The number of vacancies created in the remaining fcc part of plane B in this way is relatively large (comparable to the equilibrium vacancy concentration at a (virtual) temperature of 2200 K).

[3] In reality, atoms at the interface can take any position and are not limited to a fixed set of possible sites. Therefore a high number of random sites in the system provides a better approximation of reality. The number of random sites that can be included in the simulations is limited by the available computer hardware.

ity and for boundary self-diffusion depend on the number of random sites in the system (which allow for irregularities in the atomic structure of interfaces).

Because the change in system energy can be non-zero for atomic jumps in the boundary as opposed to atomic jumps in the bulk, the migration activation enthalpy for boundary diffusion can be larger than the migration activation enthalpy for bulk diffusion, in particular if the number of random sites in the system is low. The chance that a relatively easy jump is available for a vacancy at the interface becomes large with a high number of random sites in the system and then the migration activation enthalpy for boundary diffusion is lower than the migration activation enthalpy for bulk diffusion.

The 'migration' activation enthalpy for the interface mobility, as determined for a case of large amount of intrinsic free space at the interface, is always lower than the migration activation enthalpy for bulk diffusion, and is higher than the migration activation enthalpy for boundary diffusion provided the number of random sites in the system is high (which is the most realistic case).

Dependent on the amount of intrinsic free space at the interface, the activation enthalpy for the interface mobility can or cannot contain a contribution due to the formation enthalpy of a vacancy in the interface. On that basis the activation enthalpy for the interface mobility can be either larger or smaller than the total (= migration + formation) activation enthalpy for grain-boundary diffusion.

7. Zusammenfassung

7.1 Einführung

Für eine grenzflächen-kontrollierte Phasenumwandlung wird die Umwandlungsgeschwindigkeit von Prozessen an der Grenzfläche bestimmt. Die massive Umwandlung ist ein typisches Beispiel für eine grenzflächen-kontrollierte Phasenumwandlung. Eines der technologisch wichtigsten Beispiele ist die Austenit zu Ferrit Umwandlung, die in Eisenlegerungen als massive Umwandlung auftreten kann.

In letzter Zeit hat die massive Umwandlung erneut viel Aufmerksamkeit erhalten [2, 14, 15], wobei insbesondere der Mechanismus der Umwandlung diskutiert [16] wird. Die verfügbaren experimentellen Ergebnisse sind größtenteils erst nach der Umwandlung gemessen worden. Um den Mechanismus der Umwandlung besser zu verstehen, werden Informationen zur Grenzflächenstruktur benötigt, die während der Umwandlung gemessen werden. Hierzu gibt es nur wenige experimentelle Ergebnisse [3, 16].

Die Anwendung der "molecular dynamic" (MD) Methode zur Untersuchung der martensitischen Umwandlung hat gezeigt, daß MD Simulationen geeignet sind um die Struktur einer sich bewegenden Grenzfläche auf atomarer Ebene zu untersuchen [4–6]. Seit kurzem werden MD Simulationen auch zur Untersuchung der Bewegung ebener Grenzflächen während des Kornwachstums in Kristallen benutzt [31, 38].

Die Zeitdauer einer massiven Umwandlung ist jedoch generell zu lang um mit der MD Methode simuliert zu werden. In MD Simulationen werden die Atombewegungen kontinuierlich beschrieben. Um die Zeitdauer zu verlängern, die simuliert werden kann, können Berechnungen mit der "kinetic Monte Carlo" (kMC) Methode durchgeführt werden. Hier sind die möglichen Positionen der Atome auf diskrete ("Gitter") Plätze beschränkt, und die Bewegung der Atome verläuft über stochastische Sprünge.

Monte Carlo Methoden sind bisher erfolgreich zur Simulation von Festkörper-Gas und Festkörper-Flüssigkeit Umwandlungen eingesetzt worden [7–9, 11] . Hierbei wird aber nur von einem Kristallgitter für mögliche Positionen der Atome ausgegangen. Für Festkörper-Festkörper Umwandlungen ist es erforderlich, daß die Atome Positionen auf mindestens zwei Gitter einnehmen können, hierzu ist in dieser Arbeit eine "*multi-lattice kinetic Monte Carlo*" (mlkMC) Methode entwickelt worden.

Diese Arbeit beschreibt die neu entwickelte mlkMC Methode sowie ihre Anwendung zur Untersuchung der massiven Umwandlung von einem kubisch flächenzentrierten (fcc) Gitter zu einem kubisch raumzentrierten (bcc) Gitter für ein reines Metall (Eisen).

7.2 Die multi-lattice kinetic Monte Carlo Methode

Um ein Mehrphasensystem zu beschreiben werden in der mlkMC Methode gleichzeitig unterschiedliche Gitter als mögliche Plätze für die Atome verwendet. Zu jeder gegebenen Zeit ist nur ein Teil der Gitterpositionen besetzt. Die Umwandlung wird durch Atomsprünge von besetzten zu unbesetzten Plätze simuliert. Um es den Atomen an und nahe der sich bewegenden Grenzfläche zu ermöglichen Positionen zwischen den Gitterplätzen einzunehmen, wird eine Anordnung zufällig ausgewählter Plätze in das Simulationssystem aufgenommen. Diese Zwischenplätze lassen das Auftreten von Unregelmäßigkeiten in der Atomstruktur der Grenzfläche zu.

In dieser Arbeit werden zwei unterschiedliche Simulationsalgorithmen verwendet. Im ersten Algorithmus wird ein Atom an der Grenzfläche zufällig ausgewählt. Dann wird ein benachbarter leerer Platz zufällig als sein Zielplatz ausgewählt. Der Sprungchance, p, wird berechnet mit

$$p = \frac{\exp\left(-\frac{\Delta U}{k_B T}\right)}{1 + \exp\left(-\frac{\Delta U}{k_B T}\right)}, \tag{7.1}$$

wobei ΔU die Energieänderung durch den Sprung, T die Temperatur und k_B die Boltzmann Konstante ist. Indem man p mit einer zufällig gewählten Zahl zwischen null und eins vergleicht, wird der Sprung entweder angenommen oder zurückgewiesen. Bei diesem Algorithmus wird die Zeit in Monte-Carlo Schritten ausgedrückt.

Im zweiten Algorithmus wird die Summe der Rate, k, jedes möglichen Sprungs im System errechnet mit

$$K_{\text{sum}} = \sum_{i=1}^{N_{\text{jump}}} k_i. \tag{7.2}$$

Als nächstes wird der erste Sprung, a, mit

$$\sum_{i=1}^{a} k_i \geq R_1. \tag{7.3}$$

ausgewählt, wobei R_1 eine zufällig gewählte Zahl zwischen null und eins ist.

Mit diesem Algorithmus kann die Zeit zwischen den Sprüngen, Δt, berechnet werden mit

$$\Delta t = -\left(\frac{1}{K_{\text{sum}}}\right) \ln(R_2), \tag{7.4}$$

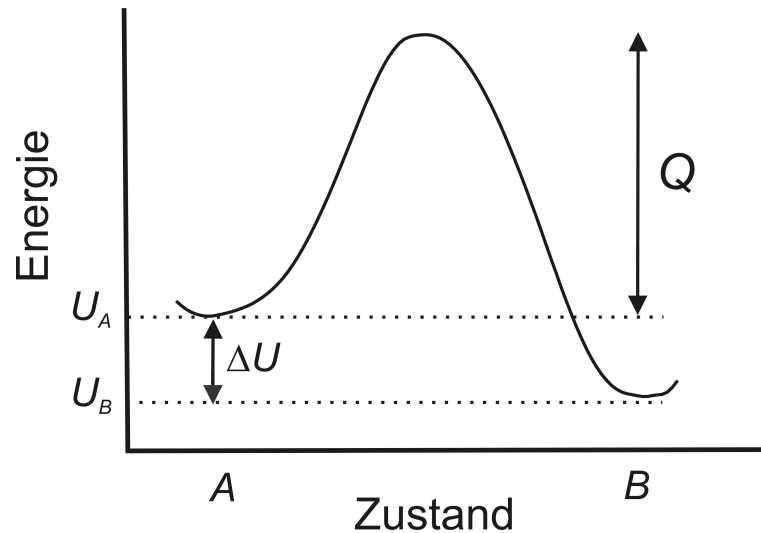wobei R_2 eine zweite zufällig gewählte Zahl zwischen null und eins ist.

Fig. 7.1: Schematische Änderung der Energie entlang des Pfades eines Atomsprungs von Platz A zu Platz B.

Die Sprungrate wird mit Hilfe der "simple transition state theory" (s. z.B. Ref. [24]) berechnet mit

$$k = \nu_0 \exp\left(-\frac{E^a}{k_B T}\right),$$ (7.5)

wobei ν_0 ein konstanter präexponentieller Faktor und E^a die Aktivierungsenergie für den Sprung ist.

Zur Berechnung vom E^a in Gleichung (7.5) gibt es zwei Möglichkeiten. Einmal wird angenommen, daß jeder Sprung die gleiche Energiebarriere Q aufweist, (s. Abbildung 7.1). Damit ergibt sich für Gleichung (7.5)

$$k = \begin{cases} \nu_0 \exp\left(-\frac{Q+\Delta U}{k_B T}\right) & \text{falls } (\Delta U > 0) \\ \nu_0 \exp\left(-\frac{Q}{k_B T}\right) & \text{sonst} \end{cases}.$$ (7.6)

E^a kann auch für jeden Sprung bestimmt werden. Dazu wird das springende Atom in kleinen Schritten in Richtung des Zielplatzes bewegt. Nach jedem Schritt wird die Energie des Systems mit einer "constrained conjugate gradient" (CCG) Methode minimalisiert. E^a ist dann die Differenz zwischen der höchsten auftretenden Energie und der Ausgangsenergie des Systems.

Zur Berechnung von ΔU wird ein Modell für die atomare Wechselwirkungen benötigt. In dieser Arbeit werden zwei Modelle benutzt: ein einfaches Bindungsmodell und das *"embedded atom method"* [18, 19] (EAM) Potential. Im Bindungsmodell wird für alle Bindungen eine konstante Energie unabhängig von der Entfernung zwischen den Atomen angenommen. In der Simulation einer Phasenumwandlung von fcc zur bcc gibt es insgesamt fünf unterschiedliche Bindungsenergien: u_{bb} für eine bcc-bcc Bindung, u_{ff} für eine

fcc-fcc Bindung, u_{bf} für eine gemischte bcc-fcc Bindung, u_{rf} für eine Bindung zwischen einem fcc Atom und einem Atom auf einem zufälligen Platz und u_{rb} für eine Bindung zwischen einem bcc Atom und einem Atom auf einem zufälligen Platz.

Das Bindungsmodell hat den Vorteil, daß die Triebkraft für die Umwandlung ($\Delta U_{bcc,fcc}$ = $\frac{1}{2}(8u_{bb}-12u_{ff})$) und die Grenzflächenenergie fast beliebig gewählt werden können. Das EAM Potential erzeugt dagegen realistischere Werte für die Wechselwirkungsenergie.

Die CCG Methode zur Minimalisierung der Systemenergie, notwendig zur Bestimmung von E^a, kann nicht in Kombination mit dem Bindungsmodell benutzt werden. Die Berechnung von E^a ist sehr rechenaufwendig und kann deshalb nicht direkt in der Simulation angewendet werden ohne zu unakzeptabel langen Rechenzeiten zu führen. Es ist aber möglich ein neurales Netz mit Daten von einigen zehntausend Sprüngen zu trainieren (die mit der CCG Methode zur Minimalisierung der Systemenergie ausgerechnet werden können). Mit dem trainierten neuralen Netz kann E^a während einer Simulation für jeden Sprung einzeln ausgerechnet werden. Das neurale Netz benötigt folgende Eingabe-Parameter: die Systemenergie vor und nach dem Sprung, die Sprunglängen sowie die Abstände von 14 Nachbarn, die der Linie zwischen Start- und Zielposition des springendes Atoms am nächsten liegen. Mit diesen Parametern kann E^a mit einer mittleren Abweichung kleiner als zwei Prozent berechnet werden.

7.3   Simulationsszenarien

Die Mehrheit der Simulationen wurde mit der gleichen fcc(111)//bcc(110) und fcc[11$\overline{2}$]// bcc[00$\overline{1}$] Grenzflächenorientierung ausgeführt. Es werden die Grenzflächen eines reinen Metalls betrachtet, wobei die fcc (111) und die bcc (110) Ebenen die gleiche Flächedichte haben. Eine typische Ausgangskonfiguration zeigt Abbildung 7.2.

Es wurden Simulationen zur Untersuchung folgender Phänomen durchgeführt:

Wachstumsverhalten Der Einfluß der gewählten Bindungsenergie-Werte auf das Wachstumsverhalten wurde untersucht.

Keimbildung Das zwei-dimensionale Keimbildungsverhalten der bcc Phase wurde durch die Bildung von kreisförmigen Keimen in Ebene B (s. Abbildung 7.2) untersucht. Die Simulationen wurden mit dem einfachen Bindungsmodell durchgeführt.

Grenzflächenmobilität Um die Aktivierungsenergie der Grenzflächenmobilität zu untersuchen, wurden Simulationen des laterale Wachstums von einem Keim in Ebene B (s. Abbildung 7.2) mit dem zweiten Algorithmus ausgeführt. Die Energieberechnungen wurden sowohl mit dem einfachen Bindungsmodell als auch mit einem Eisen-EAM-Potential [33] durchgeführt. Es wurden sowohl Simulationen mit kon-
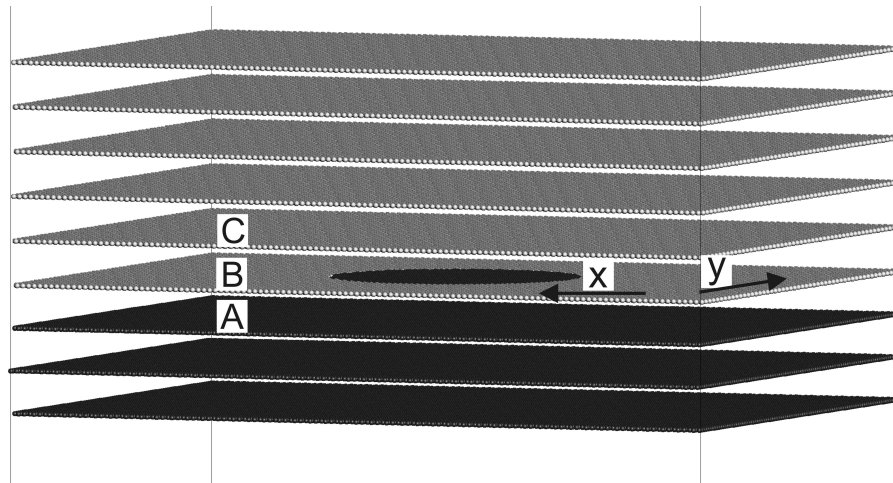
Fig. 7.2: Eine typische fcc(111)//bcc(110) Konfiguration. Der zusätzliche Abstand zwischen den Ebenen dient nur der Veranschaulichung. Bcc Atome sind dunkel eingezeichnet, fcc Atome grau. Für die x und y Richtungen wurden periodische Randbedingungen verwendet.

stantem Q-Wert, als auch mit Q-Werten, die für einzelne Atom-Sprünge mit dem neuralen Netz berechnet wurden, durchgeführt.

Grenzflächendiffusion Um die Aktivierungsenergie der Grenzflächenselbstdiffusion zu untersuchen, wurde die Bewegung einer Leerstelle in Ebene B (s. Abbildung 7.2, aber ohne bcc Keim) mit dem zweiten Algoritmus simuliert. Die Energieberechnungen wurden mit der Eisen-EAM-Potential durchgeführt. Es wurden Simulationen mit Q-Werten, die für einzelne Atom-Sprünge mit dem neuralen Netz berechnet wurden, durchgeführt.

In fast allen Simulationssystemen sind zufällig ausgewählte Plätze aufgenommen worden, die nach einer begrenzt zufälligen Verteilung hinzugefügt wurden. Hierzu wird zuerst das System in kleine kubische Zellen mit einer Länge von $1.4r_b$ aufgeteilt (r_b ist der nächste Nachbarn Abstand im bcc Gitter) und dann werden die Zellen nach einer stetigen Gleichverteilung mit zufälligen Plätze gefüllt.

7.4   Ergebnisse

7.4.1   Wachstumsverhalten

In Simulationen mit dem einfachem Bindungsmodell wird die Triebkraft für die Umwandlung durch die Differenz der Bindungsenergie einer bcc-bcc und einer fcc-fcc Bindung bestimmt. Für Simulationen, die mit einer ebenen Grenzfläche anfangen (s. Abbildung 7.2) wurden zwei unterschiedliche Wachstumsverhalten beobachtet. Bei großer
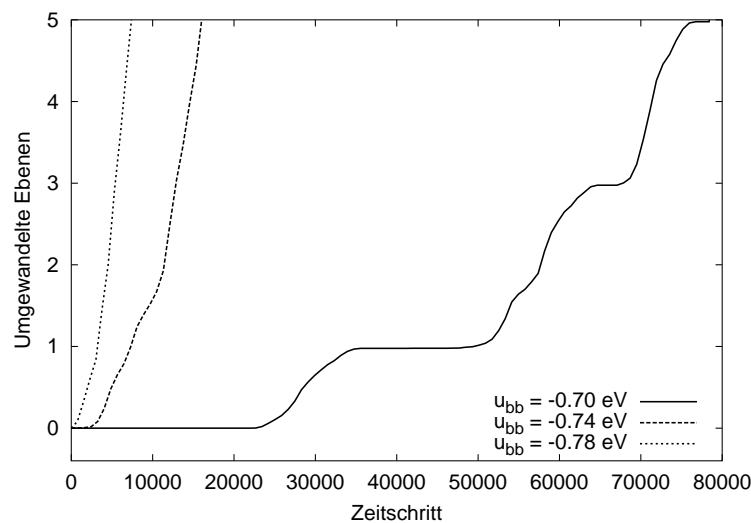
Fig. 7.3: Die drei Umwandlungskurven zeigen, wie der Wachstumsmodus sich mit ab-
nehmender bcc-bcc Bindungsenergie ändert.

Triebkraft verläuft das Wachstum kontinuierlich und die Grenzfläche erstreckt sich über
mehrere atomare Ebenen (bei Wachstumsbeginn parallel zur Grenzfläche). Bei niedri-
ger Triebkraft ändert sich das Wachstumsverhalten. Zuerst wird eine Ebene vollständig
umgewandelt bevor die Umwandlung in der nächsten Ebene anfängt. Bei diesem Wachs-
tumsverhalten ist die zweidimensionale Keimbildung von bcc in der nächsten fcc Ebene
(wie z.B. in Ebene C, s. Abbildung 7.2) schwieriger, so daß eine Wartezeit zwischen der
Umwandlung einzelner Ebenen vorliegt (s. Abbildung 7.3).

7.4.2 Keimbildung

Abbildung 7.4 zeigt die Änderung der Systemenergie wenn kreisförmige bcc Keime un-
terschiedlicher Größe in Ebene B in Abbildung 7.2 eingesetzt werden. Der kritischer
Keimsradius r^* lässt sich aus der $\Delta U(r)$ Abhängigkeit (s. Abbildung 7.4) einfach be-
stimmen. Die Simulationen haben bestätigt, daß Keime mit einem Radius kleiner als r^*
schrumpfen, während größere Teilchen wachsen. Die gestrichelte Linie in Abbildung 7.4
ist eine Fit von

$$\Delta U_{\mathrm{nucleus}} = \pi r^2 d \Delta U_V + 2\pi r d\gamma, \tag{7.7}$$

wobei r de Keimradius, ΔU_V die fcc-bcc Energiedifferenz pro Volumeneinheit, γ die
Grenzflächenenergie pro Fläche und d die Dicke einer Atomebene ist. ΔU_V und γ können
als Funktion der Bindungsenergie berechnet werden, wobei diese Werte sehr gut mit den
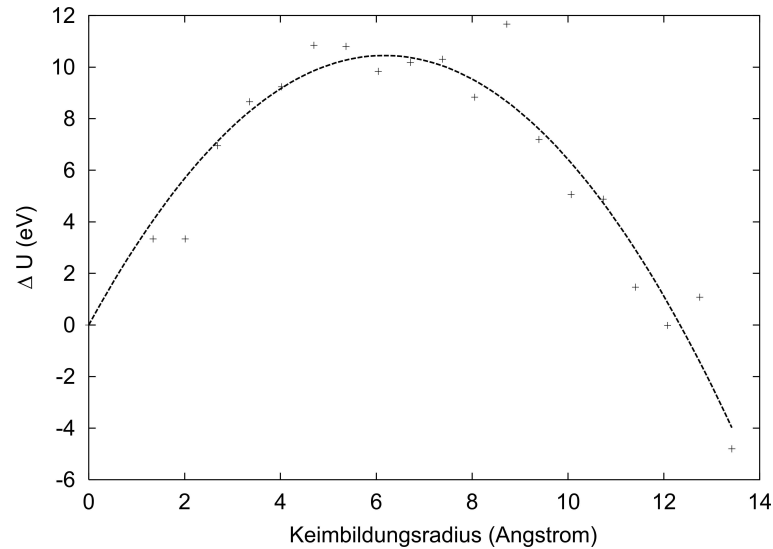Werten aus der Fit von Gleichung (7.7) übereinstimmen.

Fig. 7.4: Die Änderung der Systemenergie durch Einbringung von bcc Keimen in einer fcc Ebene an der fcc/bcc Grenzfläche. Die gestrichelte Linie zeigt den (kleinste Fehlerquadrate) Fit der Gleichung (7.7) an die "gemessenen" Daten.

7.4.3 Grenzflächenmobilität

Die Aktivierungsenergie der Grenzflächenmobilität kann durch einen Fit von

$$r_{\text{tf}}(T) = C \exp\left(-\frac{\Delta G^a}{kT}\right)\left(1 - \exp\left(-\frac{\Delta U_{bcc,fcc}}{kT}\right)\right), \tag{7.8}$$

wobei C eine Konstante und $\Delta U_{bcc,fcc}$ die fcc-bcc Energiedifferenz ist, mit den bei verschiedenen Temperaturen aus Simulationen berechneten Umwandlungsgeschwindigkeiten, r_{tf}, bestimmt werden.

Simulationen mit konstantem Q-Wert haben gezeigt, daß die Differenz zwischen Q und ΔG^a bei ansonsten gleichen Bedingungen konstant ist. Diese Differenz wird "Energieoffset" E_{off} genannt:

$$E_{\text{off}} = \Delta G^a - Q. \tag{7.9}$$

E_{off} ist immer positiv. Aus $\Delta G^a > Q$ folgt, daß die Umwandlungsgeschwindigkeit durch energetisch ungünstige Sprünge bestimmt wird ($\Delta U > 0$ s. Gleichung (7.6)).

Auf der Basis von Simulationen, bei denen alle Sprünge mit einem ΔU-Wert in der Nähe von E_{off} herausgefiltert wurden, konnte gezeigt werden, daß ΔG^a durch Gruppen von energetisch ungünstigen Atom-Sprüngen bestimmt wird. Dies bedeutet, daß der Energiepfad zwischen fcc und bcc mehrere Zwischenzustände enthält. Abbildung 7.5 zeigt ein Beispiel hierzu.

Die Sprungeffizienz ist definiert als die Anzahl der umgewandelten Atome pro Atom-Sprung. Es kann gezeigt werden, daß nur ein Energiepfad mit mehreren Zwischenzuständen zu einer Steigerung der Sprungeffizienz bei steigender Temperatur führen kann. In
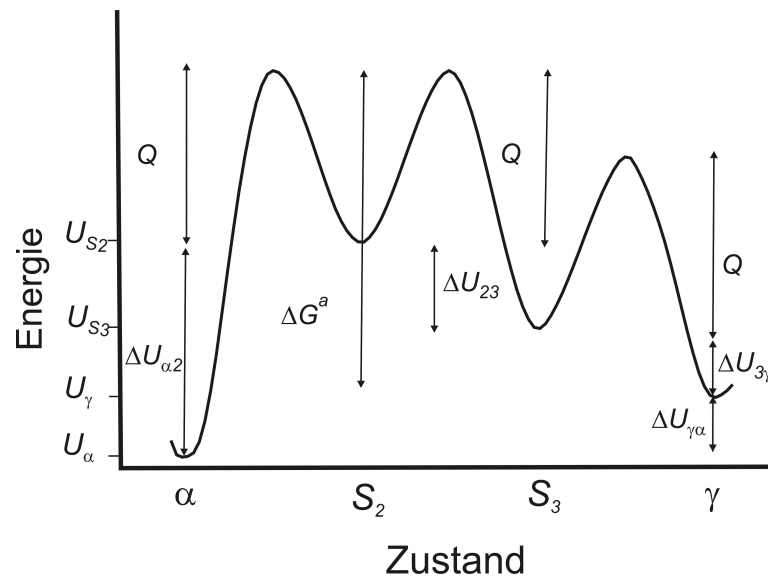
Fig. 7.5: Schematische Zeichnung eines Energiepfads von der fcc (γ) Phase zur der bcc (α) Phase mit zwei Zwischenzuständen. Die Energiebarriere zwischen allen Zuständen (für einzelnen Sprünge) ist konstant (Q). Die gesammte Aktivierungsenergie für diesen Prozess, ΔG^a, ist die Differenz zwischen der höchsten Energie und der Energie des Anfangszustands.

den Simulationen steigt die Sprungeffizienz bei steigender Temperatur, wodurch bestätigt wird, daß ΔG^a tatsächlich von Gruppen energetisch ungünstiger Sprünge bestimmt wird.

Eine detaillierte Analyse der Bewegung der Atome an der Grenzfläche hat gezeigt, daß die fcc Atome in den meisten Fällen nicht direkt auf einen bcc Gitterplatz springen können, da alle benachbarten bcc Gitterplätze von anderen Atomen blockiert werden. Ein komplizierter Umordnungsprozeß stellt einen Weg für die Atome von fcc zu bcc zur Verfügung, der über mehrfache Zwischenzuständen führt. Wenn mehr Raum an der Grenzfläche zu Verfügung steht, ist es für die Atome einfacher, einen Weg zum neuen Gitter zu finden, was zu einem niedrigeren Wert für ΔG^a führt. Dies wurde in Simulationen mit unterschiedlicher Leerstellenkonzentration gezeigt, sowie in Simulationen mit unterschiedlicher Grenzflächenorientierung.

Alle Schlussfolgerungen gelten sowohl für beide Energiemodelle (das einfache Bindungsmodell und das EAM-Potential) als auch für Simulationen mit konstanten Q-Wert und Simulationen bei dem ein neurales Netz die Q-Werte für die einzelnen Atom-Sprünge berechnet.

7.4.4 Grenzflächendiffusion

Die Wanderungs-Aktivierungsenergie der Grenzflächenselbstdiffusion, ΔG_{GB}^m wird aus "Mean Square Displacement" Messungen bestimmt. Die "Sum Squared Displacement" (SSD) wird berechnet mit

$$\mathrm{SSD}(t, t_0) = \sum_{j=1}^{N_{\mathrm{GB}}} \left(\mathbf{r}_j(t + t_0) - \mathbf{r}_j(t_0) \right)^2, \tag{7.10}$$

wobei t die Zeit, N_{GB} die Zahl der Grenzflächenatome und $\mathbf{r}_j$ die Position von Atom j ist. Falls a die Tangente einen SSD(t) Darstellung ist und für einige Temperaturen bestimmt wurde, kann ΔG_{GB}^m durch ein Fit von

$$\ln(a) = C' - \frac{\Delta G_{\mathrm{GB}}^m}{k_B T}, \tag{7.11}$$

bestimmt werden, wobei C' eine Konstante ist.

Die Simulationen haben gezeigt daß ΔG_{GB}^m von der Zahl der zufällig ausgewählte Plätze im System abhängig ist. Bei größer werdender Zahl dieser Plätze wird ΔG_{GB}^m niedriger. Bei einer Dichte von 15 zufällig ausgewählten Plätzen pro Zelle (s. Paragraph 7.3) ist ΔG_{GB}^m niedriger als der aus der Simulationen arhaltene Wert für ΔG^a.

References

[1] J. W. Christian, The theory of transformations in metals and alloys, Pergamon Press, Oxford, 2002.

[2] H. I. Aaronson, Metall. Mater. Trans. A 33A (2002) 2285–2297.

[3] J. M. Howe, W. T. Reynolds, V. K. Vasudevan, Metall. Mater. Trans. A 33A (2002) 2391–2411.

[4] P. Entel, R. Meyer, K. Kadau, Phil. Mag. B 80 (2) (2000) 183–194.

[5] J. V. Lill, Q. Broughton, Phys. Rev. B 63 (2001) 144102.

[6] K. Kadau, T. C. Germann, P. S. Lomdahl, B. L. Holian, Science 296 (2002) 1681–1684.

[7] H. J. Leamy, K. A. Jackson, J. Appl. Phys. 42 (5) (1971) 2121–2127.

[8] G. H. Gilmer, P. Bennema, J. Appl. Phys. 43 (1972) 1347–1360.

[9] H. J. Leamy, G. H. Gilmer, J. Cryst. Growth 24/25 (1974) 499–502.

[10] A. Das, E. J. Mittemeijer, Phil. Mag. A 81 (11) (2001) 2725–2742.

[11] K. A. Jackson, Interface Sci. 10 (2002) 159–169.

[12] H. Müller-Krumbhaar, K. Binder, J. Stat. Phys. 8 (1) (1973) 1–24.

[13] K. Binder, Monte Carlo methods in statistycal physics, Springer-Verlag Berlin, 1986.

[14] T. B. Massalski, Metall. Mater. Trans. A 33A (2002) 2277–2283.

[15] Y. C. Liu, F. Sommer, E. J. Mittemeijer, Acta. Mater. 51 (2) (2003) 507–519.

[16] H. I. Aaronson, V. K. Vasudevan, Metall. Mater. Trans. A 33A (2002) 2445–2470.

[17] S. W. Levine, P. Clancy, Modelling Simul. Mater. Sci. Eng. 8 (2000) 751–762.

[18] M. S. Daw, M. I. Baskes, Phys. Rev. Lett. 50 (1983) 1285.

[19] M. S. Daw, M. I. Baskes, Phys. Rev. B 29 (1984) 6443.

[20] C. Bos, F. Sommer, E. J. Mittemeijer, Acta. Mater. 52 (2004) 3545–3554.

[21] H. C. Kang, W. H. Weinberg, J. Chem. Phys. 90 (5) (1989) 2824–2830.

[22] A. F. Voter, Phys. Rev. B. 34 (10) (1986) 6819–6829.

[23] K. A. Fichthorn, W. H. Weinberg, J. Chem. Phys. 95 (2) (1991) 1090–1096.

[24] P. Hänggi, P. Talkner, M. Borkovec, Rev. Mod. Phys. 62 (2) (1990) 251–341.

[25] J. Mandel, The statistical analysis of experimental data, Interscience publishers, 1964.

[26] S. Glasstone, K. J. Laidler, H. Eyring, The theory of rate processes, McGraw-Hill Book Company, New York, 1941.

[27] M. R. Plichta, H. I. Aaronson, J. H. Perepezko, Acta Metall. 26 (1978) 1293–1305.

[28] N. F. Mott, Proc. Phys. Soc. 60 (1948) 391.

[29] B. Schönfelder, D. Wolff, S. R. Phillpot, M. Furtkamp, Interf. Sci. 5 (1997) 245–262.

[30] M. Upmanyu, R. W. Smith, D. J. Srolovitz, Interf. Sci. 6 (1998) 41–58.

[31] H. Zhang, M. I. Mendelev, D. J. Srolovitz, Acta. Mater. 52 (2004) 2569–2576.

[32] C. Bos, F. Sommer, E. J. Mittemeijer, Acta. Mater. 53 (2005) 5333–5341.

[33] R. A. Johnson, D. J. Oh, J. Mater. Res. 4 (5) (1989) 1195–1201.

[34] M. Kaukonen, J. Perajoki, R. M. Nieminen, G. Jungnickel, T. Frauenheim, Physical Review B 61 (2000) 980–987.

[35] B. Müller, J. Reinhardt, M. T. Strickland, Neural networks: an introduction, Springer, Berlin, 1991.

[36] Y. C. Liu, F. Sommer, E. J. Mittemeijer, Acta. Mater. 52 (2004) 2549–2560.

[37] Y. C. Liu, F. Sommer, E. J. Mittemeijer, Phil. Mag. B 84 (18) (2004) 1853–1876.

[38] B. Schönfelder, G. Gottstein, L. S. Shvindlerman, Acta. Mater. 53 (2005) 1597–1609.

[39] P. J. Shewmon, Diffusion in solids, 2nd edition, TMS publication, 1989.

[40] C. Bos, F. Sommer, E. J. Mittemeijer, submitted for publication (2006).

[41] D. Frenkel, B. Smit, Understanding Molecular Simulation, Academic Press, San Diego, 1996.

[42] R. W. Balluffi, T. Kwok, P. D. Bristowe, A. Brokman, P. S. Ho, S. Yip, Scripta Met. 15 (1981) 951–956.

DANKSAGUNG

CURRICULUM VITAE

Persönliche Daten

Name	Cornelis Bos
geboren am	29. Mai 1978 in Enschede
Staatsangehörigkeit	Niederländisch

Schulbildung

1982-1989	Grundschule in Enschede/Niederlande
1989-1996	Ichthus College Enschede/Niederlande
	Vorbereitender Wissenschaftlicher Unterricht (VWO)

Hochschulbildung

1996-2002	Studium der Materialkunde an der Technischen Universität Delft
2002	Diplomarbeit an der Technischen Universität Delft zum Thema: "Atomistic simulation of interface dynamics during the austenite-ferrite transformation" Hauptberichter: Prof. Dr. B.J. Thijsse

Promotion

seit 10/2002	am Institut für Metallkunde, Universität Stuttgart und Max-Planck-Institut für Metallforschung, Stuttgart zum Thema: "Atomistic simulation of interface controlled solid-state phase transformations" Hauptberichter: Prof. Dr. Ir. E.J. Mittemeijer